The Pennsylvania State University

The Graduate School

Department of Materials Science and Engineering

DYNAMIC SWELLING AND CONDUCTIVITY OF ION-CONTAINING BLOCK COPOLYMER THIN FILMS

A Thesis in

Materials Science and Engineering

by

Stephanie Ann Petrina

Submitted in Partial Fulfillment
of the Requirements
for the Degree of

Master of Science

August 2010

The thesis of Stephanie Ann Petrina was reviewed and approved* by the following:

Michael A. Hickner
Assistant Professor of Materials Science and Engineering
Thesis Advisor

Nikolas J. Podraza
Research Assistant Professor of Electrical Engineering

Ralph H. Colby
Professor of Materials Science and Engineering

Joan M. Redwing
Associate Head for Graduate Studies

*Signatures are on file in the Graduate School.

ABSTRACT

Ion-containing polymers have been extensively studied in an attempt to increase the efficiency of ion transport in fuel cells. Block copolymers with an ionic phase and a hydrophobic phase represent one promising approach to improved fuel cell materials. Despite abundant research on bulk membranes composed of ion-containing block copolymers, little attention has been given to swelling and conductivity in thin films (~10-500 nm) of these materials.

Thin ion-containing polymer films play a significant role in fuel cell operation and performance by facilitating proton conduction between the catalyst layer and proton exchange membrane (PEM). By lowering the interfacial resistance between the catalyst and PEM in a fuel cell, these films become a critical component in accessing the maximum amount of reactive catalyst surface area. Typically, thin ion-containing polymer films are treated as having the same properties as measured for bulk membranes. However, in thin films, substrate and air interfaces affect material properties. The high ratio of surface area to volume in films less than 100 nm in thickness results in a large percentage of interfacial polymer with unique morphological, swelling, and conductivity characteristics compared to what is observed for bulk films.

When a PEM is exposed to increased water activity, or more commonly, relative humidity, additional water is absorbed into the film. The morphological structure and polymer chain dynamics of the film may vary with thickness, which affects the rate of water absorption, the total amount of water absorbed, and therefore, the conductivity of the films. To understand thin film conduction, the following points were investigated: the morphological differences between bulk and thin (< 100 nm) film polymers; the

effect of film thickness and morphology on water uptake and dynamic swelling; and the interactions between the ion-containing polymers and the substrate.

The microscopic structure before swelling, the change in thickness during swelling, and ion conductivity of thin films of ion-containing block copolymers were examined. The initial morphology of the films in ambient conditions was established by atomic force microscopy (AFM). Spectroscopic ellipsometry was used to measure the change in thickness and film composition in real time to characterize the dynamic water uptake. Ion conductivity was measured using AC impedance. The aim of this research is to understand the swelling behavior of thin ion-containing block copolymer films and to determine the fundamental water sorption phenomena and morphological features that may influence the conductivity of these thin films.

TABLE OF CONTENTS

LIST OF FIGURES

LIST OF TABLES

ACKNOWLEDGEMENTS

It seems appropriate to begin this document by thanking the people who have supported me in my personal and professional journey to this point. I would like to recognize and thank my advisor, Michael Hickner, for his patience and encouraging attitude. Amazingly, you always have time for students and I appreciate that you treat people as valuable assets. Your insatiable appetite for science is admirable and I envy it.

Thanks are due to Nik Podraza for introducing me to the whole new world of ellipsometry. You were immensely helpful in getting the ellipsometry aspect of this project off the ground and I hope we can conquer the (spectroscopic ellipsometry) world with future discoveries about thin film polymer dynamics. Thanks to the members of Hickner group for all the conversations, guidance, and diversions. Romesh, I'm grateful you were always willing to have a chat and/or a beer with me.

Most importantly, I thank my family and friends who have been my constant advocates and supporters. I was incredibly lucky to grow into adulthood with a group of friends at Virginia Tech that helped me make it through tedious engineering classes, a tragedy, and some immensely good times. Kristin, thanks for being goofy and smart and resetting my balance: I am lucky we could continue from VT to Penn State together. My friend, partner, and love, Josh, I look forward to a lifetime of adventures with you. Thanks to my sister, Renée, for setting the bar high for me. Most of all, I am indebted to my parents, Glenn and Gloria, for making me join swim team, do crafts after school, attend Workcamp and the Governor's School, and setting me up for a life of prosperity. You taught me to be an individual and a good person. I owe all my successes to you.

Chapter 1

Ion Conductive Polymers

1.1. Introduction

Using energy from renewable sources like hydrogen, the most abundant element on Earth, is a promising way to decrease dependence on fossil fuels. Energy conversion using hydrogen fuel cells emits water as a byproduct, as opposed to nitrogen, carbon, and sulfur emissions from internal combustion engines. Fuel cells that use hydrogen or other renewable fuels have the potential to become a common energy conversion technology for electronics and vehicles, but their performance must be improved and their cost reduced before widespread commercialization can be realized.

Proton exchange membranes (PEMs) are usually composed of sulfonated polymers, with Dupont's Nafion®, a poly(perfluorosulfonic acid) random copolymer, being the industry standard. Ion-containing polymers have been extensively studied in an attempt to increase the efficiency of ion transport in fuel cells. Fuel cells convert the chemical energy of hydrogen into electrical energy by splitting hydrogen into protons and electrons ($H_2 \rightarrow 2H^+ + 2e^-$). Figure **1-1** shows the basic function and components of a hydrogen fuel cell. The electrons are used in an external circuit and the proton exchange membrane conducts the protons from anode to cathode. At the cathode, the protons and electrons reduce oxygen from air into water. Water readily absorbs into the membrane to facilitate the proton conduction process. As the material swells, the hydrogen bonding dynamics of the absorbed water increase, more water-water interactions result, and the membrane's microscopic structure changes, all of which promote high conductivity.

Many new PEMs are based on ion-containing polymers with block copolymer motifs. Although bulk membranes composed of ion-containing block copolymers have been extensively researched, little attention has been given to thin film swelling and conductivity of the analogous materials. Omitting research on thin films in these systems is a serious deficiency in the field as ion-containing polymer films lower the interfacial barrier between the catalyst and PEM in a fuel cell, and their performance is critical to accessing all of the catalyst surface area. A layer of ionomer approximately 10 nm thick coats the catalytic particles in the cathode catalyst layer in a PEM fuel cell (PEMFC). Proper ionomer coating of catalytic particles in the catalyst layer of a PEMFC sustains the electrochemical reactions and proton transport that is vital to the functionality of a fuel cell.[1] Since the ionomer must be humidified to be proton conductive, it is essential to understand the behavior of water in a thin film proton conductive polymer.

Typically, these thin ionomer films are treated as having the same properties as measured for bulk membranes. However, in thin films, the substrate and air interfaces affect film behavior. The high ratio of surface area to volume in films less than 100 nm in thickness results in a large percentage of interfacial polymer that may have different properties than what is observed for bulk films.

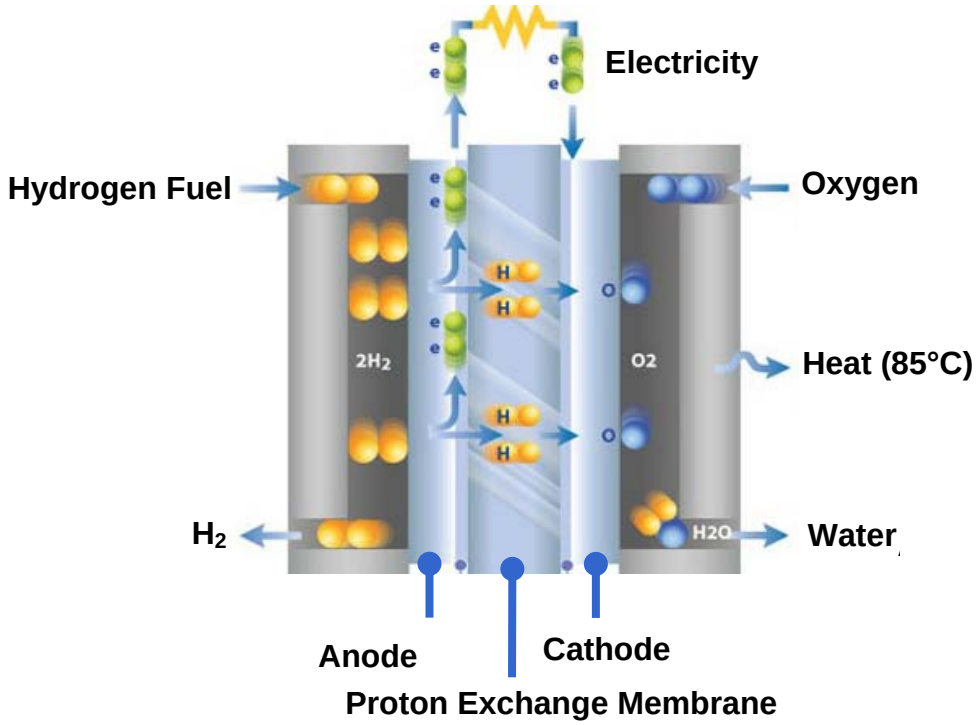

Figure **1-1**. Simplified schematic of a hydrogen powered fuel cell. Hydrogen (H_2) fuel is reduced by the catalyst layer ($H_2 \rightarrow 2H^+ + 2e^-$). The electrons are used in an external circuit and the proton exchange membrane conducts the protons from anode to cathode. At the cathode, the protons and electrons are used to reduce oxygen to water.[2]

1.2. Significance of This Work

In other works, polyelectrolye thin film (5 nm thick) swelling has been attributed to diffusion of water into the film.[3, 4] Due to the very short diffusion lengths of ultra thin films, calculated diffusion coefficients were five orders of magnitude lower than what is generally seen in bulk films of similar materials.[5] Such results are unreasonably low for water diffusivity within ion-containing polymer films, necessitating a new method to describe the dynamic interaction between water and polymer in thin polyelectrolyte films. The goal of this research is determine the fundamental water sorption phenomena and

morphological features that may influence the conductivity of thin ion-containing polymer films.

Ionic conductivity is an inherent material property that is influenced by the water activity in ion-containing polymers. When a PEM is exposed to an increased relative humidity, additional water is absorbed into the film.[1] Certain block copolymer morphologies allow for more expansion of the hydrophilic (ion conductive) phase, and thus increased water absorption, when the material is humidified. Therefore, as thin films adopt different morphologies, their conductivity is likely impacted. Establishing a definitive correlation between phase-separated order and conductivity would be an ideal way to guide the design of new PEMs.

The morphological structure and chain dynamics of the film affect the rate of water absorption and the total amount of water absorbed. These properties vary with thickness, so the conductivity of the films are likely influenced by film thickness. To better understand the relationship between water uptake and conductivity, the following points were investigated: the morphological structure differences between bulk and thin (<100 nm) film polymers; the effect of film thickness and morphology on water uptake and dynamic swelling; and the interactions between the ion-containing polymers and the substrate.

The microscopic structure before swelling, the change in thickness during swelling, and ion conductivity of thin films of ion-containing block copolymers were examined. The initial morphology of the films under ambient conditions was established by atomic force microscopy (AFM). Ellipsometry was used to measure the change in thickness and film composition in real time to characterize the dynamic water uptake.

Ion conductivity was measured using AC impedance. This study will elucidate the fundamental water uptake and morphological characteristics of thin films and will compare their properties to their bulk analogs.

References

1. Eikerling, M., Water management in cathode catalyst layers of PEM fuel cells - A structure-based model. *Journal of the Electrochemical Society* **2006,** 153, (3), E58-E70.
2. Ballard How Fuel Cells Work. http://www.ballard.com/About_Ballard/Resources/How_Fuel_Cells_Work.htm
3. Vogt, B. D.; Soles, C. L.; Lee, H. J.; Lin, E. K.; Wu, W. L., Moisture absorption and absorption kinetics in polyelectrolyte films: Influence of film thickness. *Langmuir* **2004,** 20, (4), 1453-1458.
4. Vogt, B. D.; Soles, C. L.; Lee, H.-J.; Lin, E. K.; Wu, W.L., Moisture absorption into ultrathin hydrophilic polymer films on different substrate surfaces. *Polymer* **2005,** 46, (5), 1635-1642.
5. Mangiagli, P. M.; Ewing, C. S.; Xu, K.; Wang, Q.; Hickner, M. A., Dynamic Water Uptake of Flexible Ion-Containing Polymer Networks. *Fuel Cells* **2009,** 9, (4), 432-438.

Chapter 2

Literature Review

2.1. Introduction

This literature review will begin by discussing the nature of block copolymer phase separation. These concepts will then be extended to the thin film regime with a review of block copolymer thin film literature. Thin film background will include information on the anomalous morphologies observed in the ultrathin film regime (< 100 nm) as well as kinetics of thin film diffusion, relaxation, and swelling. Since spectroscopic ellipsometry was used to study thin film sorption and swelling, a general review of ellipsometry is included, along with a review of research that uses ellipsometry to characterize swelling. Atomic force microscopy is discussed as it applies to morphological studies on ion-containing block copolymer thin films. Finally, a key piece of literature data is discussed concerning the conductivity data of thin Nafion films, which motivated the present work.

2.2. Block Copolymers

Diblock copolymers are composed of two chemically distinct polymer chains covalently bonded to each other. The miscibility of the polymers is based on the Helmholtz free energy of mixing. The polymer chains in the diblock, referred to as "A" and "B" blocks, have a positive free energy of mixing, $\Delta G_m > 0$. To lower the free energy of mixing, the system will tend to minimize the interfacial area between the A and

B blocks via phase separation. The repulsion between the two polymers manifests itself as segregation into A and B rich phases having a range of three-dimensional morphologies. The separation of the two components is called microphase separation, usually with dimensions on the order of less than 100 nm: there is no macroscopic phase separation (with dimensions of microns) because the two polymer units are covalently bonded together. The three dimensional morphological structure depends mainly on the degree of compatibility of A and B, and the molecular weight and volume fraction of each block.[1-6] Because these block copolymers naturally form repeating domains on the nanoscale, they can be used in lithography to create very small and well organized patterns on a substrate.[7-10] Traditional block copolymer behavioral laws do not necessarily extend to ionic block copolymer systems, but as there are no theoretical alternatives to describe the phase behavior of ion-containing block copolymers with strong ionic and/or dipolar interactions, traditional block copolymer principles are used to make predictions about ion-containing block copolymer behavior.

Diblock copolymers are formed via a variety of synthetic procedures. Most commonly, living polymerization is used to precisely control the molecular weight of each block and to provide relatively low polydispersity. In living polymerization, the only active species is at the chain end, so monomer B only adds to the end of a chain of polymer A. When monomer A is fully polymerized, the addition of monomer B prompts further growth from the living end of polymer A and polymerization of the B block ensues. The initiation of the reaction is much faster than the monomer propagation, giving simultaneous growth of all chains. The initiator concentration determines the

concentration of growing chains during the reaction, therefore controlling molecular weight.[11]

2.2.1. Flory-Huggins Theory

What Maurice Huggins described as the statistics of "long chain molecules" in the early 1940's laid the groundwork for the modern understanding of block copolymer thermodynamics. Paul Flory[12] and Maurice Huggins[13] simultaneously established the thermodynamic principles of polymer-solution miscibility. To minimize the Helmholtz free energy of mixing, a binary block copolymer will tend to minimize the interfacial area between the A and B blocks. Microphase separation reduces the number of A-B contacts which simultaneously lowers entropy. Qualitatively speaking, the thermodynamic properties are determined by the chemical compatibility of the two polymers and the number of contacts between them. Quantitatively, this translates into entropy (potential number of contacts between the polymers) and enthalpy (energy difference between A and B, multiplied by the number of interactions). Equation 2-1 shows the basic relationship for Helmholtz free energy of mixing, ΔG_m, with the Flory-Huggins equation shown in 2-2.

(2-1) $$\Delta G_m = \Delta H_m - T\Delta S_m$$

(2-2) $$\Delta G_m = RT\left[N_A \ln \phi_A + N_B \ln \phi_B + N_A \phi_B \chi_{AB}\right]$$

In diblock copolymers, the parameters that affect phase behavior are: i) the degree of polymerization, N, (where $N=N_A+N_B$); ii) the composition of the copolymer, $f = N_A/N$,

and iii) the Flory-Huggins parameter, χ. The χ parameter represents the free energy cost per mole of monomer contacts between differing monomer units.[6] χ is based on the difference between the solubility parameters of the two materials, δ_A and δ_B, the molar volume of a monomer unit, V_o, the gas constant, R, and temperature, T, as seen in Equation 2-3:[14]

(2-3)
$$\chi = \frac{V_o(\delta_A - \delta_B)^2}{RT}$$

The product of χ and the degree of polymerization (or number of monomers in a block), N, dictates the degree to which the A and B blocks segregate. Along with volume fraction of each block, f, these parameters are the most important indicators of phase behavior in the molten state.[15, 16] The mean field phase diagram in Figure **2-1** [17] demonstrates the resulting phase equilibria. The schematic shows that as the compositional fraction of block A increases, different equilibrium structures are observed. The phase morphologies that correspond to the letters L (lamellar), G (gyroid), C (cylindrical), S (spherical), and S_{cp} (close-packed spherical) in Figure **2-1** are illustrated in Figure **2-2**.

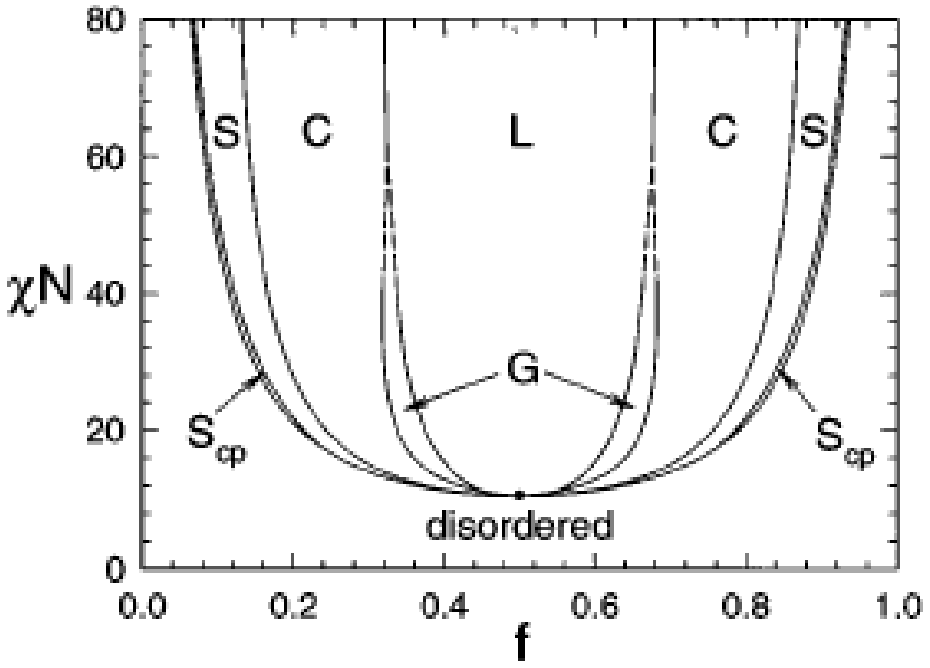

Figure **2-1**. Mean-field phase diagram for diblock copolymer melts. The ordered phases are labeled as L (lamellar), G (gyroid), C (cylindrical), S (spherical), and S_{cp} (close-packed spherical). The dot marks a mean-field critical point, and the dashed curves denote extrapolated phase boundaries, which could not be calculated due to numerical limitations.[18]

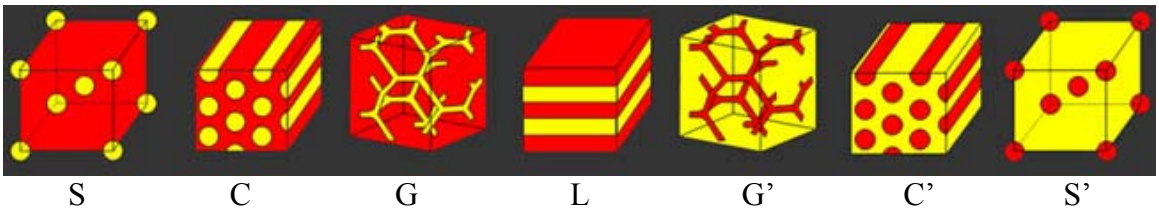

Figure **2-2**. Three dimensional structures of ordered block copolymer phases including S (spherical), C (cylindrical), G (gyroid), and L (lamellar).[19]

The mean field approximation assumes that the interaction one molecule experiences is an average of all the possible configurations of the system. This theory can be used to calculate the change in enthalpy and entropy to determine the free energy of a system at a particular temperature. [2, 15, 20]

The thickness of the molecular structures, also known as the domain spacing, scales with molecular weight.[2, 21, 22] Equation 2-4 exemplifies how the domain spacing, D, is related to the characteristic monomer length, a, the degree of polymerization, N and the Flory Huggins interaction, χ:[2]

$$D \propto aN^{2/3}\chi^{1/6} \tag{2-4}$$

Simply put, longer polymer chains will create thicker lamellae (or other periodic structures).

2.2.2. Application of Block Copolymer Theory to Ion-Containing Block Copolymers

Theoretical solubility parameters (δ) for ionic constituents used in block copolymers, namely sulfonated polystyrene, have been experimentally determined.[23] Experimentally derived δ values for ionic moieties are estimates because the Coulombic interactions among ionic groups are not accounted for in the χ calculation[24, 25] (Equation 2-3). The χ value for interaction between fully sulfonated polystyrene and polymethyl methacrylate is 10.28, which, in itself, already falls in the strong segregation regime.

2.3. Thin Film Block Copolymers

Morphology in thin film block copolymers is greatly influenced by interfacial surface energies and the symmetry of those energies. The focus of this section is on substrate-supported thin films with an open air surface, where the system has asymmetric surface energies. When the thickness of the film is less than the domain spacing of the polymer ($t < L_o$), surface energetics dominate the entropic contributions in thin films. Attraction of one component of the block copolymer to the surface will lead to a

concentrated A- or B-rich phase at the surface. Concentrations of each block will be found at either surface based on their affinity for that interface. The substrate will induce chain confinement of the polymer, while the air interface allows for conformational expansion and lowered surface tension.[26]

It has been established that in bulk form diblocks naturally phase separate to form structures that reduce the interaction between the chemically different polymers, forming an energetically favorable morphology. In thin-film block copolymers, the phase separated morphology is more ordered because of the structural support of the substrate. Thin films have a high surface area to volume ratio, so a large portion of the polymer is in contact with either a substrate or air interface. These interfaces affect polymer mobility and confinement and the interfaces also affect how block copolymers adopt various morphologies in thin films. Figure **2-3** [26] shows a schematic of the distribution of A and B rich blocks as the thickness of the film decreases from the characteristic domain size, L_o.

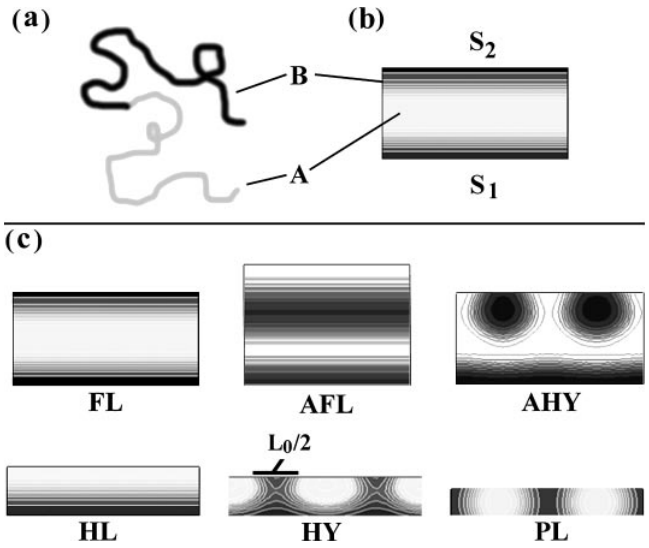

FL: symmetric surface-parallel full lamella

AFL: anti-symmetric surface-parallel lamella

AHY: anti-symmetric hybrid structure

HL: half-lamella

HY: symmetric hybrid structure

PL: surface-perpendicular lamellae

Figure **2-3**. Diblock copolymer thin film morphologies. (*a*) Schematic representation of volume symmetric diblock with A (light) and B (dark) type segments. (*b*) Diagram of BC film system in cross section indicating the bottom (1) and top (2) surfaces, with surface interaction energies *S1* and *S2*, respectively. (*c*) Summary of diblock thin film morphologies as film thickness decreases from L_0. These calculated cross sections indicate the density of B-type segments, i.e., Black = 100% B, white =100% A. These structures are referred to in the text with the abbreviations included under each diagram. [26]

As the thickness of a block copolymer film decreases from L_o, the phase separated A and B domains form unique structures based on the symmetry of domains at a given thickness. The blocks will still separate into A- and B-rich phases based on preferential wetting: the polymer will segregate to the surface that has the most compatible surface energy (depicted as S_1 and S_2 in Figure **2-3**) to minimize the entropic expense.[26-29]

When a block preferentially wets either surface, as seen in the half-lamella structure in Figure **2-3**, the film is anti-symmetric at equilibrium. The intermediate structures in anti-symmetric films are stable only when the thickness is some increment of the lamellar spacing, where $t = (n + ½)L_o$ for n = 1, 2, 3, 4. For symmetric films like the full lamellar form at $t = L_o$, the films are stable at increments of $t = nL_o$.[26] The

symmetry of surface energies plays a major role in the morphology of thin film block copolymers. For most applications, films are not sandwiched between identical surfaces and the most common thin film system is substrate supported on one face, creating asymmetric surface energies and asymmetric structures.[26, 29]

When dealing with thin films, it is important to consider the effects of the substrate and air interface on film behavior, especially morphology, chain mobility, and thermodynamics.[30] When polymer chains selectively deposit on the substrate, conformational entropy and surface tension are reduced. Not only is the mobility and natural reptation of the polymer hindered at this solid interface, but the substrate can also have an attractive, repulsive, or neutral interaction with the polymer. This concentration of material at the substrate creates a greater amount of free volume at the free surface,[31] affecting the glass transition temperature (T_g),[1, 32-35] relaxation time,[1, 31, 34, 36-39] small molecule diffusivity,[28, 31, 36-45] physical aging,[46] and swelling characteristics.[30, 39, 43, 47-49] The high surface area to volume ratio of thin films creates a large percentage of this unique interfacial polymer.

2.3.1. Small Molecule Diffusion in Thin Polymer Films

Figure **2-4** [50] depicts the two types of diffusion in polymers. The most common case for softer polymers is Fickian diffusion, where the solvent molecules penetrate the free surface based on a concentration gradient.[39, 44, 50, 51] In Case II diffusion, most of the polymer maintains its glassy state, with a layer of swollen gel-like material only at the free surface in contact with the diffusing medium, as depicted in Figure **2-4b**. Case II diffusion is usually dependent on temperature and film thickness. In thin films,

relaxation at the glassy to gel polymer interface is the main determinant of diffusion character. The resistance to diffusion in the swollen fraction of the polymer increases as that interface propagates into the material. The diffusion resistance is negligible in thin films due to the short diffusion lengths encountered.[50] A material can follow Fickian, Case II diffusion, or, often, some combination of the two.[40, 41, 50, 52, 53]

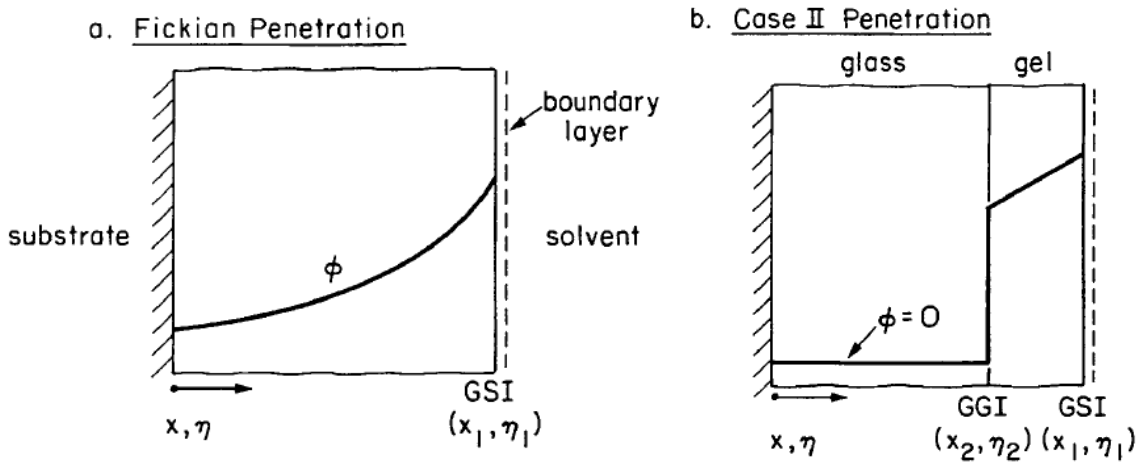

Figure **2-4**. The two types of diffusion are shown (a) Fickian diffusion and (b) anomalous Case II diffusion. [50]

If a solvent does not solvate the polymer, it will only swell the polymer. A good solvent, with a similar solubility parameter as the polymer matrix, will swell the polymer and also induce chain relaxation and disentanglement at the free surface.[6, 50, 54] Corresponding dissolution and swelling equations for each case can be found in Papanu, et. al.,[50] but those details are beyond the scope of this review.

As the film thickness approaches the radius of gyration (R_g) of the polymer, confinement effects are observed at the substrate interface, but even for films at thicknesses less than R_g, Gaussian chain statistics still apply.[43] Chain confinement hinders both the diffusivity of chains and small molecules such as water. The calculated

diffusivity of water decreased by orders of magnitude in relation to film thickness based on Fickian diffusion coefficients in Equation 2-5 [30, 40, 43]

(2-5) $$\frac{M_t}{M_\infty} = \frac{2}{d}\sqrt{\frac{Dt}{\pi}}$$

where M_t is the mass uptake of water at time t, M_∞ is the mass uptake of water at equilibrium, t is time, d is film thickness, and D is diffusion coefficient. Eq. 2-5 is a simplified relationship for short diffusion times, and is used to calculate the mass uptake of water from the initial linear portion of a solvent uptake curve only. It does not describe diffusion when the mass uptake plateaus and the material equilibrates with its environment. Due to the very short diffusion lengths of ultra thin films, the calculated diffusivity values are decidedly low. Based on calculations from Equation 2-5, ultra thin films (<100 nm) exhibit diffusion coefficients on the order of 10^{-13} cm sec^{-1}, as seen in Figure **2-5**. These values are five orders of magnitude less than diffusivity in bulk ionic polymer films,[55] which is not feasible for water diffusivity within ionic polymer films, necessitating a new method to describe the dynamic interaction between water and polymer in thin polyelectrolyte films. In reality, the relationship between diffusion and film thickness is not accurately described with one simple diffusion model. Chain relaxation due to plasticization from increased solvent content counterbalances the diminished diffusion rate which often necessitates a two part diffusion model of small molecules in polymer films.[30, 56, 57]

The effects of chain relaxation on diffusion have been described in bulk polymer films [30] as well as thin films. Relaxation is especially significant in the study of solvent

sorption in thin polymer films because of the confinement at the substrate interface. To determine the significance of the polymer-substrate interaction, Tan, et. al. [58] used X-ray reflectivity techniques to compare moisture absorption in hygroscopic polyimide on two types of substrates: native oxide on Si wafers and wafers coated with a silane coupling agent. For films of identical thickness, the silane coupling agent, γ-aminopropyltrimethoxysilane (APTMS), reduced the total amount of water absorption, leading to the conclusion that a hydrophilic substrate, the SiO_x, creates a more humidified layer at the substrate interface. Subsequently, their ultrathin films (7-100 nm) were considered to have a bilayer structure including an interfacial and bulk region.[58] Their observation implies that the polymer, which experiences chain confinement due to the substrate interface, is plasticized by the accumulation of more moisture at the substrate interface.

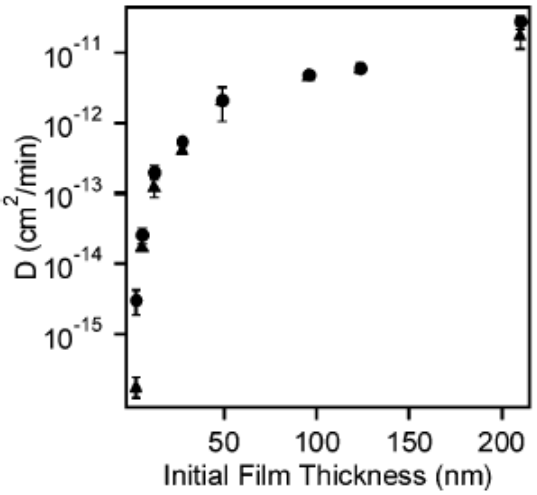

Figure **2-5**. Water diffusion coefficients into thin films as a function of poly(4-ammonium styrenesulfonic acid) film thickness as determined by (▲) Fickian and (●) two-stage absorption models. [43]

Tan, et. al. also found that, when exposed to 80% relative humidity (RH) for 16 hours, thinner films had a higher thickness increase relative to their dry thicknesses $100*(t_{RH}-t_{dry})/t_{dry}$, as seen in Figure **2-6**. This effect held true for both bare and APTMS coated substrates, but a physical explanation for this anomaly was not explored in the paper. For a polymer which absorbs only up to 5 wt % water, it was surprising to find this effect. In studies of more hydrophilic polymers, there is no change in water absorption for a range of film thicknesses of 3-200 nm (30-2000 Å).[43]

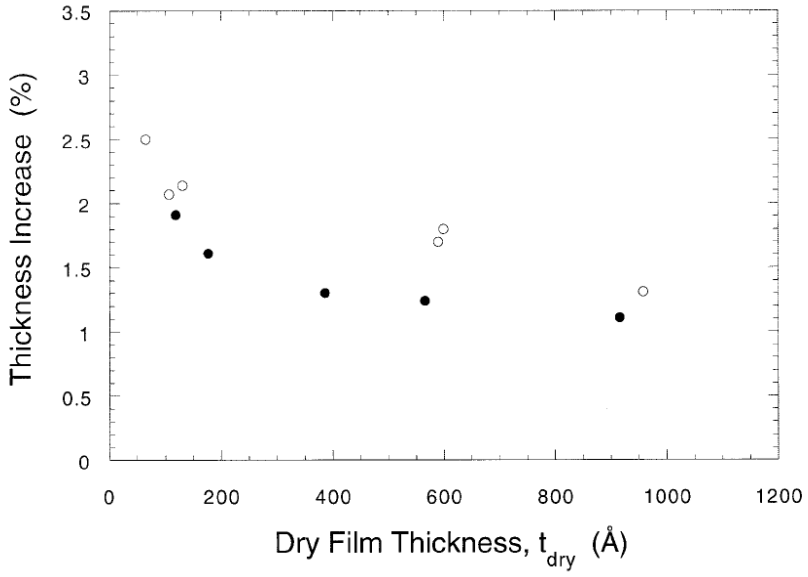

Figure **2-6**. Percentage increase in film thickness induced by a 16-h exposure to an 80% RH environment vs. thickness of the same film measured under dry, evacuated conditions. Films prepared with a silane coupling agent (●) and without a silane coupling agent (○). All measurements at 23ºC. [58]

Vogt, et al. [30] performed a similar study with a different polymer, measuring water uptake of various thickness poly(vinyl pyrrolidone) (PVP) films on hydrophilic and hydrophobic substrates. They, too, observed reductions in the absorption of water for the films less than 100 nm thick on hydrophobic substrates. Using x-ray reflectivity and

quartz crystal microbalance (QCM), the gravimetric uptake of water was observed in PVP films 3-200 nm thick, on native oxide on silicon as well as silicon wafers coated with hydrophobic hexamethyldisilazane (HMDS). The volume fraction of water at equilibrium swelling in saturated vapor for the thickest film (150 nm) on HMDS was identical to that of films on silicon's native oxide, as seen in Figure **2-7**. Despite the thickness effect of the hydrophobic substrate treatment on the uptake of water, films on hydrophilic SiO_x absorbed the same volume fraction of water (0.47) for thicknesses varying from 3 to 150 nm. Similar results were observed for a thin polyelectrolyte film of poly(4-ammonium styrenesulfonic acid) in Figure **2-8**.[43] Both QCM and X-ray reflectivity showed a similar water uptake for thicknesses ranging from 2 to 120 nm on silicon (oxide) substrates.

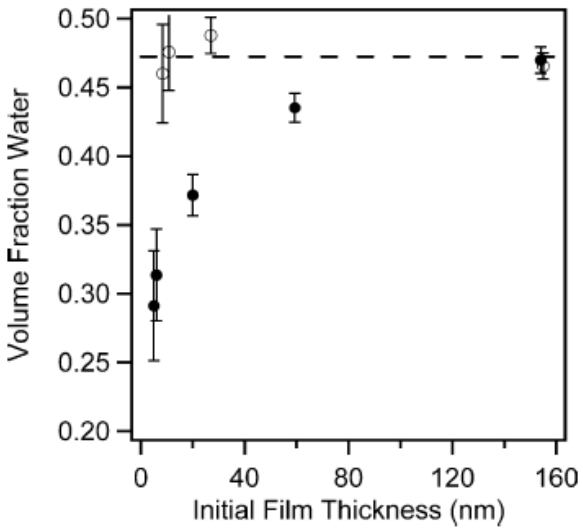

Figure **2-7**. Influence of poly(vinyl pyrrolidone) (PVP) film thickness on moisture absorption as measured by reflectivity. The water volume fraction absorbed in the films from saturated vapor is dependent for the thin films upon the substrate, either (○) SiO_x or (●) HMDS treated silicon. The dashed line is a guide to show that the absorption in PVP on the silicon oxide substrate is independent of film thickness.[30]

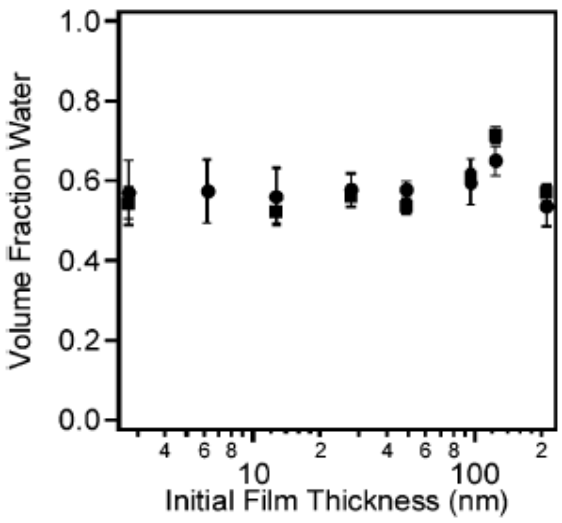

Figure **2-8**. Equilibrium water absorption in different thickness poly(4-ammonium styrenesulfonic acid) films as determined by (●) XR and (■) QCM measurements. [43]

The interfacial concentration of water was also affected by relative humidity. The absorption isotherm for PVP films on HMDS samples showed a discontinuity in the volume fraction of water absorbed after 40% relative humidity due to plasticization of the polymer, which corresponds to the transition from a glassy to rubbery state.[35, 53, 59] At this point, the polymer is relaxing as it swells and is plasticized with water. Figure **2-9** shows calculated diffusion coefficients of small molecules (using Eq. 2-5).

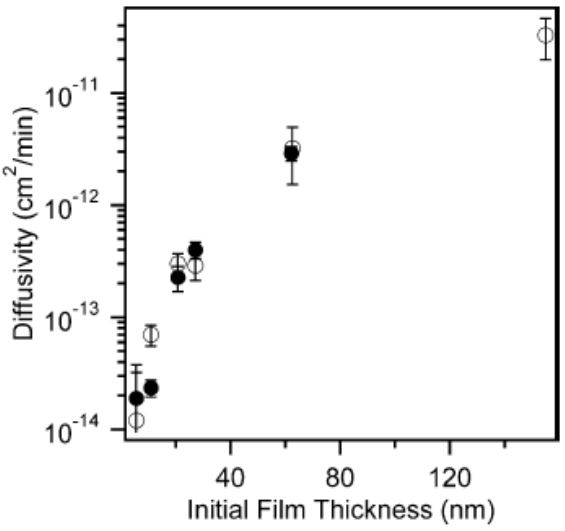

Figure **2-9**. Effective water diffusion coefficients in PVP films. The diffusivity decreases by three orders of magnitude as the film thickness decreases from 155 to 5.6 nm. There is no discernable effect of the substrate, (○) SiO_x or (●) HMDS, on the diffusivity. [30]

Equation 2-5 describes diffusivity based on the slope of the mass uptake (M_t/M_∞) versus time$^{1/2}$/thickness during initial diffusion into the film. This analysis does not represent the additional absorption of water due to polymer relaxation or the behavior of the polymer once it is plasticized.

Even in films as thin as 5 nm, there is little difference in diffusivity for films on HMDS versus SiO_x substrates. Small molecule diffusion in other thin film systems have shown no dependence on polymer-substrate affinity in 50 nm thick films.[42] The complex interactions involved in these systems between the polymers and the surface still lend much contention as to how the heterogeneity of thin films contributes to their absorption properties.[51, 60]

2.3.2. Thin Film Diffusion and Relaxation

During solvent sorption into a polymer, two processes occur simultaneously: the solvent diffuses into the free volume of the polymer, and the polymer chains relax as they are plasticized by the solvent. The plasticization process subsequently allows further solvent absorption. This relationship between diffusion and polymer relaxation can be described by the Berens-Hopfenberg model.[61, 62] The model distributes the total solvent mass (M_t) absorbed by the polymer between mass attributed to Fickian diffusion ($M_{t,F}$) and extra mass acquired during relaxation ($M_{t,R}$) in Equation 2-6:

(2-6) $$M_t = M_{t,F} + M_{t,R}$$

The first order rate equation derived from this relationship exemplifies the underlying connection between diffusion and relaxation: relaxation leads to more diffusion until the mass uptake of water reaches equilibrium at $M_{\infty,R}$. This equation can be rearranged to solve for the relaxation rate constant, k_R through Equations 2-7, 2-8, and 2-9 [61-63]:

(2-7) $$\frac{dM_{t,R}}{dt} = k_R(M_{\infty,R} - M_{t,R})$$

(2-8) $$\frac{dM_{t,R}}{(M_{\infty,R} - M_{t,R})} = k_R \cdot dt$$

(2-9) $$M_{\infty,R} - M_{t,R} = \exp(-k_R t + c)$$

Now it is possible to solve for the ultimate mass uptake due to relaxation can via Equation 2-10 [61-63]:

(2-10) $$M_{t,R} = M_{\infty,R}\left[1 - \exp(-k_R t)\right]$$

Another consideration of ultrathin film dynamics that is coupled with diffusion is the relaxation profile of ultrathin films. Thin films of poly(isobutyl methacrylate) and poly(2-vinyl pyridine), both of which have a relatively strong interactions with native silicon oxide, showed no difference in diffusion for films as thin as 50 nm, indicating that polymer-substrate interaction effects extend less than 40 nm into the bulk of the film.[31] The substrate effects extend to half of one lamellar period of the film.

In ultrathin films, T_g decreases because the high density of chains at substrate surface reduces surface tension and conformational entropy.[28, 64] This substrate-chain interaction would create more free volume at the free surface, in turn lowering the glass transition temperature and number of chain entanglements and increasing chain mobility and diffusivity.[6, 32, 64] The value that represents the penetration of surface effects is R_g. Interfacial effects are usually felt no more than two times the radius of gyration of the polymer. [31]

It has been established that the unique structures of thin and ultrathin films affect the polymer dynamics, and, naturally, that includes polymer self-diffusion and relaxation. The anomalous relaxation of thin films is inherently linked to the change in T_g, and both have been extensively studied.[1, 28, 32-34, 37, 46, 51, 60, 65, 66] In bulk melts, the glass transition temperature is often characterized using rheological techniques, which are not appropriate for thin film characterization. Techniques to measure the T_g of thin films include ellipsometry,[46, 47, 49] x-ray reflectivity,[2, 43, 48, 58, 60] optical birefringence,[65] neutron scattering,[43, 60] second harmonic generation,[31, 33, 34, 65] and optical waveguide spectroscopy.[31]

As previously established, the polymer chains in thin films experience different levels of molecular motion and confinement based on their location relative to either interface. Chains with significant free volume (as at the free surface) will relax much faster than chains experiencing confinement (at the substrate surface). Subsequently, thin film polymers will experience a larger distribution of relaxation times as compared to bulk films.[1, 31, 33, 34, 37, 51, 66] This broadening is especially evident on the shorter relaxation time scales which has implications for small molecule diffusion, and, consequently, swelling. Figure **2-10**[31] shows measured distributions of relaxation times for 23 and 520 nm thick polymer films using SHG. Relaxation times less than 10 seconds show a significantly broader distribution. Figure **2-10**[66] is another example of thickness dependent relaxation for poly(vinyl acetate) (PVAc) as characterized by broadband dielectric spectroscopy. Relaxation times become more varied as film thickness decreases because of the gradient in the density of polymer chains in thin films.

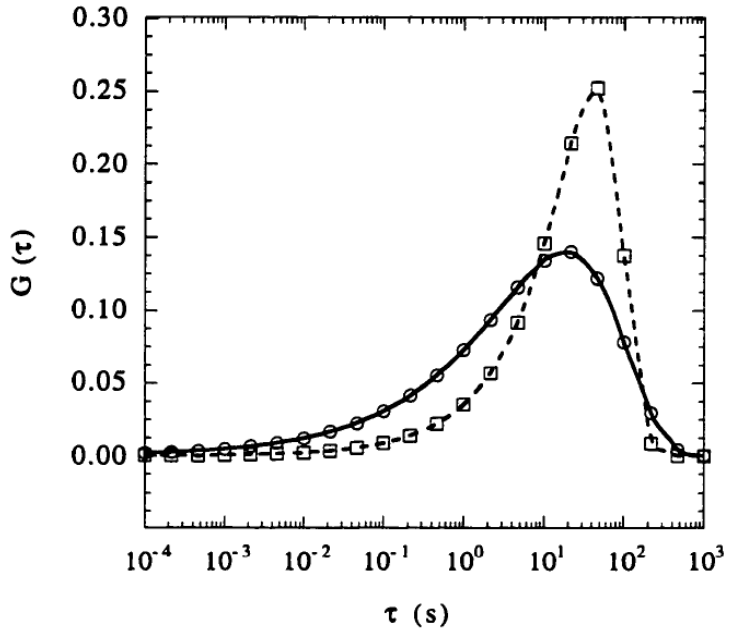

Figure **2-10**. Discrete distributions of relaxation times for (○) 23 and (□) 520 nm thick films at 98ºC (5º above T_g). Curves are drawn to guide the eye. [31]

Since interfacial effects have a great influence on thin film behavior, studying film relaxation and small molecule diffusion as a function of film thickness will aid in understanding thin film ion conductivity.

2.4. Thin Films of Ion-containing Polymers: Morphology and Conductivity

Thin film ion conductivity is an unexplored field with deep potential: little attention has been given to the area of thin film (< 100 nm) ion-containing block copolymer swelling and conductivity. At the interface between the catalyst and PEM layers in a fuel cell membrane electrode assembly, thin ionic polymer films strike a balance that facilitates conductivity and gas diffusion, both of which are required for high performance fuel cell electrodes.[67, 68] The study of thin ionic polymer films unites two developed but not fully understood fields: properties unique to thin film polymers and fundamental mechanisms of ion conductivity. Morphology and conductivity are interconnected in ion-containing block copolymers because the structural arrangement of ionic groups controls ionic movement.[69]

Thin film ionic block copolymers have been studied more in recent years for their applications as electrochemical sensors and catalysts,[63, 70-75] to increase ion-exchange selectivity,[70, 76, 77] and as conductive coatings to reduce Schottky barriers between materials with different resistivities.[67, 68] Despite this wide range of studies, the underlying morphological influence on conductivity in thin films of ion containing polymers has not been fully described. Bertoncello, et al., who have extensively studied thin films of layered amphiphiles (Langmuir-Schaefer films) including Nafion® for sensing applications,[71-75] have also investigated thin film morphologies, yet their work

mostly compares the morphological and voltammetric effects of cation loading. The research did not examine the fundamental effects that film thickness has on morphology of bulk and thin film forms of ion conducting polymer species. Figure **2-11**[71] shows morphologies obtained via AFM. The thickness of these films was in the range of 13-17 nm and they were deposited on an oxidized silicon surface. Figure **2-11a** shows a largely uniform surface with only several void spaces. As ionic compounds (ferrocene derivative ferrocenyltrimethylammonium cation, FA^+ (Figure **2-11b**), or tris(2,2'-bipyridyl)ruthenium(II), $Ru(bpy)_3^{2+}$ (Figure **2-11c**))[71] are added to the solution a morphology more typical of bulk Nafion® forms,[78] exhibiting ion cluster-like formations.

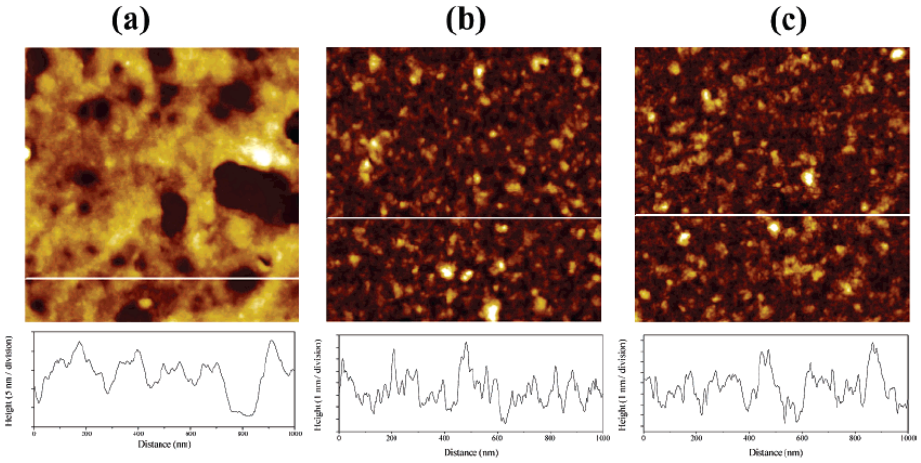

Figure **2-11**. AFM topography images (1 µm x1 µm) of Nafion® LS films in air: 10 layers deposited on a silicon oxide substrate (a) before and (b) after loading in 5 x 10^{-4} M FA^+ and (c) 5 x 10^{-4} M $Ru(bpy)_3^{2+}$.[71]

Dilute solutions of Nafion® were spin coated onto flat substrates at thicknesses of 5 to 20 nm. AFM was used to characterize Nafion® morphology on indium tin oxide (ITO) substrates. Figure **2-12a** shows a 135 nm thick layer of ITO on a glass surface (Z range 10.6 nm), and Figure **2-12b** shows a 7 nm thick layer of spin cast Nafion® on ITO. The bumpy ITO surface affects the morphology of the Nafion® polymer, but Figure **2-**

12b shows that the film has smoothed over and evenly coated the rough surface. The AFM height image shows a co-continuous "island" morphology of phase separated sulfonated domains (Z range 7.5 nm). Figure **2-12c** shows the electronic nature of Figure **2-12b**, with the uncovered ITO appearing in red and Nafion® as yellow-green.

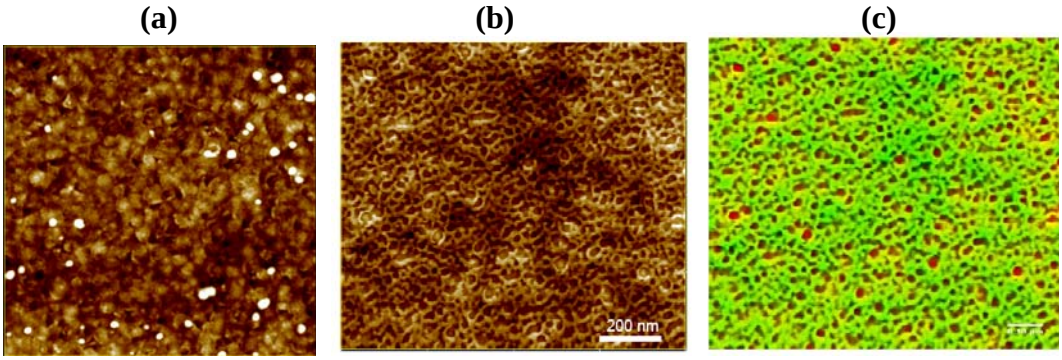

Figure **2-12**. Atomic force micrograph of (a) 135 nm thick ITO film (tapping mode) and (b, c) 7 nm thick Nafion film on ITO (tapping mode). (c) is a color coded version of (b) which shows uncoated ITO in red.[73]

Figure **2-11** shows that even for the same material at similar thicknesses, a range of morphologies still exist. The wide array of observed morphologies can be attributed to differing substrate roughness, surface energy, and processing conditions yet initial studies show that there is still a vast range of forms that these thin films may assume. These different morphologies, no doubt, will lead to differences in ion conductivity.

Yasuda, et al.[67] provided the initial report on thin film ion conductivity via impedance spectroscopy, which is discussed further in Chapter 6. They found that the film conductivity decreased as the thickness of the film on silicon decreased. As conductivity is an intrinsic material property, it is not anticipated to change for films with varying thickness, but Yasuda, et al. found a logarithmic relationship that extended from 10 nm to 100 μm between the conductivity of thin film recast Nafion®. It is unknown what interfacial effects could be taking place over such large of a range of thicknesses.

One possibility is that thin films absorb less water, thus lowering conductivity, providing the basis for this investigation. But in literature, thin films have been shown to expand by more of their original thickness than thicker films, as seen in Figure **2-6**. The relationship between thin film swelling and conductivity is explored in Chapters 5 and 6.

2.5. Ellipsometry

Ellipsometry is a technique that uses reflection and polarization of light to determine optical properties of thin film materials. More specifically, it involves the refraction (and ultimately, reflection) of light as it passes through the interfaces that exist between layers of a material, as seen in Figure **2-13**. Ellipsometry can be measured using either a single wavelength of light or a spectrum of light, as in spectroscopic ellipsometry. Spectroscopic ellipsometry gives more information about a material than single wavelength ellipsometry as it interacts with a wide range of photon energies. Figure **2-13**[79] shows the angle of incidence of light Φ_i, reflected angle Φ_r, transmitted angle Φ_t, and the refractive index of air n_0, and the refractive index of the first layer of a material, n_1.

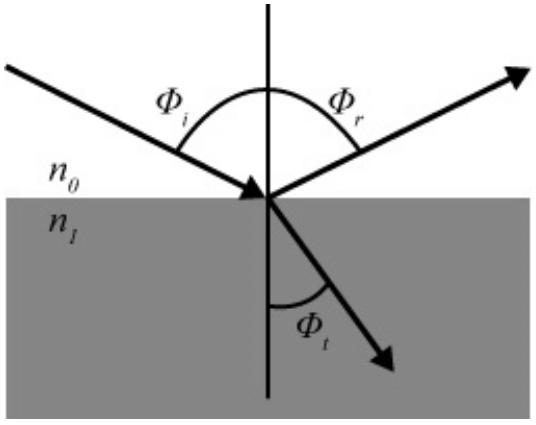

Figure **2-13**. Reflection of light off of a surface showing angle of incidence, reflection and transmission. Refractive index of air, n_0, and material, n_1.

Ellipsometry measures the polarization of light as it passes through layers of a material with different refractive indices. Fresnel reflection coefficients r_s and r_p are measurements of reflected light as it oscillates perpendicular (s) and parallel (p) to the plane of incidence, and are orthogonal to each other. The schematic in Figure **2-14** shows how the p and s components of a wave (wave 1 and 2, respectively, in the figure) combine to form an ellipse (from which the name ellipsometry is derived) while Figure **2-15** shows the polarization of the s and p planes as light is reflected off of a planar surface.

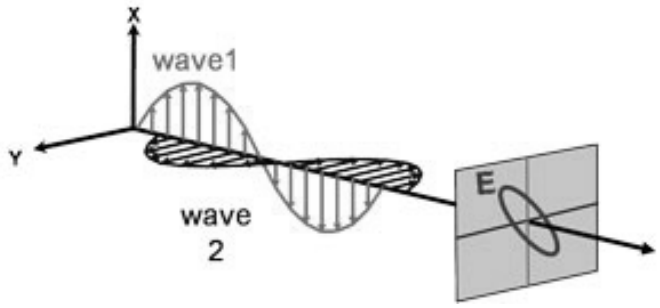

Figure **2-14.** Orthogonal waves combined to demonstrate elliptical polarization of light.[79]

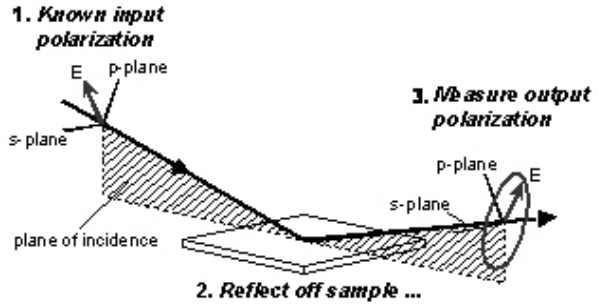

Figure **2-15**. Typical ellipsometry configuration, where linearly polarized light is reflected from the sample surface and the polarization change is measured to determine the sample response.[79]

The fundamental ellipsometry relationship is given in Equation 2-13 by the ratio of the reflection coefficients, which relates the amplitude and phase of a light wave:

tan(ψ) represents the wave amplitude ratio upon reflection and Δ represents the phase shift of light upon reflection. Because an ellipsometer measures these components relative to each other, it is an extremely accurate tool.[49, 79-83]

(2-11) $$\rho = \frac{r_p}{r_s} = \tan(\Psi)e^{i\Delta}$$

The refractive index is composed of both real and imaginary components, where N = (n + ik), $\varepsilon = (\varepsilon_1 + i\varepsilon_2)$, and $\varepsilon = N^2$. The imaginary (i-based) component of refractive index includes an extinction coefficient, k, which is related to the depth of light penetration (i.e. if the material is fully transparent or a perfect vacuum, k = 0). The penetration depth is given by Equation 2-12. The complex dielectric function is determined by the complex refractive index via Equations 2-13.

(2-12) $$D_p = \frac{\lambda}{4\pi k}$$

(2-13) $$\varepsilon = N^2 \qquad \varepsilon_1 = n^2 - k^2 \qquad \varepsilon_2 = 2nk$$

These parameters can all derive essential information about the optoelectrical properties of individual layers of a material, making ellipsometry a powerful characterization tool for characterizing thickness, complex refractive index, and complex dielectric function.

Ellipsometry is a commonly used for real time dynamic measurements of a material as it is exposed to a changing environment. The dual rotating compensator multichannel ellipsometer, the type used in this study, was first introduced in 2004.[84] The experimental setup of an ellipsometer allows for a measurement to be made through

non-polarizing windows, so a material can be placed in a controlled environment cell and optoelectronic properties can be measured in real time as the conditions inside the sample cell change. An example schematic of a controlled environment cell is given in Figure **2-16**.[85] The angle of incidence of light is optimized so as not to polarize the light before it reflects off the sample surface.

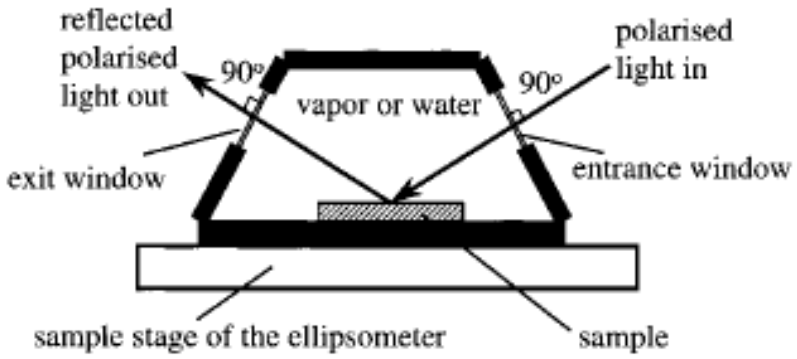

Figure **2-16**. Schematic diagram of the sample cell for ellipsometric measurements. [85]

The ability to do in-situ measurements with high temporal resolution makes ellipsometry an excellent tool for measuring thickness changes during material deposition [80, 82, 86] and swelling.[47, 49, 58, 80, 81, 85, 87, 88] In the same way that water uptake was derived via gravimetric measurements in Equation 2-5,[40, 52] water uptake can also be estimated by thickness increase during swelling via *in situ* dynamic ellipsometry.[63] As the film increases in volume, f_t, due to the change in thickness, d_t, multiplied by area, A, during swelling, and volume and mass are related via density, then a relationship between mass, M, and thickness, d, can be assumed via a proportionality constant, C as in Equations 2-15 and 2-16.

(2-15) $$f_t = A \cdot d_t$$

(2-16) $$M = C \cdot d$$

The proportionality constant C then relates the mass uptake at times t, M_t, and at equilibrium, M_∞, to the diffusion at time 0, t, and equilibrium via:

(2-17) $$M_t = C(d_t - d_0)$$

(2-18) $$M_\infty = C(d_\infty - d_0)$$

The same way the gravimetric uptake of water can be calculated by the ratio of diffusion coefficients, volumetric water uptake can be derived by determining the change in refractive index. Volumetric water uptake can be calculated by matching the refractive index of the swollen film to a mixed refractive index of water and the dry polymer.[63]

(2-19) $$\frac{M_t}{M_\infty} \approx \frac{d_t - d_0}{d_\infty - d_0}$$

(2-20) $$\frac{M_t}{M_\infty} \approx \frac{n_t - n_\infty}{n_\infty - n_0}$$

The refractive index of the swollen polymer can be used to directly calculate the volume fraction of water in the film using the Bruggemann mixing equation.[89]

(2-21) $$\frac{n^2 - n_{pol}^2}{n^2 + 2n_{pol}^2} = \phi_{v/v} \frac{n_{water}^2 - n_{pol}^2}{n_{water}^2 + 2n_{pol}^2}$$

Where n is the dry refractive index, n_{water} is the refractive index of water, n_{pol} is the refractive index of the dry polymer, and $\varphi_{v/v}$ is the volume fraction of water in the polymer. The value for the refractive index of the swollen material is determined by ellipsometric measurements and the equation can be solved for the volume fraction of water in the polymer.[85]

Figure **2-17** shows the phase (Ψ) and amplitude (Δ) shifts for poly(methoxytriethylene glycol acrylate) (P(MTGA*r*-AA)) at relative humidities from 0

to 95%. As the polymer film absorbs water, the peak in the phase and amplitude shift to longer wavelengths, and therefore lower photon energies (eV). This shift means that light interacts more with the polymer as the material becomes denser with added water. Figure **2-18** shows the increase in thickness and decrease in refractive index as relative humidity is increased. As the relative humidity increases, the polymer swells and a larger portion of the material is composed of water. Subsequently, the thickness increases and the refractive index decreases because the refractive index of water is less than that of the polymer, $n_{water} = 1.333 < n_{pol} = 1.512$.

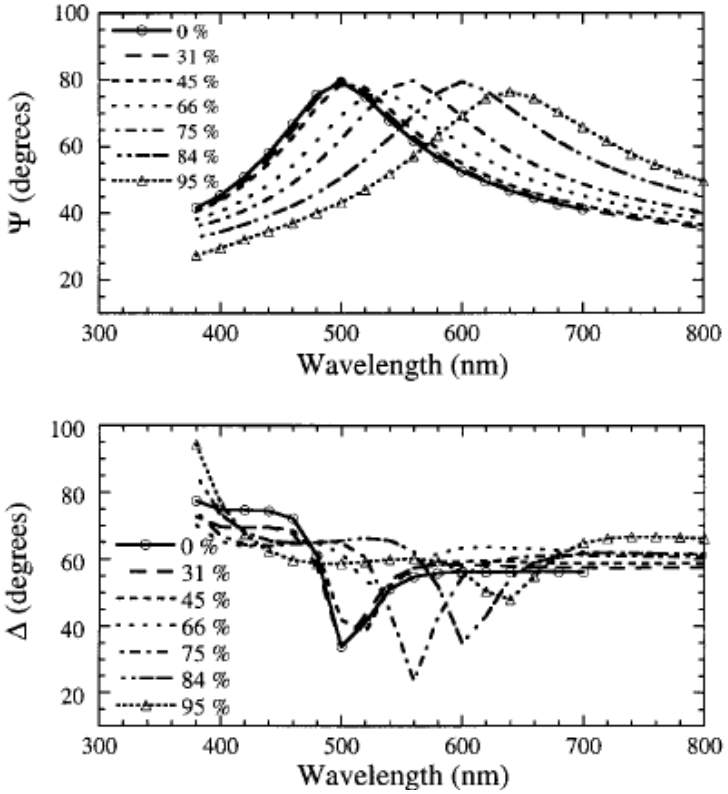

Figure **2-17**. Ellipsometric angles Ψ and Δ as a function of wavelength for a series of humidities for P(MTGA-r-AA).[85]

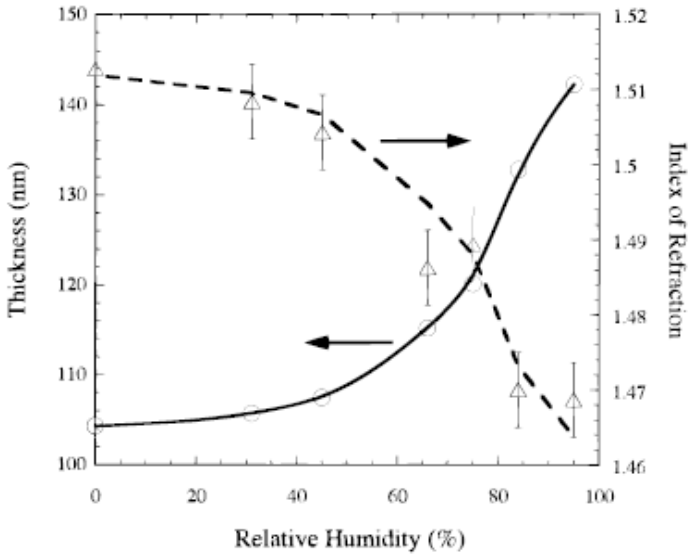

Figure **2-18**. Ellipsometric thickness and index of refraction of P(MTGA-r-AA) as a function of humidity. The dashed line is the refractive index estimation determined from measured thickness values.[85]

2.6. Summary

This chapter summarized the important features of block copolymers and the behavioral differences between thin and bulk films. Thin film behavior includes the importance of polymer-substrate interactions, diffusion, relaxation, and swelling.

References

1. Agra, D. M. G.; Schwab, A. D.; Kim, J. H.; Kumar, S.; Dhinojwala, A., Relaxation dynamics of rubbed polystyrene thin films. *Europhysics Letters* **2000,** 51, (6), 655-660.
2. Bates, F. S.; Fredrickson, G. H., Block Copolymer Thermodynamics - Theory and Experiment. *Annual Review of Physical Chemistry* **1990,** 41, 525-557.
3. Noshay, A., *Block copolymers : overview and critical survey* Academic Press: 1977; p 516.
4. Painter, P. C., *Essentials of Polymer Science and Engineering*. DEStech Publications, Inc.: 2008; p 525.
5. Painter, P. C., *Fundamentals of polymer science : an introductory text* 2nd ed.; 1997; p 478.
6. Rubinstein, M.; Colby, R., *Polymer Physics*. Oxford University Press: Oxford, 2003; p 433.
7. Edwards, E. W.; Montague, M. F.; Solak, H. H.; Hawker, C. J.; Nealey, P. F., Precise control over molecular dimensions of block-copolymer domains using the interfacial energy of chemically nanopatterned substrates. *Advanced Materials* **2004,** 16, (15), 1315-+.
8. Stoykovich, M. P.; Nealey, P. F., Block copolymers and conventional lithography. *Materials Today* **2006,** 9, (9), 20-29.

9. Wang, Q.; Nath, S. K.; Graham, M. D.; Nealey, P. F.; de Pablo, J. J., Symmetric diblock copolymer thin films confined between homogeneous and patterned surfaces: Simulations and theory. *Journal of Chemical Physics* **2000,** 112, (22), 9996-10010.
10. Yang, X. M.; Peters, R. D.; Nealey, P. F.; Solak, H. H.; Cerrina, F., Guided self-assembly of symmetric diblock copolymer films on chemically nanopatterned substrates. *Macromolecules* **2000,** 33, (26), 9575-9582.
11. Wang, Q., MatSE 575: Functional Polymeric Materials. In Penn State University: 2007.
12. Flory, P. J., Thermodynamics of High Polymer Solutions. *The Journal of Chemical Physics* **1941,** 9, (8), 660.
13. Huggins, M. L., Solutions of Long Chain Compounds. *The Journal of Chemical Physics* **1941,** 9, (5), 440.
14. Maynard, H. D.; Lyu, S. P.; Fredrickson, G. H.; Wudl, F.; Chmelka, B. F., Syntheses of nanophase-segregated poly(vinyl acetate)-poly(dimethylsiloxane) and poly(vinyl acetate)-poly(styrene) graft copolymers. *Polymer* **2001,** 42, (18), 7567-7574.
15. Leibler, L., Theory of Microphase Separation in Block Copolymers. *Macromolecules* **1980,** 13, (6), 1602-1617.
16. Matsen, M. W.; Schick, M., Stable and Unstable Phases of a Diblock Copolymer Melt. *Physical Review Letters* **1994,** 72, (16), 2660-2663.
17. Bates, F. S.; Maurer, W.; Lodge, T. P.; Schulz, M. F.; Matsen, M. W.; Almdal, K.; Mortensen, K., Isotropic Lifshitz Behavior in Block Copolymer-Homopolymer Blends. *Physical Review Letters* **1995,** 75, (24), 4429-4432.
18. Matsen, M. W.; Bates, F. S., Block copolymer microstructures in the intermediate-segregation regime. *Journal of Chemical Physics* **1997,** 106, (6), 2436-2448.
19. Wiesner http://people.ccmr.cornell.edu/~uli/pages/research.htm.
20. Bates, F. S., Polymer-Polymer Phase-Behavior. *Science* **1991,** 251, (4996), 898-905.
21. Hashimoto, T.; Tanaka, H.; Hasegawa, H., UNIFORMITY OF MICRODOMAIN SIZE OF BLOCK POLYMERS AS COMPARED WITH UNIFORMITY OF THEIR MOLECULAR-WEIGHTS. *Macromolecules* **1985,** 18, (10), 1864-1868.
22. Douzinas, K. C.; Cohen, R. E.; Halasa, A. F., EVALUATION OF DOMAIN SPACING SCALING LAWS FOR SEMICRYSTALLINE DIBLOCK COPOLYMERS. *Macromolecules* **1991,** 24, (15), 4457-4459.
23. Lu, X. Y.; Weiss, R. A., Development of miscible blends of Bisphenol A polycarbonate and lightly sulfonated polystyrene ionomers from intrapolymer repulsive interactions. *Macromolecules* **1996,** 29, (4), 1216-1221.
24. Zhou, N. C.; Xu, C.; Burghardt, W. R.; Composto, R. J.; Winey, K. I., Phase behavior of polystyrene and poly (styrene-ran-styrene sulfonate) blends. *Macromolecules* **2006,** 39, (6), 2373-2379.
25. Park, M. J.; Balsara, N. P., Phase behavior of symmetric sulfonated block copolymers. *Macromolecules* **2008,** 41, (10), 3678-3687.
26. Fasolka, M. J.; Mayes, A. M., Block copolymer thin films: Physics and applications. *Annual Review of Materials Research* **2001,** 31, 323-355.
27. Mayes, A. M.; Russell, T. P.; Bassereau, P.; Baker, S. M.; Smith, G. S., Evolution of Order in Thin Block-Copolymer Films. *Macromolecules* **1994,** 27, (3), 749-755.
28. Frank, B.; Gast, A. P.; Russell, T. P.; Brown, H. R.; Hawker, C. J., Polymer mobility in thin films. *Macromolecules* **1996,** 29, (20), 6531-6534.
29. Fasolka, M. J.; Banerjee, P.; Mayes, A. M.; Pickett, G.; Balazs, A. C., Morphology of ultrathin supported diblock copolymer films: Theory and experiment. *Macromolecules* **2000,** 33, (15), 5702-5712.
30. Vogt, B. D.; Soles, C. L.; Lee, H.-J.; Lin, E. K.; Wu, W.-l., Moisture absorption into ultrathin hydrophilic polymer films on different substrate surfaces. *Polymer* **2005,** 46, (5), 1635-1642.

31. Hall, D. B. Experimental studies of relaxation phenomena and diffusion in thin and ultrathin polymer films. Ph.D. Thesis. . Ph.D. Dissertation, Northwestern University 1999.
32. de Gennes, P. G., Glass transitions in thin polymer films. *European Physical Journal E* **2000,** 2, (3), 201-203.
33. Hall, D. B.; Hooker, J. C.; Torkelson, J. M., Ultrathin polymer films near the glass transition: Effect on the distribution of alpha-relaxation times as measured by second harmonic generation. *Macromolecules* **1997,** 30, (3), 667-669.
34. Mundra, M. K.; Ellison, C. J.; Rittigstein, P.; Torkelson, J. M., Fluorescence studies of confinement in polymer films and nanocomposites: Glass transition temperature, plasticizer effects, and sensitivity to stress relaxation and local polarity. *European Physical Journal-Special Topics* **2007,** 141, 143-151.
35. Buera, M. D.; Levi, G.; Karel, M., Glass-Transition in Poly(vinyl pyrrolidone): Effect of Molecular-Weight and Dilutents. *Biotechnology Progress* **1992,** 8, (2), 144-148.
36. Fujita, H.; Kishimoto, A., Diffusion-Controlled Stress Relaxation in Polymers. 2. Stress Relaxation in Swollen Polymers. *Journal of Polymer Science* **1958,** 28, (118), 547-567.
37. Hall, D. B.; Miller, R. D.; Torkelson, J. M., Molecular probe techniques for studying diffusion and relaxation in thin and ultrathin polymer films. *Journal of Polymer Science Part B: Polymer Physics* **1997,** 35, (17), 2795-2802.
38. Kishimoto, A.; Fujita, H., Diffusion-Controlled Stress-Relaxation in Polymers, I. *Kolloid Zeitschrift* **1956,** 1, (150), 11.
39. Kishimoto, A.; Hiroshi, F., Diffusion-controlled stress relaxation in polymers. III. Stress relaxation in a swelling polymer. *Journal of Polymer Science* **1958,** 28, (118), 569-585.
40. Burnett, D. J.; Garcia, A. R.; Thielmann, F., Measuring moisture sorption and diffusion kinetics on proton exchange membranes using a gravimetric vapor sorption apparatus. *Journal of Power Sources* **2006,** 160, (1), 426-430.
41. Edwards, D. A., Non-Fickian diffusion in thin polymer films. *Journal of Polymer Science Part B-Polymer Physics* **1996,** 34, (5), 981-997.
42. Hall, D. B.; Torkelson, J. M., Small molecule probe diffusion in thin and ultrathin supported polymer films. *Macromolecules* **1998,** 31, (25), 8817-8825.
43. Vogt, B. D.; Soles, C. L.; Lee, H. J.; Lin, E. K.; Wu, W. L., Moisture absorption and absorption kinetics in polyelectrolyte films: Influence of film thickness. *Langmuir* **2004,** 20, (4), 1453-1458.
44. Vrentas, J. S.; Duda, J. L., Molecular-Diffusion in Polymer-Solutions. *Aiche Journal* **1979,** 25, (1), 1-24.
45. Vrentas, J. S.; Jarzebski, C. M.; Duda, J. L., Deborah Number for Diffusion in Polymer-Solvent Systems. *Aiche Journal* **1975,** 21, (5), 894-901.
46. Baker, E. A.; Rittigstein, P.; Torkelson, J. M.; Roth, C. B., Streamlined Ellipsometry Procedure for Characterizing Physical Aging Rates of Thin Polymer Films. *Journal of Polymer Science Part B-Polymer Physics* **2009,** 47, (24), 2509-2519.
47. Papanu, J. S.; Hess, D. W.; Bell, A. T.; Soane, D. S., In-Situ Ellipsometry to Monitor Swelling and Dissolution of Thin Polymer Films. *Journal of the Electrochemical Society* **1989,** 136, (4), 1195-1200.
48. Singh, A.; Mukherjee, M., Swelling dynamics of ultrathin polymer films. *Macromolecules* **2003,** 36, (23), 8728-8731.
49. Sirard, S. M.; Green, P. F.; Johnston, K. P., Spectroscopic ellipsometry investigation of the swelling of poly(dimethylsiloxane) thin films with high pressure carbon dioxide. *Journal of Physical Chemistry B* **2001,** 105, (4), 766-772.
50. Papanu, J. S.; Soane, D. S.; Bell, A. T.; Hess, D. W., Transport Models for Swelling and Dissolution of Thin Polymer-Films. *Journal of Applied Polymer Science* **1989,** 38, (5), 859-885.
51. Jones, R. A. L., The dynamics of thin polymer films. *Current Opinion in Colloid & Interface Science* **1999,** 4, (2), 153-158.

52. Sun, Y. M., Sorption/desorption properties of water vapour in poly(2-hydroxyethyl methacrylate) .2. Two-stage sorption models. *Polymer* **1996,** 37, (17), 3921-3928.
53. Crowley, K. J.; Zografi, G., Water vapor absorption into amorphous hydrophobic drug/poly(vinylpyrrolidone) dispersions. *Journal of Pharmaceutical Sciences* **2002,** 91, (10), 2150-2165.
54. Hansen, C. M., *Hansen solubility parameters : a user's handbook* CRC Press: Boca Raton, 2007; p 519.
55. Mangiagli, P. M.; Ewing, C. S.; Xu, K.; Wang, Q.; Hickner, M. A., Dynamic Water Uptake of Flexible Ion-Containing Polymer Networks. *Fuel Cells* **2009,** 9, (4), 432-438.
56. Neogi, P., Anomalous Diffusion of Vapors through Solid Polymers. 2. Anomalous Sorption. *Aiche Journal* **1983,** 29, (5), 833-839.
57. Sanopoulou, M.; Petropoulos, J. H., Systematic analysis and model interpretation of micromolecular non-Fickian sorption kinetics in polymer films. *Macromolecules* **2001,** 34, (5), 1400-1410.
58. Tan, N. C. B.; Wu, W. L.; Wallace, W. E.; Davis, G. T., Interface effects on moisture absorption in ultrathin polyimide films. *Journal of Polymer Science Part B-Polymer Physics* **1998,** 36, (1), 155-162.
59. Webber, S. E., *Solvents and self-organization of polymers* Kluwer: 1996; p 509.
60. Soles, C. L.; Douglas, J. F.; Wu, W. L.; Peng, H. G.; Gidley, D. W., Comparative specular X-ray reflectivity, positron annihilation lifetime spectroscopy, and incoherent neutron scattering measurements of the dynamics in thin polycarbonate films. *Macromolecules* **2004,** 37, (8), 2890-2900.
61. Berens, A. R., Diffusion and Relaxation in Glassy Polymer Powders: 1. Fickian Diffusion of Vinyl-Chloride in Polyvinyl Chloride. *Polymer* **1977,** 18, (7), 697-704.
62. Berens, A. R.; Hopfenberg, H. B., Diffusion and Relaxation in Glassy Polymer Powders. 2. Separation of Diffusion and Relaxation Parameters. *Polymer* **1978,** 19, (5), 489-496.
63. Pantelic, N. Mass Transport Properties in Thin Ion–Exchange Polymer Films and Related Phenomena. Ph.D. Thesis. University of Cincinnati, 2007.
64. Brown, H. R.; Russell, T. P., Entanglements at polymer surfaces and interfaces. *Macromolecules* **1996,** 29, (2), 798-800.
65. Schwab, A. D.; Agra, D. M. G.; Kim, J. H.; Kumar, S.; Dhinojwala, A., Surface dynamics in rubbed polymer thin films probed with optical birefringence measurements. *Macromolecules* **2000,** 33, (13), 4903-4909.
66. Serghei, A.; Tress, M.; Kremer, F., Confinement effects on the relaxation time distribution of the dynamic glass transition in ultrathin polymer films. *Macromolecules* **2006,** 39, (26), 9385-9387.
67. Siroma, Z.; Ioroi, T.; Fujiwara, N.; Yasuda, K., Proton conductivity along interface in thin cast film of Nafion (R). *Electrochemistry Communications* **2002,** 4, (2), 143-145.
68. Siroma, Z.; Kakitsubo, R.; Fujiwara, N.; Ioroi, T.; Yamazaki, S. I.; Yasuda, K., Depression of proton conductivity in recast Nafion (R) film measured on flat substrate. *Journal of Power Sources* **2009,** 189, (2), 994-998.
69. Rubatat, L.; Li, C. X.; Dietsch, H.; Nykanen, A.; Ruokolainen, J.; Mezzenga, R., Structure-Properties Relationship in Proton Conductive Sulfonated Polystyrene-Polymethyl Methacrylate Block Copolymers (sPS-PMMA). *Macromolecules* **2008,** 41, (21), 8130-8137.
70. Kaval, N.; Seliskar, C. J.; Heineman, W. R., Spectroelectrochemical sensing based on multimode selectivity simultaneously achievable in a single device. 16. Sensing by fluorescence. *Analytical Chemistry* **2003,** 75, (22), 6334-6340.
71. Bertoncello, P.; Ciani, I.; Li, F.; Unwin, P. R., Measurement of apparent diffusion coefficients within ultrathin Nafion Langmuir-Schaefer films: Comparison of a novel scanning electrochemical microscopy approach with cyclic voltammetry. *Langmuir* **2006,** 22, (25), 10380-10388.

72. Bertoncello, P.; Ciani, I.; Marenduzzo, D.; Unwin, P. R., Kinetics of solute partitioning into ultrathin Nafion films on electrode surfaces: Theory and experimental measurement. *Journal of Physical Chemistry C* **2007,** 111, (1), 294-302.
73. Bertoncello, P.; Peruffo, M.; Li, F.; Unwin, P. R., Functional electrochemically-active ultra-thin Nafion films. *Colloids and Surfaces a-Physicochemical and Engineering Aspects* **2008,** 321, (1-3), 222-226.
74. Bertoncello, P.; Ugo, P., Preparation and voltammetric characterization of electrodes coated with Langmuir-Schaefer ultrathin films of Nafion (R). *Journal of the Brazilian Chemical Society* **2003,** 14, (4), 517-522.
75. Bertoncello, P.; Wilson, N. R.; Unwin, P. R., One-step formation of ultra-thin chemically functionalized redox-active Langmuir-Schaefer Nafion films. *Soft Matter* **2007,** 3, (10), 1300-1307.
76. Szentirmay, M. N.; Martin, C. R., Ion-exchange selectivity of Nafion films on electrode surfaces. *Analytical Chemistry* **1984,** 56, (11), 1898-1902.
77. Rocha, L. S.; Pinheiro, J. P.; Carapuca, H. M., Ion-exchange voltammetry with nafion/poly(sodium 4-styrenesulfonate) mixed coatings on mercury film electrodes: Characterization studies and application to the determination of trace metals. *Langmuir* **2006,** 22, (19), 8241-8247.
78. Hickner, M. A.; Fujimoto, C. H.; Cornelius, C. J., Transport in sulfonated poly(phenylene)s: Proton conductivity, permeability, and the state of water. *Polymer* **2006,** 47, (11), 4238-4244.
79. Co., J. W. Ellipsometry Tutorial: Light and Materials.
80. Azzam, R.; Bashara, N., *Ellipsometry and Polarized Light*. North-Holland Publishing Company: New York, NY, 1977; Vol. 1, p 529.
81. Scharf, T., *Polarized Light in Liquid Crystals and Polymers*. John Wiley & Sons, Inc: Hoboken, NJ, 2007; p 400.
82. H. G. Tompkins, W. A. M., *Spectroscopic Ellipsometry and Reflectometry*. John Wiley & Sons Inc: 1999.
83. Tompkins, H. G., *A Users's Guide to Ellipsometry*. Academic Press Inc: London, 1993.
84. Chen, C.; An, I.; Ferreira, G. M.; Podraza, N. J.; Zapien, J. A.; Collins, R. W., Multichannel Mueller matrix ellipsometer based on the dual rotating compensator principle. *Thin Solid Films* **2004,** 455, 14-23.
85. Chen, W. L.; Shull, K. R.; Papatheodorou, T.; Styrkas, D. A.; Keddie, J. L., Equilibrium swelling of hydrophilic polyacrylates in humid environments. *Macromolecules* **1999,** 32, (1), 136-144.
86. Barbero, C.; Kotz, R., Nanoscale Dimensional Changes and Optical Properties of Polyaniline Measured by *in-situ* Spectroscopic Ellipsometry. *Journal of the Electrochemical Society* **1994,** 141, (4), 859-865.
87. Gilchrist, V. A.; Lu, J. R.; Keddie, J. L.; Staples, E.; Garrett, P., Adsorption of penta(ethylene glycol) monododecyl ether at the solid poly(methyl methacrylate)-water interface: A spectroscopic ellipsometry study. *Langmuir* **2000,** 16, (2), 740-748.
88. Li, Y.; Park, E. J.; Lim, K. T. L.; Johnston, K. P.; Green, P. F., Role of interfacial interactions on the anomalous swelling of polymer thin films in supercritical carbon dioxide. *Journal of Polymer Science Part B-Polymer Physics* **2007,** 45, (11), 1313-1324.
89. Born, M.; Wolf, E., *Principles of Optics*. University Press: Cambridge, 1997.

Chapter 3

Experimental Procedures for Sample Preparation and Characterization

3.1. Introduction

In this chapter, explicit details of sample preparation and characterization are given. Sample preparation procedures include the sulfonation of poly(styrene)-*b*-poly(methyl methacrylate) (sPS- *b*-PMMA), bulk and thin film casting, substrate treatment preparation, as well as fabrication of electrodes for thin film conductivity measurements. Details about the design and fabrication of electrodes are explained, including photolithography, mask design, and metal evaporation. Characterization procedures include techniques for measuring morphology with atomic force microscopy (AFM), conductivity with AC impedance (for thin and bulk films), and swelling with spectroscopic ellipsometry. Since conductivity and swelling were measured as a function of relative humidity, custom environmental chambers with flow-through humidity control were created to work in conjunction with each piece of equipment to maintain a consistent humid sample environment while not interfering with the measurement.

3.2. Film Fabrication

The way that sulfonated poly(styrene)-*b*-poly(methyl methacrylate) films are cast influences block copolymer morphology and conductivity. Three types of films were fabricated for conductivity measurements: bulk films (50 to 100 μm thick), films drop cast onto silicon substrates (1 to 10 μm thick), and thin films spin cast onto silicon

substrates (20 to 400 nm thick). Spectroscopic ellipsometry is sensitive to surface roughness and film thickness on the angstrom scale, so the films used for ellipsometry measurements were spin cast to achieve uniform thickness. Morphology was investigated as a function of film thickness for both spin cast and drop cast films. The surface roughness of free-standing bulk films was too large to accommodate the z range of the AFM, so bulk film morphology could not be characterized. Substrate supported films for ellipsometry and AFM measurements were cast onto treated substrate to characterize the how the polymer-substrate interaction influences morphology and swelling. Chapters 4, 5, and 6 elaborate on the relationship between film processing conditions and morphology, swelling, and conductivity, respectively.

3.2.1. Substrate Treatments

AFM and ellipsometry samples were created on three types of silicon substrates: native oxide covered silicon, hexamethyldisilazane (HMDS)-coated silicon, and 3-aminopropyltri-methoxysilane (APTMS)-coated silicon. Silicon substrates were cleaned with piranha solution (7:3 H_2SO_4 to 30% H_2O_2 heated to 100°C) then rinsed three times with Millipore (18.5 MΩ, pH 6.0) water and dried with compressed air. To create a hydrophobic substrate, HMDS was spin cast at 3000 rpm onto cleaned wafers and baked at 100 ºC for 1 minute. Hydrophilic substrates were created by spin casting 0.5 v/v % APTMS in 95:5 w:w ethanol to water solution at 3000 rpm onto cleaned silicon wafers.

Native oxide silicon wafers as well as wafers coated with HMDS and APTMS substrate treatments were examined with spectroscopic ellipsometry to determine how the treatments themselves might contribute to the optical properties and thickness change of

the films. To examine any contribution to swelling from the substrate treatments, wafers were prepared with the three treatments (APTMS, HMDS, and bare silicon with a native oxide) and exposed to 0 to 90 % relative humidity using the same procedure for the testing of the polymers films. It was found that the APTMS treatment swells as it absorbs water. Neither the hydrophobic HMDS treatment nor the bare wafer showed any appreciable change in thickness when exposed to humid environments. The APTMS layer was found to swell 31 % percent of its original thickness at 90 % RH as seen in Figure **3-1**. During modeling of ellipmetry data, it was confirmed that there is no difference in the refractive index of the polymer and the substrate treatments (HMDS, APTMS or bare wafers).

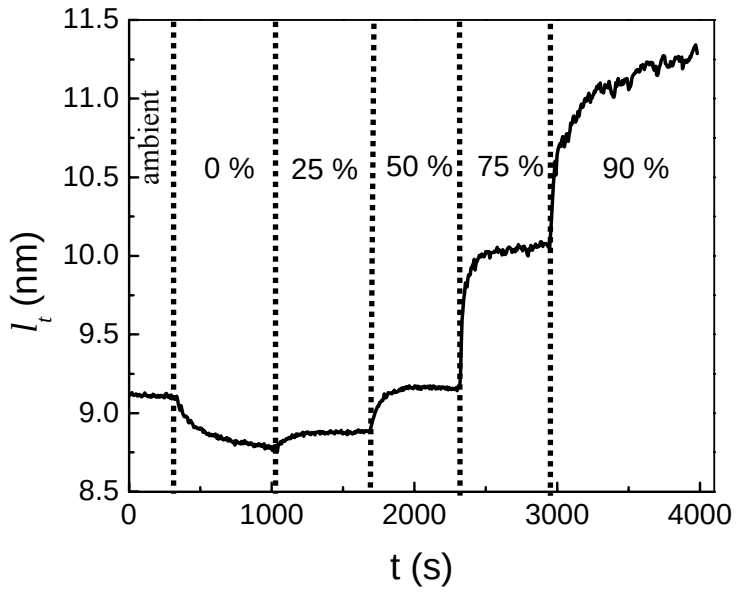

Figure **3-1**. In situ swelling of 8.75 nm thick (when dry) APTMS film on silicon as it is exposed to increasing humidity, measured by spectroscopic ellipsometry. Thickness change, l_t, (nm) is shown in real time, t, in seconds and as a function of relative humidity, RH (%), labeled on the graph.

The slightly visible APTMS layer is much thicker than the HMDS layer, which is not visible to the naked eye. The APTMS layer can be as thick as 8.75 nm in the dry state, implying that it is not a monolayer of silane, but instead a multilayer build-up of APTMS molecules created during rapid spin coating. While the HMDS treatment creates nearly a monolayer less than 1 nm thick, the APTMS film contributes significant bulk to ultra thin polymer films.

3.2.2. Thin Film Fabrication

Films less than 1 μm thick are fragile and must be supported by substrates. These thin films were created via spin coating. In this process, polymer solution was dropped onto a static silicon wafer, which was then spun at several thousand rotations per minute, spreading the solution over the surface and rapidly evaporating the solvent. This technique created films with very uniform thickness, which was vital for accurate ellipsometry, and thus swelling, measurements. Spin coating of thin polymer films was performed using a Headway Research model R485 spin coater at room temperature. Solutions of 1 and 5 w/w % sPS-*b*-PMMA in N,N-dimethylformamide (DMF) were stirred for at least 24 h before being filtered through a 0.45 μm PTFE® filter and casted into molds. Film thickness was varied via spin speed (1000-3000 rpm) and solution concentration, as shown in Table **3-1**.

Table **3-1**. Approximate film thicknesses based on processing conditions for dried spin cast thin films created from 1 or 5 w/w % solutions at spin speeds of 1000 or 3000 rpm.

Spin speed	1 w/w % solution	5 w/w % solution
1000 rpm	45 nm	350 nm
3000 rpm	25 nm	190 nm

3.2.3. Fabrication of Bulk Films

Bulk films were made by casting concentrated polymer solutions (~5 w/w %) into Teflon® molds. The amount of polymer needed to create a bulk film was calculated by the multiplying the area of the mold (1 in × 1 in) by the desired thickness (50 μm). This volume was divided by the density of the polymer to find the desired sample mass. The calculated mass of polymer was added to DMF and stirred for at least 24 h before filtering. Solutions were filtered through a 0.45 μm PTFE® filter and cast into molds. Teflon molds containing polymer solution were placed on level casting trays in chemical fume hoods and covered with a glass plate to evaporate the solvent slowly. DMF evaporated over a minimum of 10 days. Once the films appeared to be fully dry, the molds were dried under vacuum for 24 h at 50ºC to remove all residual solvent. Films extracted from the Teflon® molds were sectioned into pieces to test the conductivity of bulk films using an in-plane method.[1]

3.3. Electrode Fabrication

Thin film conductivity measurements were performed by casting a polymer film onto a substrate patterned with platinum or gold electrodes. A schematic of the electrode layout can be seen in Figure **3-2**. Custom designed electrodes were fabricated on prime, 3 inch silicon wafers with a 90 nm thick thermal oxide coating. The pattern was created using traditional photolithography and the metal was evaporated onto the patterned wafers with a Semicore evaporator. To promote adhesion to the substrate, a 5 nm thick layer of titanium was applied as a base, followed by a 45 nm thick layer of platinum or gold. The wafer-supported electrodes have four probes spaced 220 μm apart. The electrodes are 20 μm wide and 11mm long and the probe pads were 3 mm x 3mm.

3.3.1. Mask Fabrication

Electrodes were fabricated by depositing metal onto a silicon wafer patterned with photoresist. These wafers were created in the NNIN Nanofabrication Laboratory at the Materials Research Institute at Penn State. A lithographic mask pattern designed using L-edit software was etched onto a 4 in × 4 in quartz plate using a Heidelberg DWL66 Laser Writer. The laser writer removes the chrome from the areas of the pattern where photoresist was exposed to UV light, developed and removed, and metal was eventually be deposited. The pattern was designed for use with 3 inch diameter silicon wafers and positive photoresist.

3.3.2. Photolighography

Photolithography utilizes a photosensitive polymer to create features with characteristic dimensions on the order of microns. This type of process is especially popular in semiconductor manufacturing for the ease of repeatability and low material cost. Ultraviolet light shines through a lithographic mask onto a wafer covered in the photosensitive polymer, called photoresist. As positive photoresist is exposed to light, the light induces chain scission, degrading the chains. These fragmented chains in the unmasked areas dissolve in the developer solution, exposing the bare substrate in the same pattern as the mask. To create electrodes, the wafers are then coated with metal after removal of the exposed resist. The sharpness of feature corners and edges can be optimized by varying: exposure time, photoresist thickness, gap between the mask and substrate (alignment gap), and development time. The minimum feature size in this

custom pattern is 20 μm. The schematic in Figure **3-2** shows the basic layout of one of the four point electrode probe arrays.

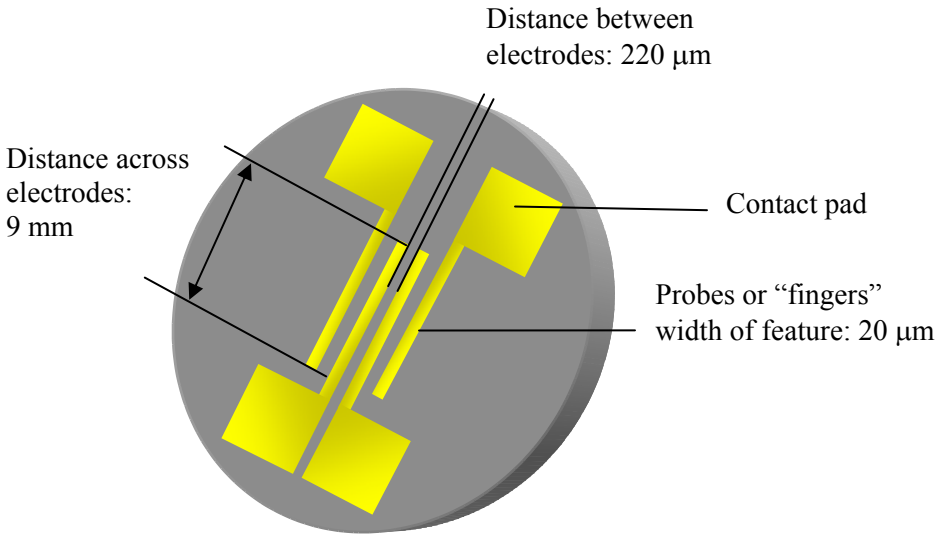

Figure **3-2**. Schematic of the electrode design for thin film conductivity measurements. The substrate is a prime silicon wafer with a 90 nm thick thermal oxide coating. Drawing is not to scale.

Sharp feature edges were attained using the following procedure:

Application of resist:
- Thermally coated wafers were baked at 95°C, coated with hexamethyldisilazane (HMDS) at 3000 rpm, and post baked at 95°C for 1 minute
- 3 mL SPR 3012 photoresist (Shippley) was spin cast statically at 3000 rpm

UV Exposure in Karl Suss MA-6 Contact Aligner:
- Hard contact of mask to wafer
- Alignment gap of 20 μm
- 8 second exposure

Photoresist Development:
- Wafers were placed in CD-26 (0.26 N tetramethyl ammonium hydroxide) for 1 minute to develop the UV-exposed photoresist

Metal Deposition in Semicore Electron-beam Evaporator:
- 5 nm thick layer of Titanium deposited to bond Pt to SiO_x substrate
- 45 nm thick layer of Platinum deposited to create electrode

Removal of photoresist:
- Photoresist was removed by rising and sonicating wafers in acetone

After testing the resistivity of the 90 nm coated SiO_2 on Si wafer, it was found to have immeasurably high resistance in DC conductivity measurements, but there was some response during AC impedance tests. It was discovered that the HMDS layer is not fully removed with acetone, so in the future, electrode wafers will be cleaned with oxygen plasma after stripping the photoresist. All procedures not included in this summary are standard operating procedure for the equipment used. Machine specifications and capabilities can be found at http://www.mri.psu.edu/facilities/NNIN/Facilities.asp. More information on procedures can be found by contacting the staff member who oversees each piece of equipment.

3.4. Conductivity

The conductivity of the samples was measured by AC impedance with a Solartron 1260A Impedance Gain/Phase analyzer over a frequency range of 100,000 to 10 Hz with a drive signal of 100 mV. The DC resistive component of the impedance was determined by fitting the impedance response with an ideal resistor or RC equivalent circuit model. Equation 3-1 shows how the resistance of a sample is used to compute the conductivity.

(3-1) $$\sigma = \frac{\ell}{R \cdot A}$$

where σ is the proton conductivity, *l* is the path length between electrodes, A is the cross sectional area of the film available for proton transport, and R is the measured resistance. The cross sectional area, A, was calculated by multiplying the thickness of the dry film, l_0, by the width of the film in contact with the electrodes.

To characterize conductivity as a function of relative humidity in sPS-*b*-PMMA films, conductivity was measured while the films were exposed to relative humidities of

20, 35, 50, 75, and 90%. Humidity was controlled with different techniques for bulk and thin films. An Espec environmental chamber was used to regulate humidity in bulk films, while a flow-though humidity system was used to equilibrate the thin films.

3.4.1. Bulk Film Conductivity

Conductivity of bulk and thin films were measured with two different techniques. As previously mentioned, conductivity of bulk, free-standing films (>50 μm thick) was measured using a Solatron 1260A Impedance/Gain Phase Analyzer and humidity was controlled using an Espec environmental chamber. Conductivity was measured as a function of relative humidity while the films were exposed to relative humidities of 20, 35, 50, 75, and 90 %. At each level of humidity, the films were allowed to equilibrate for 90 minutes to ensure uniform hydration. Electrical contact was made by clamping films into a parallel plate cell as described in literature.[1]

3.4.2. Thin Film Conductivity

Thin film conductivity measurements must be performed using a Karl Suss PM5 probe station. Since the probe station cannot be contained within an environmental chamber, the chamber had to be created around the sample. For films cast on top of electrodes, a plastic dome was placed over the sample to contain the humidity and allow for the probe tips to make contact with the electrodes on the sample surface, as seen in the side view (Figure **3-3)** and top view (Figure **3-4**) schematics. These electrodes are the same ones as pictured in Figure **3-2**. For experiments using flow tube humidity

generators, humidity was controlled by manually adjusting the ratio of dry air and humidified air as shown in in Table **3-2**.

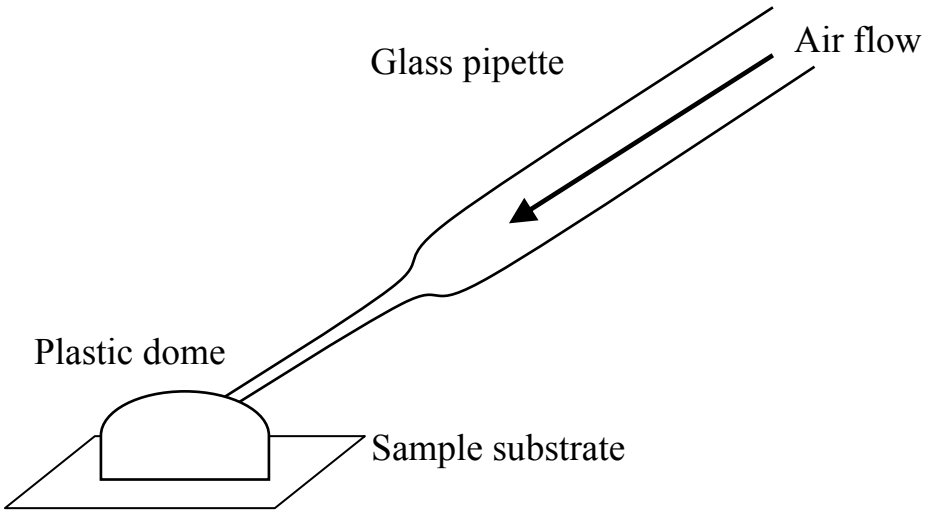

Figure **3-3**. Side view schematic of the method for maintaining the humid environment around thin film sPS-PMMA samples while measuring AC impedance on electrode substrates.

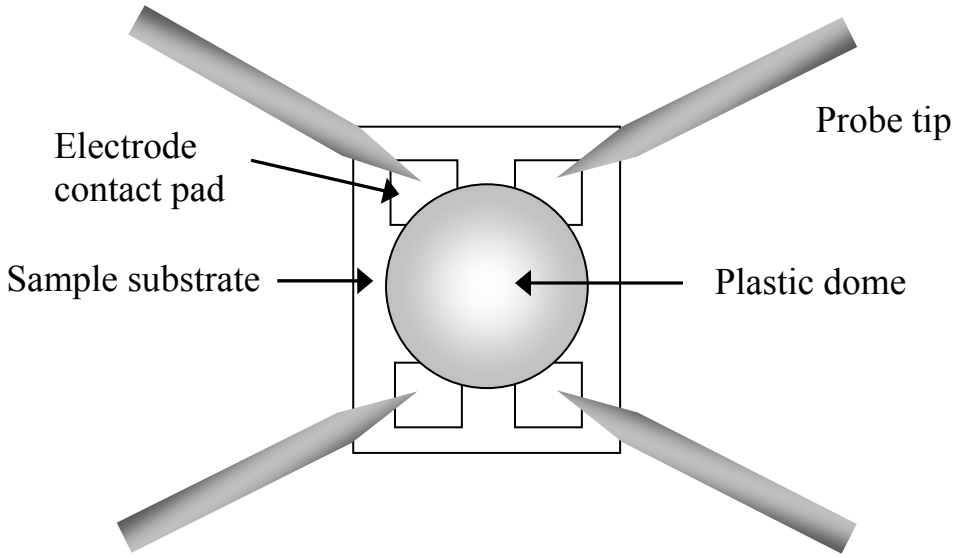

Figure **3-4**. Top view schematic of the method for maintaining the humid environment around thin film sPS-PMMA samples while measuring AC impedance on electrode substrates. For clarity, this image does not include the tube that feeds humidity into the plastic dome.

Table **3-2**. Flow rates for humidity measurements.

%RH	Humid air flow		Dry air flow		Real humidity	Total Air flow	
	mm	ccm	mm	ccm	%	mm	ccm
ambient	0	0	0	0	ambient	0	0
0	0	0	90	528	0	90	528
25	25	110	76	444	20	101	554
50	47	260	47	260	50	94	520
75	75	440	26	115	79	101	555
90	95	558	14	59	90	109	617

3.5. Spectroscopic Ellipsometry

A spectroscopic ellipsometer measures the change in amplitude and phase of light when refracted from a sample to determine the optical properties in the form of the complex index of refraction and thickness of each layer. Spectroscopic ellipsometry was used to characterize swelling in real time (~ 1 s temporal resolution) as films 20-400 nm in thickness were exposed to relative humidities of 0, 25, 50, 75 and 90 %. Experiments were performed using an RC2-XI dual rotating compensator multichannel spectroscopic ellipsometer manufactured by the J.A. Woollam Co. Photon spectra from 240 – 1700 nm (0.75-5.15 eV) were measured as a function of relative humidity and time and spectra were analyzed using CompleteEASE software to determine thickness change (in angstroms). Since different optical properties are exhibited over a range of energies (eV) or wavelengths, collecting data over a larger spectral range gives more information about the optical features of the film compared to single wavelength ellipsometry.

3.5.1. Analyzing Spectroscopic Ellipsometry Data

After the ellipsometry spectra are collected as a function of photon energy (eV) they must be analyzed using a model to derive the optical properties and thickness of the material. The model must be created so that it reasonably represents the physical properties of the material. It is then fit to the experimental data by changing the refractive index and thickness of the model components and minimizing the unweighted error function.[3] The basic starting optical property parameterization was a Lorentz oscillator model.[4]

To determine if the treatments were optically different from the polymer film, and should therefore be modeled as a different layer, the film thickness was modeled and compared using three and four layer models. The four layer model of a polymer film on APTMS included bulk silicon, the native oxide on silicon, and two distinct material layers, one of which included the optical values for the dry substrate layer. It was found that APTMS and HMDS cannot be detected separately from the polymer layer. Therefore, the model has three layers considered: bulk silicon, the native oxide on silicon, and the bulk film thickness. During data modeling, surface roughness was often found to be negligible, so for consistency, it was fixed at zero and thus absent from the analysis.

3.5.2. Environmental Chamber for Ellipsometry

To measure thin film swelling *in situ* in real time, an environmental cell was used to expose the sample to a consistent humidity while transmitting light from the ellipsometer. Figure **3-5** shows a schematic of the environmental cell used in ellipsometry measurements. The frame was made with basic acrylic sheeting, and non-polarizing quartz windows were added in to transmit a maximum amount of light.

Seventy degrees was the optimum angle for sensitivity of films on crystal silicon since the Brewster angle is 70º for crystalline silicon. The red arrows indicate the incident light of the ellipsometer and an identical angle of light reflected off the sample that is collected by the detector. The humidity in the chamber was isotropic and non-absorbing across the spectral range.

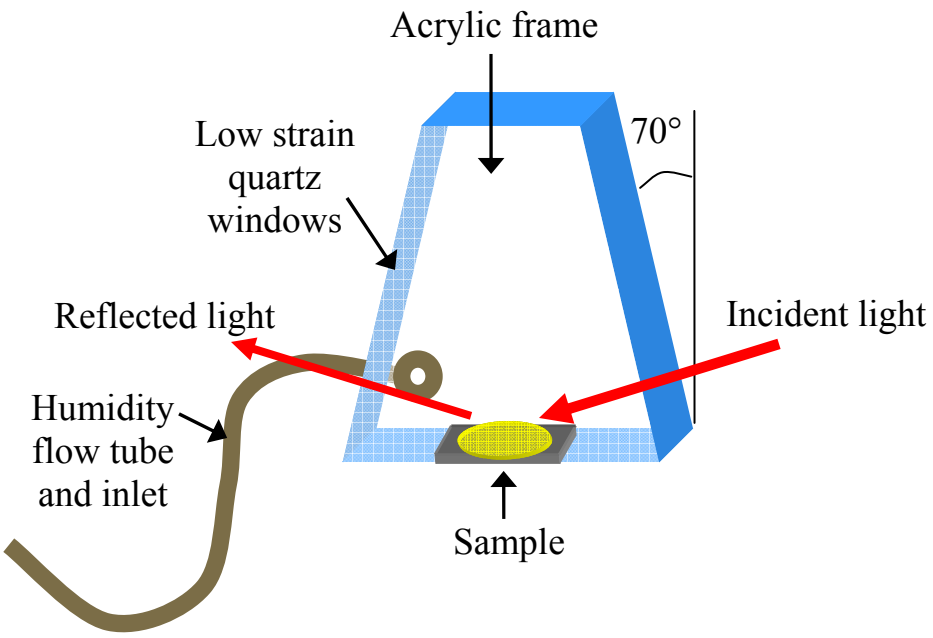

Figure **3-5**. Environmental cell created to maintain a consistent humid environment for swelling samples characterized with spectroscopic ellipsometry.

3.6. Atomic Force Microscopy

Atomic force microscopy (AFM) was used to determine the morphology of sPS-*b*-PMMA films. Atomic force microscopy was performed on a Veeco™ Digital Instruments Dimension 3100 Atomic Force Microscope in tapping mode. AFM tips were purchased from Nanosensors, with a spring constant of k = 40 and radius < 7 nm. All

AFM height and phase images included in this study were 3 μm × 3μm. AFM images show that surface treatment has a great influence on the structure of these thin films (25 nm). Lighter domains in the AFM phase images correspond to the softer sulfonated poly(styrene) phase.

3.7. Properties and Synthesis of Sulfonated Poly(styrene)-*b*-poly(methyl methacrylate)

Sulfonation of PS-*b*-PMMA was conducted using acetyl sulfate in 1,2-dichloroethane (Figure **3-6**), following a reference procedure.[5] Acetyl sulfate solution (1 M solution, 50 mL) was generated via the sequential addition of sulfuric acid (2.67 mL, 0.05 mol) and acetic anhydride (5.96 mL, 0.063 mol) in 1,2-dichloroethane (41.37 mL) at 0 °C. A 2 molar excess of acetyl sulfate compared to polystyrene repeat unit was added to the reaction mixture and the reaction proceeded for 24 h at 50 °C. The resulting reaction mixture was precipitated in hexanes and washed with water. The separated sulfonated PS-*b*-PMMA was dried in a reduced pressure for 48 h at 50 °C. The starting material, poly(styrene)-*b*-poly(methyl methacrylate), was purchased from Polymer Source, Inc. Sulfonation of PS-*b*-PMMA was performed by Tomonori Saito. ^{1}H NMR was used to determine the degree of sulfonation and corresponding IEC of sulfonated PS-*b*-PMMA. The degree of sulfonation was calculated using the shift of aromatic protons next to sulfonic acid in ^{1}H NMR resonance from 6.8 – 7.2 ppm to 7.2 – 7.6 ppm. The sPS-*b*-PMMA in this study has a molecular weight of 203-165 kg mol^{-1}, polydispersity index of 1.20, degree of sulfonation of 100%, and ion exchange capacity of 3.0 mmol g^{-1}, as shown in Table **3-4**, unless otherwise noted.

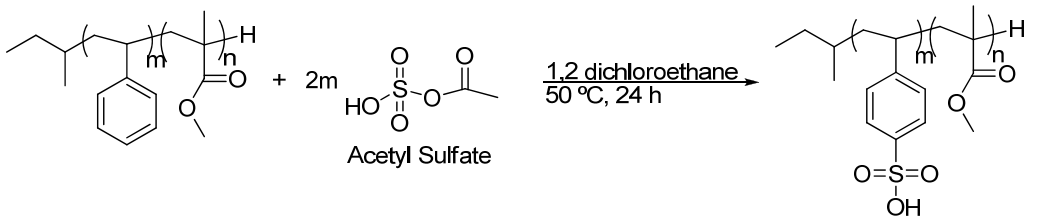

Figure **3-6.** Sulfonation of PS-*b*-PMMA using acetyl sulfate.

The solubility parameter for sulfonated polystyrene was derived in literature[6] while others were taken from Hansen's solubility parameter text.[7] The molar volume for sulfonated polystyrene was calculated by the group contribution method.[5] A theoretical density was calculated by dividing molar mass by molar volume.

Table **3-3**. Solubility parameters and molecular properties of materials used in this study including N,N-dimethylformamide (DMF), poly(styrene) (PS), sulfonated poly(styrene) (sPS), poly(methyl methacrylate) (PMMA) and water.

	δ $(J/cm^3)^{0.5}$	δ $(cal/cm^3)^{0.5}$	Molar mass $(g\ mol^{-1})$	Density $(g\ cm^{-3})$	Molar volume $(mol\ cm^{-3})$
DMF	24.86	12.15	73.09	0.944	77.43
PS	18.61	9.10	104.15	1.05	99.19
sPS	33.96	16.60	184.21	1.43	129.10
PMMA	18.27	8.93	100.12	1.17	85.57
Water	47.9	23.40	18.02	1.00	18.02

Molecular weights given by Polymer Source, Inc. for the original poly(styrene)-*b*-poly(methyl methacrylate) were then used to calculate molecular weight of sulfonated poly(styrene)-*b*-poly(methyl methacrylate) based on the molar mass of sulfonated poly(styrene), the fractional degree of sulfonation, φ, the degree of polymerization, N, and the molar mass, m, using Equation 3-2.

(3-2) $$MW_{sPS} = \phi N m_{sPS} + (1-\phi) N m_{PS}$$

Values for sulfonated and unsulfonated PS-PMMA molecular weights are included in Table **3-4**, along with the polydispersities of the original PS-PMMA and IECs measured by NMR.

Table **3-4**. Original molecular weights and calculated molecular weights after sulfonation of poly(styrene) (PS), sulfonated poly(styrene) (sPS), and poly(methyl methacrylate) (PMMA).

Samples	MW_{PS} (kg mol^{-1})	MW_{sPS} (kg mol^{-1})	MW_{PMMA} (kg mol^{-1})	PDI (M_W/M_N)	DS %	IEC^{NMR} (mmol g^{-1})
TS1-20A	235	403	263	1.18	74	2.8
TS1-20B	105	186	106	1.13	100	3.4
TS1-20C	52	80	52	1.09	93	3.3
TS1-65A	68	120	90	1.25	100	3.1
TS1-65B	96	170	128	1.06	100	3.1
TS1-65C	115	203	165	1.20	100	3.0

References

1. Einsla, B. R.; Kim, Y. S.; Hickner, M. A.; Hong, Y.-T.; Hill, M. L.; Pivovar, B. S.; McGrath, J. E., Sulfonated naphthalene dianhydride based polyimide copolymers for proton-exchange-membrane fuel cells: II. Membrane properties and fuel cell performance. *Journal of Membrane Science* **2005,** 255, (1-2), 141-148.
2. Rubatat, L.; Li, C. X.; Dietsch, H.; Nykanen, A.; Ruokolainen, J.; Mezzenga, R., Structure-Properties Relationship in Proton Conductive Sulfonated Polystyrene-Polymethyl Methacrylate Block Copolymers (sPS-PMMA). *Macromolecules* **2008,** 41, (21), 8130-8137.
3. Cong, Y.; An, I.; Vedam, K.; Collins, R. W., Optical Characterization of a 4-Medium Thin-Film Structure by Real-Time Spectroscopic Ellipsometry- Amorphous-Carbon on Tantalum. *Applied Optics* **1991,** 30, (19), 2692-2703.
4. Collins, R. W.; Ferlauto, A. S., *Handbook of Ellipsometry*. William Andrew Publishing: Norwich, NY, 2005; p 870.
5. Saito, T.; Mather, B. D.; Costanzo, P. J.; Beyer, F. L.; Long, T. E., *Macromolecules* **2008**, (41), 3503-3512.
6. Lu, X. Y.; Weiss, R. A., Development of miscible blends of Bisphenol A polycarbonate and lightly sulfonated polystyrene ionomers from intrapolymer repulsive interactions. *Macromolecules* **1996,** 29, (4), 1216-1221.
7. Hansen, C. M., *Hansen solubility parameters: a user's handbook* CRC Press: Boca Raton, 2007; p 519.

Chapter 4

Thin Film Morphology of Ionic Block Copolymers

4.1. Introduction

It was reviewed in Chapter 2 that diblock copolymers naturally phase separate to form structures that reduce the interaction between the chemically different polymers, forming an energetically favorable morphology. The addition of the ionic component in ionic block copolymers creates very strong phase separation due to the large difference in the polymethyl methacrylate (PMMA) and sulfonated polystyrene (sPS) solubility parameters.[1] Furthermore, thin film block copolymers have a high surface area to volume ratio, so a large portion of the polymer is in contact with a substrate or air interface, affecting wetting, chain mobility, and confinement. This chapter investigates how film morphology is affected by film thickness, processing, and the underlying substrate treatment in substrate-supported films 20 nm to 5 μm in thickness.

The arrangement of ionic aggregates within block copolymer domains can determine the structure-property relationships in ionic block copolymers. Clustering the ions on a particular location of the polymer chain, as in a block, may lead to improved connectivity of the ionic domains and thus is an important area of research in the proton exchange membrane field. Atomic force microscopy (AFM) was used to visually characterize the continuity of domain structures. AFM data then was compared with ionic conductivity and water uptake to infer how processing, thickness, surface treatment, molecular block length, morphology, and conductivity correlate with one another. The

following morphological investigations will lead to conclusions in subsequent chapters about how morphology influences swelling characteristics and the ion conductivity of thin ionic block copolymer films.

4.1.1. Correlation between Morphology and Conductivity

The inherent connection between morphology and conductivity in ionic block copolymers is somewhat disputed in literature. Studies draw conflicting conclusions about the trend between the degree of sulfonation and the phase separated morphology. It is generally true that the higher the ionic content of a material, the higher the conductivity, but Elabd, et al.[2] found a decrease in order as the level of sulfonation increased, while Rubatat, et al.[3] report findings to the contrary. Elabd illustrates in Figure **4-1a** the correlation between ion content and phase geometry. As ion content increases in sulfonated poly (styrene-*b*-isobutylene-*b*-styrene) triblock copolymer, phases transform from periodic, lamellar structures to continuous, interconnected domains lacking organization. Rubatat found that as the degree of sulfonation was increased (up to 37%) in sPS-PMMA there was an increase in the order of polymer phases. Figure **4-1b** shows phases transitioning from disordered to cylindrical to hexagonal closed packed as the degree of sulfonation increases from 10 to 18 to 33%, respectively.[3] This increase in sulfonation also corresponds to an increase in the conductivity (normalized by volume fraction of water + PS+ sPS) by several orders of magnitude.

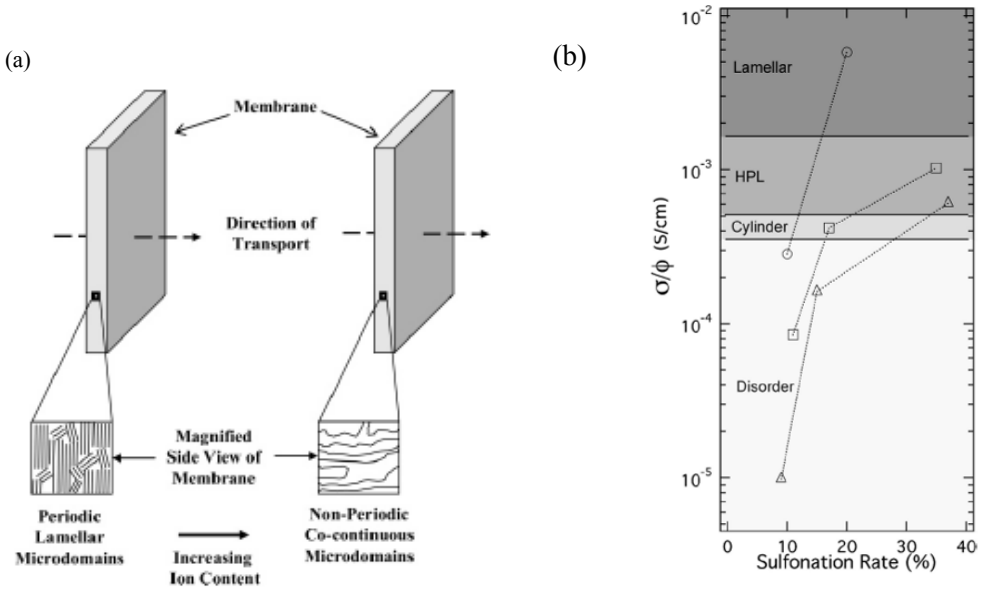

Figure **4-1**. (a) Illustration depicting the morphological change with increasing ion content. At low ion contents, a periodic lamellar morphology exists, where the microdomains are predominantly oriented perpendicular to the direction of transport. At higher ion contents, and degrees of sulfonation up to 82% a nonperiodic cocontinuous morphology exists providing less resistance for transport. (b) The normalized proton conductivity σ/Φ as a function of the sulfonation degree for the three series: 20 kg mol^{-1} (circle), 52.5 kg mol^{-1} (square), and 78 kg mol^{-1} (triangle). Φ refers to the volume fraction of the PS + sPS + water domains. [2]

Establishing a definitive correlation between phase-separated order and conductivity would be an ideal way to guide the design of new PEM membranes. Rubatat speculates as to how conductivity and phase morphology might directly correspond with the schematic in Figure **4-2**.[3] Proton conductivity increases as phases transition from complete miscibility to a lamellar structure. Figure **4-1b** shows that for similar levels of sulfonation (15 and 17%, respectively) the lamellar morphology exhibits a significantly higher normalized conductivity than the cylindrical sPS morphology. In the hexagonal morphology, the perforating PMMA cylinders restrict the expansion of the domains, and the d spacing does not change when hydrated. In the lamellar morphology, the ion conductive sPS phase has more freedom to swell and the d-spacing increases by 25% when the film is fully hydrated.[3] In the work reported here, morphologies of thin

film sPS-PMMA were investigated with atomic force microscopy to determine how the structure influences swelling characteristics of thin ionic block copolymer films.

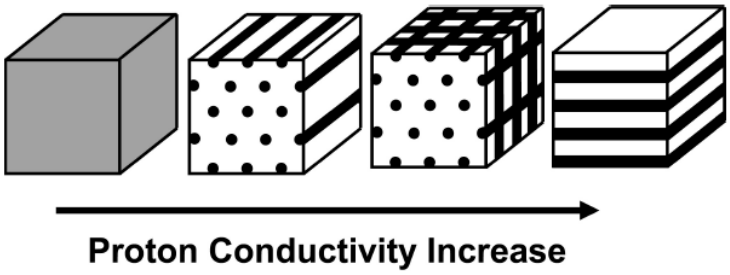

Figure **4-2**. A schematic of the increase in proton conductivity as morphology becomes more ordered in sPS-PMMA systems.[3]

4.1.2. Atomic Force Microscopy

Atomic force microscopy (AFM) revolutionized the characterization of surface morphologies in the mid 1980's. Until that point, there was no comparable method to investigate surface morphology other than via visual characterization with scanning and transmission electron microscopy. The electron beams used in these techniques often prove fatal to soft polymeric materials, destroying the sample before it can be properly imaged. AFM has several unique and important assets: it is a non destructive technique, it boasts truly atomic resolution, and the technique requires no special sample preparation. One disadvantage of AFM is that only the top surface of the material can be probed. Thus, the images can be influenced by surface energies and careful interpretation is needed as AFM gives no indication of the cross sectional morphology of a film.

In this study, morphology is investigated as a function of film thickness, film processing, and substrate wettability in AFM tapping mode. The sulfonated PS-PMMA block copolymers showed distinct separation for films thinner than the characteristic

domain size. Morphologies of films that were slowly dried created more organized structures than spin cast films, and films created at various thicknesses and spin casting speeds exhibited similar morphologies. Film thickness had little effect on films that were processed in the same way, e.g. drop versus spin casting. The surface treatment had the greatest influence on morphology. Ultra thin (~ 25 nm) films cast onto HMDS-coated, APTMS-coated, and bare silicon substrates exhibited distinctly different morphologies, which lead to different swelling characteristics, as will be discussed in Chapter 5.

4.2. Effects of Film Processing

Film morphology was greatly affected by processing. The films in this study were prepared in two ways: via spin casting or drop casting. Solvent based solutions were used to drop cast thin films (1-10 μm) onto a silicon wafer or bulk films (~50 μm) into a Teflon® mold. Morphologies of bulk films could not be characterized because the surface roughness of the freestanding films was out of the Z range capabilities of the AFM. Drop cast films were allowed to dry slowly for up to a week. Spin cast films were created by dropping solution onto a substrate rotating at 1000 to 3000 rpm. More details about film fabrication can be found the experimental section in Chapter 3. In the AFM images, ambient conditions lend some moisture to the film, so the sPS block absorbs some water from the air and exhibits itself as the softer domain. The lighter domains in the height and phase images correspond to a raised profile and softer phase, respectively, of the sulfonated polystyrene.

The slow drying process allowed the highly sulfonated polystyrene block to fully organize in the film without forming smaller, percolated domains as was observed with spin casting. Figure **4-3** shows that slowly drying the 5 μm film from solution formed

regular periodic structures with what appears to be sPS cylinders aligning perpendicular to the surface in the PMMA matrix.

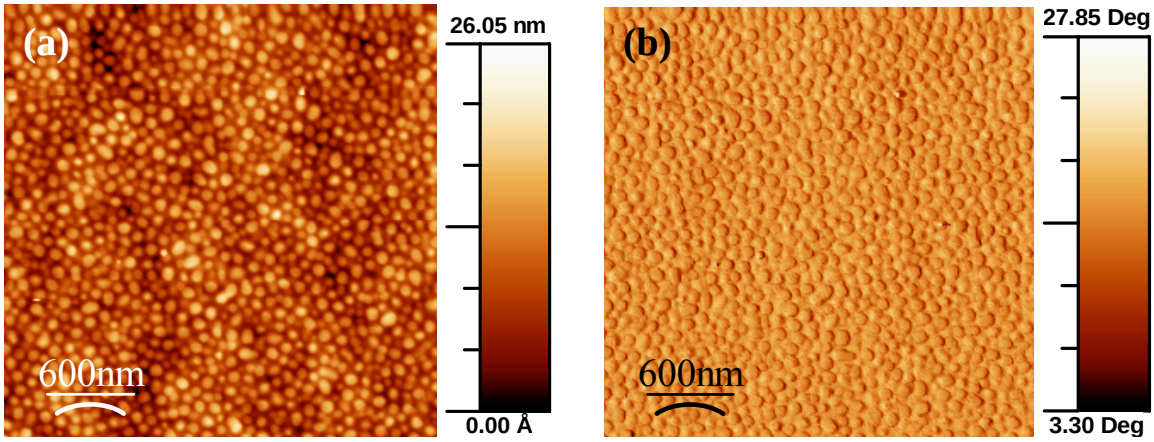

Figure **4-3**. AFM (a) height and (b) phase morphology of drop cast 203-165 kg mol^{-1} sPS-*b*-PMMA film on a wafer with native oxide surface. Slowly drying the film from solution allowed for a more periodic morphology with sPS cylinders aligning perpendicular to the surface in a PMMA matrix.

Figure **4-4** shows little difference between the morphologies observed for a 1% solution spin cast at 1000 versus 3000 rpm. The film cast at 1000 rpm seems to have slightly less defined domain edges, which may be due to higher shear forces at higher rpm speeds. Since the 1000 rpm film is cast at a slower speed, less solution is cast off of the wafer, leaving behind a thicker film. The film cast from 1% solution at 1000 rpm is 49 nm thick while the same concentration of solution cast at 3000 rpm results in a 23 nm thick film. In Figure **4-5**, a 5% solution is cast at 1000 and 3000 rpm resulting in films 184 nm thick and 380 nm thick, respectively. These thicker films show better phase separation than the 1% solution cast films, while the 380 nm thick film seems to show a greater difference in height between the sulfonated polystyrene and PMMA phases. Films cast from the same concentration of solution resemble each other more closely than films cast at the same spin speed but different concentrations. When films are created

using spin casting it seems that solution concentration and viscosity (i.e. thickness) have a greater influence on morphology than casting speed.

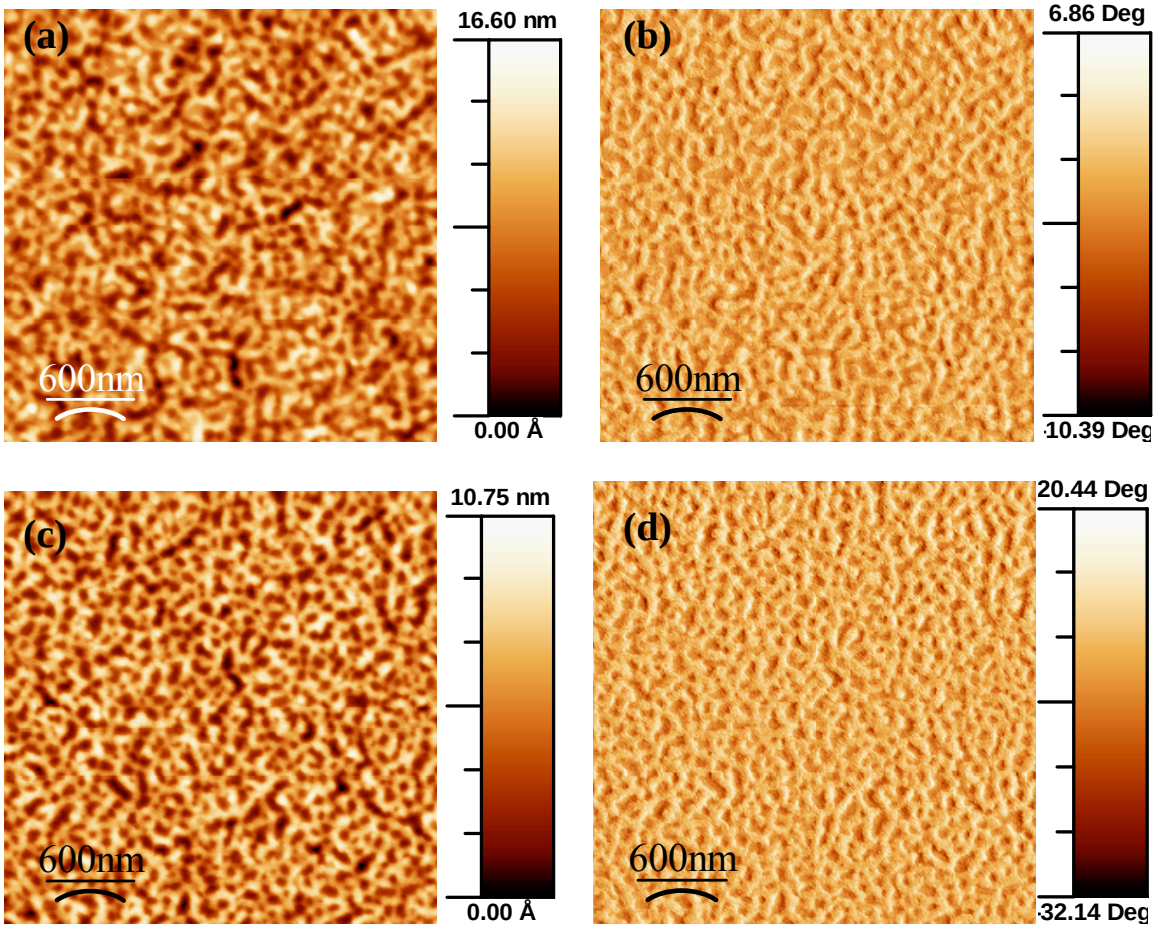

Figure **4-4**. AFM (a) height and (b) phase morphology of a 49 nm thick film created by spin casting at 1000 rpm onto a bare wafer. AFM (a) height and (b) phase morphology of a 23 nm thick film created by spin casting at 3000 rpm onto a bare wafer. Both films were cast from 1% w/w 203-165 kg mol^{-1} sPS-PMMA solution in DMF.

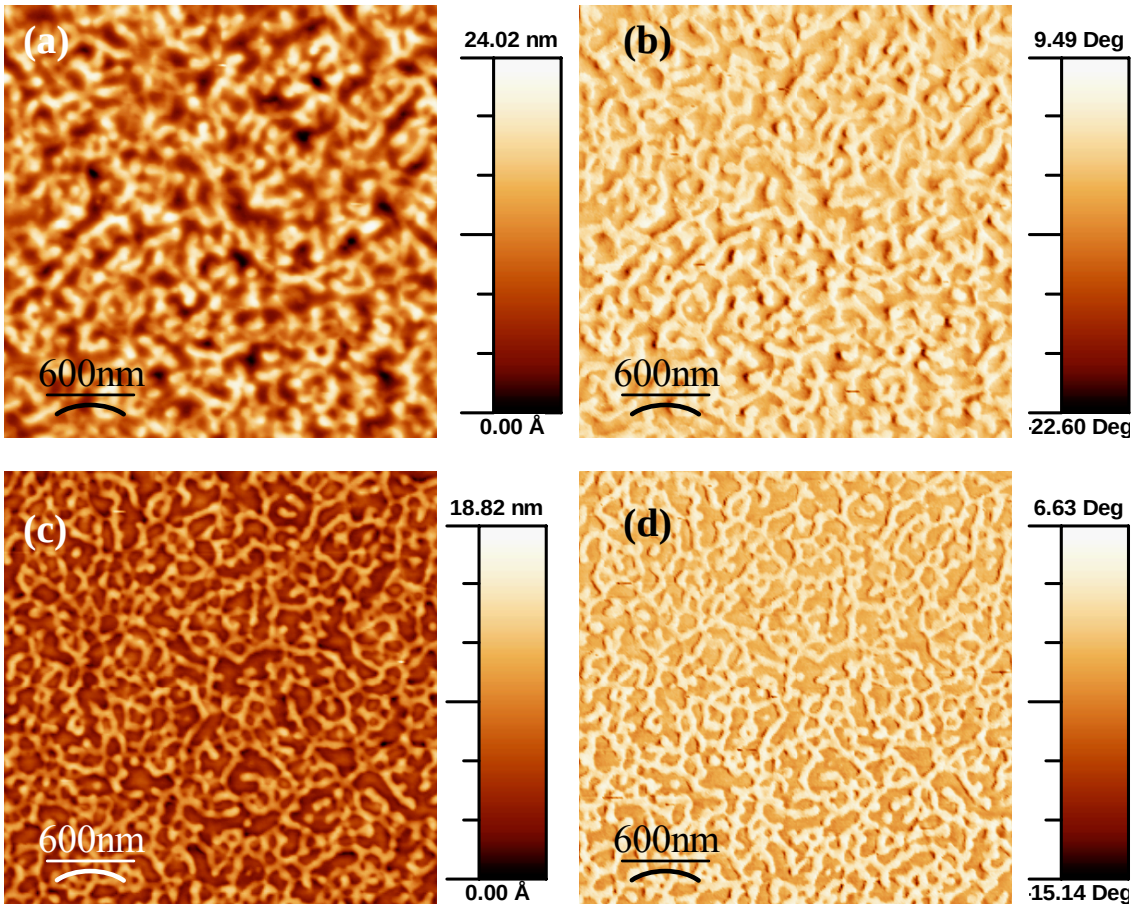

Figure **4-5**. AFM (a) height and (b) phase morphology of a 380 nm thick film created by spin casting at 1000 rpm onto a bare wafer. AFM (c) height and (d) phase morphology of a 184 nm thick film created by spin casting at 3000 rpm onto a bare wafer. Both films were created from 5% w/w 203-165 kg mol^{-1} sPS-PMMA solution in DMF.

To determine how ionic groups affect the morphology during spin cast processing, unsulfonated poly(styrene)-*b*-poly(methyl methacrylate) (PS-*b*-PMMA) was spin cast under the same conditions as sPS-*b*-PMMA from a 1% solution in toluene. The film was prepared on a neutral polystyrene brush according to literature procedures[4] and Figure **4-6** shows the resulting AFM micrographs. In the case of non-ionic block copolymers, the faster spin speed (thinner film) shows wider domains and more defined phase separation. The greater shear of the higher spin speed induced phase ordering in the non-ionic block copolymer system. Phase mixing is evidenced by the blurry phase

borders. Since the solubility parameters for PS and PMMA are closer than that of sPS and PMMA, there is weaker phase segregation. Figure **4-6** images c and d are similar to the corresponding sPS-*b*-PMMA film processed at the same spin speed from the same concentration of solution. Although these films were created using the same procedure, toluene has a lower boiling point than DMF, so the solvent evaporates faster in the PS-*b*-PMMA film casting. The differences in solvent evaporation rates and film drying could explain the similarities: although ionic groups cause kinetic trapping of domains, DMF evaporates slower than toluene, allowing for the sPS-PMMA polymer time to arrange.

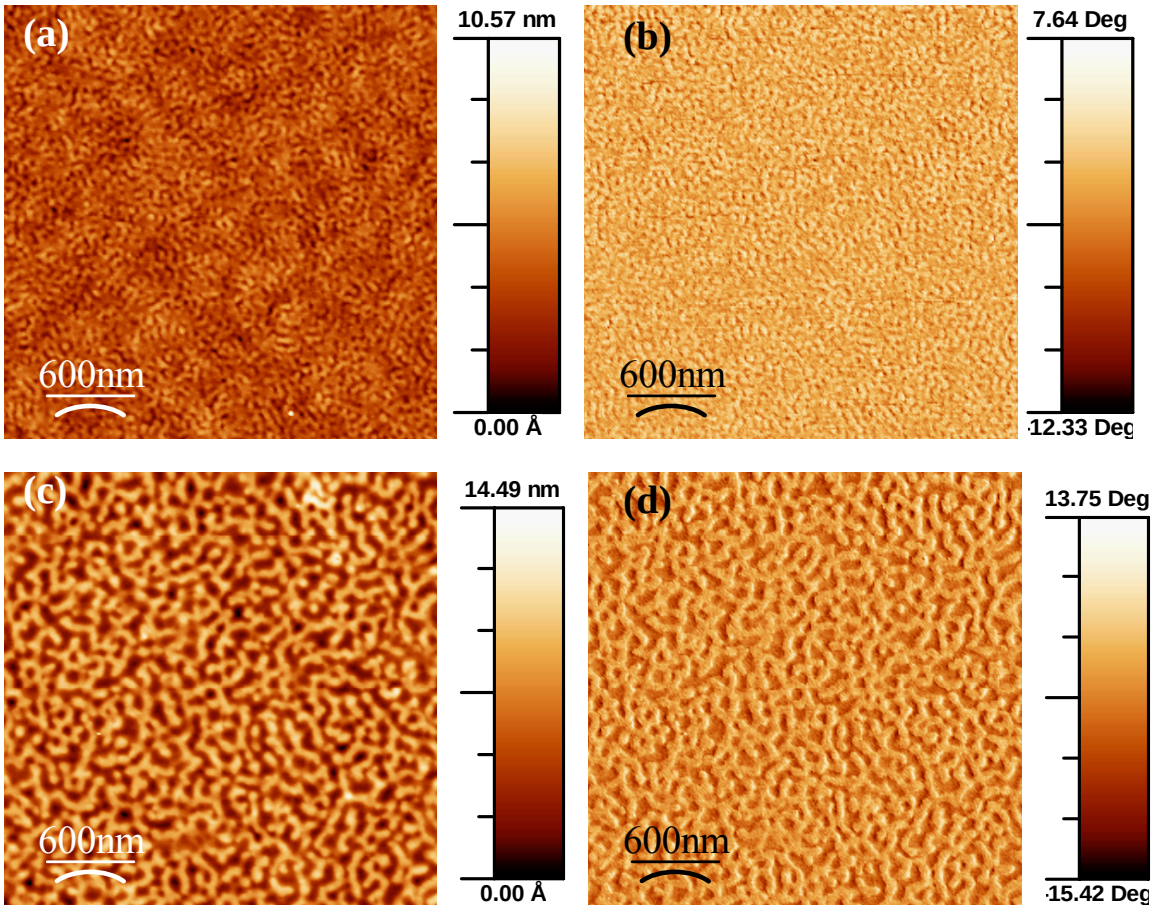

Figure **4-6**. AFM (a) height and (b) phase morphology of a 400 nm thick film, created by spin casting at 1000 rpm onto a bare wafer. AFM (a) height and (b) phase morphology of a 200 nm thick film created by spin casting at 3000 rpm onto a bare wafer.

4.2.1. Effect of Substrate Treatments

In ultrathin block copolymer films, the properties of the substrate greatly influence the film morphology. As discussed in Chapter 2, surface energy has a large affect on the structure of a thin film, so each block will be attracted to the surface it is most compatible with. This configuration lowers the interfacial free energy of the film: a strong driving force in materials with such a high surface area to volume ratio. If one of the blocks has an affinity for the substrate surface, the morphology will tend to align parallel to the surface with the more compatible polymer block wetting the substrate. A neutral substrate will induce a morphology perpendicular to the surface because both wet the surface equally. These concepts were exemplified in the ultra thin (22-29 nm thick) films as shown in Figure **4-7**.

In Figure **4-7c**, hydrophobic, glassy PMMA was driven to share more surface area with the hydrophobic HMDS-coated substrate. A PMMA-rich layer was created at the substrate interface and drove the sulfonated polystyrene to the free surface. The phase image in **4-7c** shows that the surface is largely covered with the softer sPS phase. At the free surface the sPS-PMMA film on the bare substrate in Figure **4-7a** showed an equal mix of both sulfonated polystyrene and polymethyl methacrylate, implying that it attracted both blocks equally, creating long, continuous domain structures. The APTMS surface coating (Figure **4-7b**) created small percolated sPS phases intermixed with the PMMA matrix.

	AFM height image	AFM phase image
a) 23 nm thick film on bare wafer	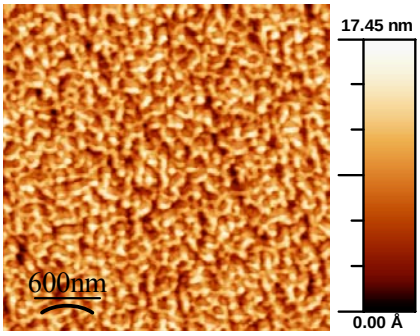	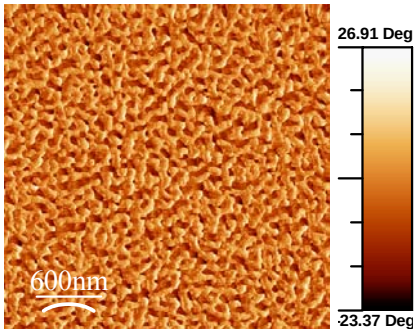
b) 29 nm thick film on APTMS coated wafer	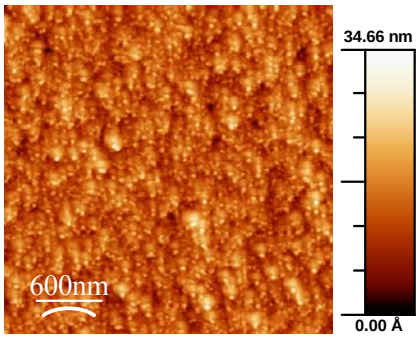	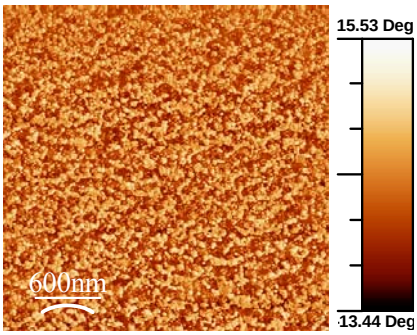
c) 22 nm thick film on HMDS coated wafer	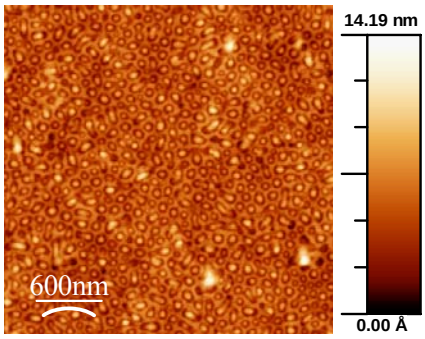	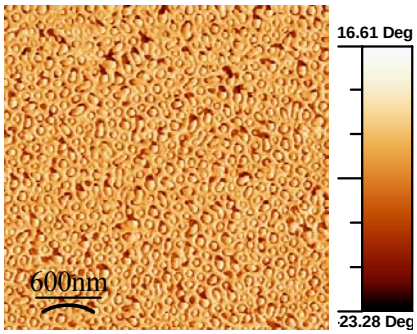

Figure **4-7**. AFM height and phase images show the differences in morphology for thin polymer films (22-29 nm thick) on a) bare silicon wafers b) APTMS coated silicon wafer and c) HMDS coated silicon wafer. Films were prepared by spin coating a 1% w/w solution of 203-165 kg mol^{-1} sPS-PMMA on the substrate at 3000 rpm.

As discussed in later chapters, domain size and continuity had a significant effect on how much these films would swell. The strongly hydrophobic HMDS-coated substrate induced the most phase separation because the interfacial area between sPS and PMMA in Figure **4-7** is minimized. Since a largely unrestricted hygroscopic phase was created at the free surface, the polymer on the hydrophobic substrate swelled the most in ellipsometry measurements. Similarly, the thin polymer film on the bare wafer exhibited almost as much swelling because it had larger and more continuous phase separated domains. Swelling in the popcorn-like structure formed on the APTMS-coated wafer was restricted because sPS was confined to small domains surrounded by the structural PMMA block.

4.3. Conclusions

The conflicting accounts in literature of how order affects conductivity demonstrates that the relationship between conductivity and morphology is still not completely understood in ionic block copolymer films. To draw conclusions about the relationship between morphology, swelling, and conductivity, the morphology of thin sulfonated poly(styrene)-*b*-poly(methyl methacrylate) films was analyzed using atomic force microscopy. Film morphology was studied as a function of processing conditions, thickness, solution concentration, and substrate treatment. It was established that substrate treatment has the largest effect on film morphology, which will be shown in subsequent chapters to influence swelling behavior and conductivity in thin films.

4.4. Future work

Because through-plane membrane conductivity is most important in a fuel cell, it is important to also understand the cross sectional morphology of these films. Since AFM can only be used to characterize surfaces, new characterization techniques must be sought out to determine how sPS-PMMA phase separates from the top to the bottom of the film. Focused ion beam milling was used to excise a cross section in substrate-supported thin films, but subsequent field emission scanning electron microscopy was not capable of imaging the cross section. At the necessary resolution to image nanometer scale domains, the ion beam would burn away the material and showed no sign of distinct phase separation. In the future, cross sectional morphology will be imaged using transmission electron microscopy.

References

1. Lu, X. Y.; Weiss, R. A., Development of miscible blends of Bisphenol A polycarbonate and lightly sulfonated polystyrene ionomers from intrapolymer repulsive interactions. *Macromolecules* **1996,** 29, (4), 1216-1221.
2. Elabd, Y. A.; Napadensky, E.; Walker, C. W.; Winey, K. I., Transport properties of sulfonated poly (styrene-b-isobutylene-b-styrene) triblock copolymers at high ion-exchange capacities. *Macromolecules* **2006,** 39, (1), 399-407.
3. Rubatat, L.; Li, C. X.; Dietsch, H.; Nykanen, A.; Ruokolainen, J.; Mezzenga, R., Structure-Properties Relationship in Proton Conductive Sulfonated Polystyrene-Polymethyl Methacrylate Block Copolymers (sPS-PMMA). *Macromolecules* **2008,** 41, (21), 8130-8137.
4. Bosworth, J. K.; Paik, M. Y.; Ruiz, R.; Schwartz, E. L.; Huang, J. Q.; Ko, A. W.; Smilgies, D. M.; Black, C. T.; Ober, C. K., Control of self-assembly of lithographically patternable block copolymer films. *Acs Nano* **2008,** 2, (7), 1396-1402.

Chapter 5

Swelling of Thin Ion-Containing Block Copolymer Films

5.1. Introduction

Chapter 4 established how film morphology is affected by film thickness, processing conditions, and substrate treatment. Morphology of the hydrophilic and hydrophobic domains is an important factor in determining the material's uptake and swelling by water as well as ionic conductivity of ion-containing block copolymer thin films. For the same degree of sulfonation, conductivity has been shown to increase by an order of magnitude for morphologies that favor water uptake.[1] Water uptake can be characterized volumetrically (by change in thickness via swelling) or gravimetrically (by change in mass). In this chapter, spectroscopic ellipsometry was used to investigate volumetric water uptake as a function of film thickness, substrate wettability, and morphology. A series of 12 films were studied (shown in Table **5-1**) to systematically quantify how the sample characteristics mentioned previously influence thin film swelling behavior. Films were spin cast onto substrates with various surface treatments and exposed to increasing humidity. Time-resolved spectroscopic ellipsometry was used to measure the optical properties, in the form of the complex index of refraction and thickness change, of ionic block copolymer films in response to changes in the sample environment relative humidity. Ellipsometry proved to be an insightful and innovative tool to characterize *in situ* transitions in optical properties and thickness as the composition of the films changed with water absorption.

Sulfonated poly(styrene)-*b*-poly(methyl methacrylate) is hygroscopic, so a sPS-PMMA film readily absorbs water as it is exposed to humidity. It has been established that the polymer component with the most compatible surface energy will segregate to the surface, influencing the morphology, and thus the swelling characteristics of the film. Film thickness may affect swelling because the concentration of polymer chains varies from the substrate to free surface more in thin films. As such, substrate treatment is a factor in film swelling because, as presented in Chapter 4, substrate wettability influences film morphology. It was found that thin proton exchange membrane films on hydrophobic substrates swelled the fastest and to the greatest extent. This behavior was an unexpected result because while hydrophobic substrates allow block copolymer thin films to swell more, as discussed in Chapter 2, they cause homopolymer thin films to swell less.[2, 3] The large difference in water uptake for thin films of various thickness and substrate treatment showed that thin films were much more sensitive to substrate treatments, indicating a strong correlation between film morphology and swelling in thin films. Thick films (>320 nm thick) displayed similar equilibrium swelling profiles regardless of the underlying substrate, implying that substrate treatment effects permeate a finite distance into the polymer films.

Spectroscopic ellipsometry was used to characterize swelling in real time as polymer films 20-400 nm in thickness were exposed to relative humidity from 0 to 90% at room temperature and a flow rate of 550 cm^3 min^{-1}. Ellipsometry measurements were performed over a spectral wavelength range of 240-1700 nm (0.75 to 5.15 eV). Results were used to understand contributions of polymer-substrate interaction and film thickness

to the swelling behavior in thin films of sulfonated poly(styrene)-*b*-poly(methyl methacrylate).

Spectroscopic ellipsometry detects changes in both the amplitude and polarization state of light reflected from a layered material and is used to determine the complex refractive index and thickness of each layer. Ellipsometry is commonly used to measure material properties *in-situ* in real time because the experimental setup of an ellipsometer allows a sample to be characterized in non-contact fashion in an environmental cell.[4] A sample chamber with non-polarizing windows was created to transmit the maximum amount of light while offering an environment with a controllable humidity. Details about the experimental set up for this series of experiments can be found in Chapter 3, while more information about spectroscopic ellipsometry background can be found in Chapter 2.

5.2. Thin Film Swelling

As a PEM film absorbs water, its composition changes, altering the film thickness, refractive index, and dielectric properties. Figure **5-1** shows the thickness change in real time of a film as it is exposed to ambient, 0, 25, 50, 75, and 90 % relative humidity, (RH %), as delineated by the vertical dashed lines above the data. The thickness at time t, l_t, decreases as the film is exposed to dry (0% RH) air, and subsequently expands as the relative humidity in the sample cell was increased. Figure **5-1** shows that at higher relative humidities the film expanded more per step. Data in Figures **5-2** through **5-12** is taken from the curve in Figure **5-1,** as indicated by the dotted and solid lines and arrows. The solid black lines and arrows indicate how the thickness

change was characterized at 50 and 75 % RH, as plotted in Figure **5-2** and **5-6**. The grey line indicates the slope of water uptake for 50 and 75 % RH, which is included in Figures **5-7** and **5-8**. The dotted lines and arrows indicate the percent swelling from dry film thickness for every RH, which is plotted again in Figures **5-9** through **5-12**.

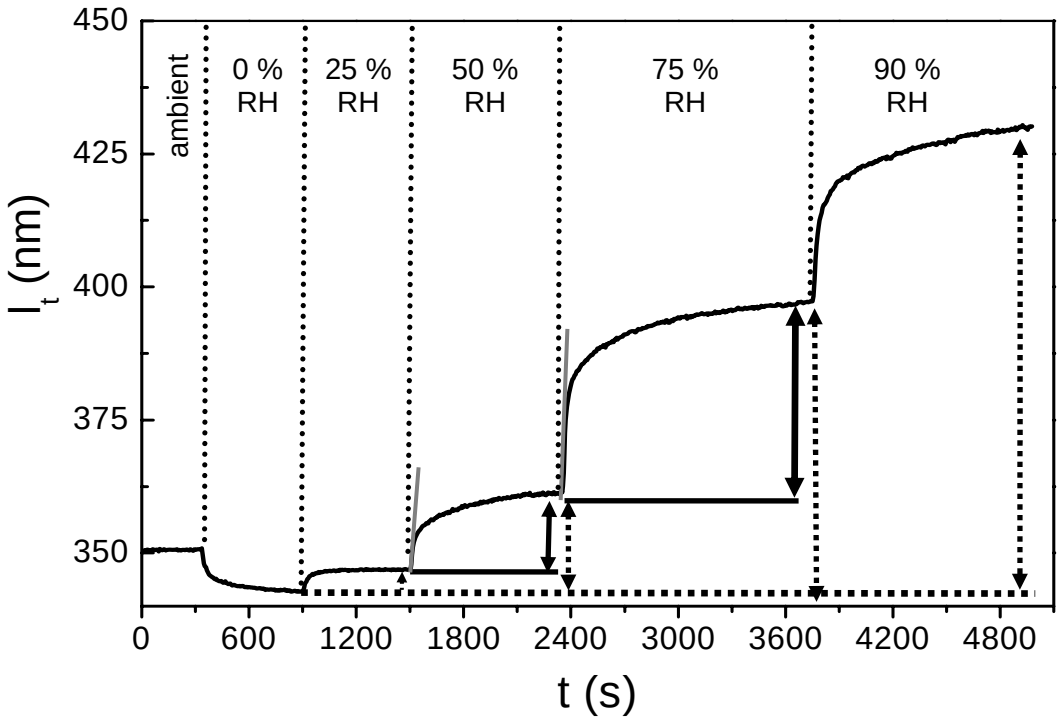

Figure **5-1.** Thickness change, l_t, of a 350 nm thick (at ambient) sPS-*b*-PMMA film as it is exposed to increasing humidity, measured by spectroscopic ellipsometry. The humidity levels listed at the top were incremented as indicated by the circular dotted drop lines. Data taken from the curve is indicated by the dotted square lines, solid lines and arrows. The grey line indicates the slope of water uptake for 50 and 75 % RH, the solid black lines and arrows indicate the thickness change for 50 and 75 % RH, and the dotted lines and arrows indicate the percent swelling from dry film thickness for every RH.

Table **5-1**. Fabrication details for the 12 films investigated in ellipsometric swelling experiments. Films were created at 4 thicknesses (in columns, 2 spin casting speeds, 2 solution concentrations) and on three different substrate treatments (across rows).

	1% solution, 3000 rpm	**1% solution, 1000 rpm**	**5% solution, 3000 rpm**	**5% solution, 1000 rpm**
Native oxide	23.2 nm	41.4 nm	180.0 nm	343.0 nm
APTMS	28.9 nm	49.0 nm	184.0 nm	380.0 nm
HMDS	22.8 nm	43.0 nm	184.5 nm	323.0 nm

5.2.1. Description of the Swelling Process

Swelling curves could not be fit to a first order diffusion equation, indicating that the swelling was not due to diffusion alone. As the polymer is plasticized by water, chains relax, allowing for more water to be absorbed, thus increasing the thickness of the film. In an attempt to calculate a rate constant for the rate of swelling, data was modeled using the following diffusion-based water uptake equation. [5]

$$\alpha` = \alpha`_{\infty}\left[1 - \exp\left(-\frac{k_1}{\alpha`_{\infty}}t\right)\right] \tag{5-1}$$

where α'_{∞} is the equilibrium degree of swelling, k_1 is the rate constant of swelling, t is time and the degree of swelling, α', has be defined as follows:

$$\alpha' = \frac{l_t - l_0}{l_t} \tag{5-2}$$

where l_t is thickness at time t and l_0 is the original thickness. Figure **5-2** shows *in-situ* swelling data along with a curve described by equation 5-1 that was fit to the data with lowest mean square error. The diffusion equation is obviously a poor fit for the water uptake data, with some films taking over 20 min to fully equilibrate. A method for fitting dielectric relaxation using the Kohlrausch-Watts-Williams (KWW) or stretched exponential equation was used to fit the data more closely.[6]

$$\alpha' = \alpha'_{\infty}\left[1 - \exp\left(-\left(\frac{k}{\alpha'_{\infty}}t\right)^{\beta}\right)\right] \tag{5-3}$$

The stretched exponential represents dynamic relaxation by using a rate constant, k, to determine deviation from an exponential function and allows for data comparison.

Table **5-2** shows the calculated swelling rates, k, and degree of decay, as given by how much β is than 1, where $0 < \beta < 1$.

Although the diffusion coefficient of water sorption into ultra thin films has been calculated using a Fickian model,[2, 7] swelling in this study cannot be described by Fickian diffusion alone. Simple diffusion would only account for the immediate absorption of water into the thin film. As discussed in Chapter 2, polymer chains will selectively deposit on the substrate to reduce surface tension. This concentration of material at the substrate creates a greater amount of free volume at the free surface,[8] affecting relaxation time,[8-14] small molecule diffusivity,[7, 8, 10-13, 15-20] and swelling characteristics.[2, 7, 13, 21-23] Therefore, the dynamics of these films are dominated by relaxation of the polymer, rather than diffusion of water. Other quantitative models for the relaxation behavior are being explored.

Table **5-2**. Values of calculated swelling rates, k, and exponential decay, β, for the thinnest and thickest sPS-*b*-PMMA films on native oxide silicon, HMDS-, and APTMS-coated silicon for the 50 and 75 % relative humidity increments.

		50% RH	75% RH	50% RH	75% RH
Thickness (nm)	Substrate	K	k	β	B
23	Bare	0.061	0.087	0.543	0.553
23	HMDS	0.210	0.240	0.523	0.541
29	APTMS	0.101	0.167	0.648	0.631
343	Bare	0.090	0.141	0.542	0.577
323	HMDS	0.158	0.114	0.557	0.543
380	APTMS	0.093	0.122	0.560	0.540

The rates of swelling, k, are the most descriptive for which films absorbed water the fastest, with the thinnest film on HMDS swelling the fastest. The films all show

similar amounts of exponential decay, β, and there is no trend in β. Figure **5-2** shows the comparison of the fit of Equations 5-1 and 5-3 for when the swelling is incremented from 25 to 50 % RH for the ultrathin film on HMDS, which is the fastest swelling sample. Similar results are represented by the slopes shown in Figures **5-7** and **5-8**.

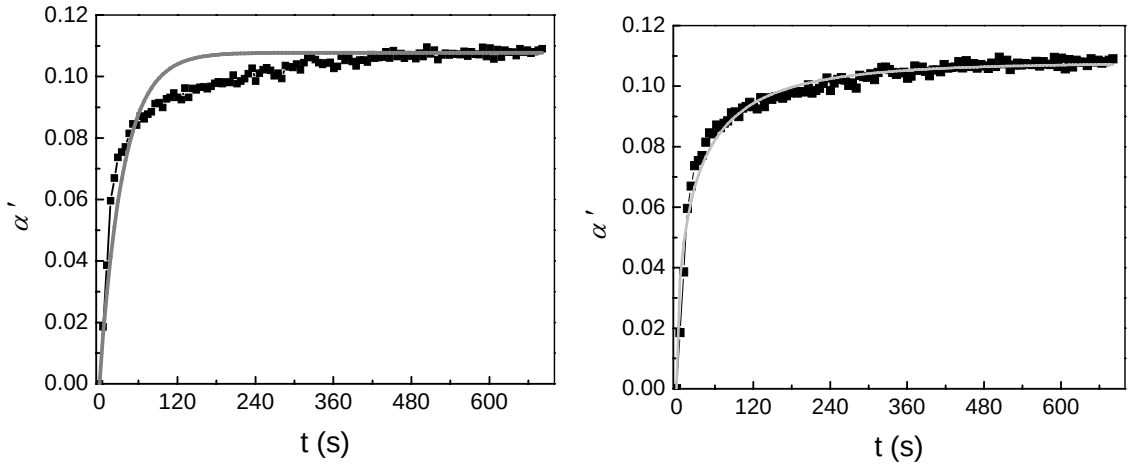

Figure **5-2**. Swelling of l_0 =21.7 nm thick film on HMDS (■) showing dynamic degree of swelling, α', as humidity is increased from 25% RH to 50% RH. The grey line shows the lowest mean square error model fit of α'. The model on the left, calculated using Equation 5-1, does not accurately describe the initial rate of uptake or the secondary swelling towards equilibrium, proving that this type of swelling is not a first order diffusion process. The model on the right shows the stretched exponential that is a much better fit to the data, as calculated using Equation 5-3.

5.2.2. Thickness Change at Equilibrium

It has been found that thin polymer films on hydrophobic substrate treatments swelled less in comparison to thicker films (150 nm), while films 3 to 100 nm in thickness on hydrophilic substrates absorbed the same volume fraction of water.[2] This effect is attributed to the polymer-substrate interactions. The native oxide on the bare silicon wafer induces hydrogen bonding between the polymer and the substrate. On hydrophobic HMDS substrate treatments, the polymer is not attracted to the substrate, and the polymer is less confined at the substrate interface, resulting in a higher overall

degree of swelling for ultra thin polymer films. As explained in Chapter 4, it was found that a hydrophobic substrate attracted the hydrophobic block to the substrate interface, allowing hydrophilic polymer to spread over the free surface. Subsequently, the ultrathin block copolymer films on hydrophobic substrates swelled the most because the hydrophilic polymer was able to expand without restriction. Figure **5-3** shows the swelling of the thinnest (~25 nm) sPS-PMMA films on HMDS, APTMS, and bare substrates. To compare the swelling rate and total equilibrium swelling for a range of sample thicknesses, data was normalized to its original thickness using Equation 5-4. Normalized thickness, l_n, was given as the ratio of thickness at time t, l_t, to original thickness, $l_{0\infty}$, (equilibrium swelling at previous humidity level). Data in Figures **5-3** through **5-8** are based on this normalized thickness, l_n.

$$l_n = \frac{l_t}{l_{0_\infty}} \tag{5-4}$$

The l_n scale shows how much the film has swelled since the equilibrium thickness at the last humidity step, so in Figure **5-3**, thin films on HMDS and APTMS coated substrates swell 3.8 % when the humidity is incremented from 25 % RH to 50 %. The film on bare silicon swelled 2.7 % during the same humidity increment. For the 50 % RH step in Figure **5-3**, the thinnest films on HMDS and APTMS had the largest equilibrium degree of swelling. In Figure **5-4**, the thinnest film on HMDS swelled 11.6 % during the 50 % RH to 75 % RH increment while the film on native oxide silicon swelled 8.2 % and on APTMS swelled 7.4 % during the RH change. The greater swelling changes on HMDS surfaces can be attributed to the largely unrestricted sulfonated phase blanketing air surface of the film as seen in Figure **4-7c**.

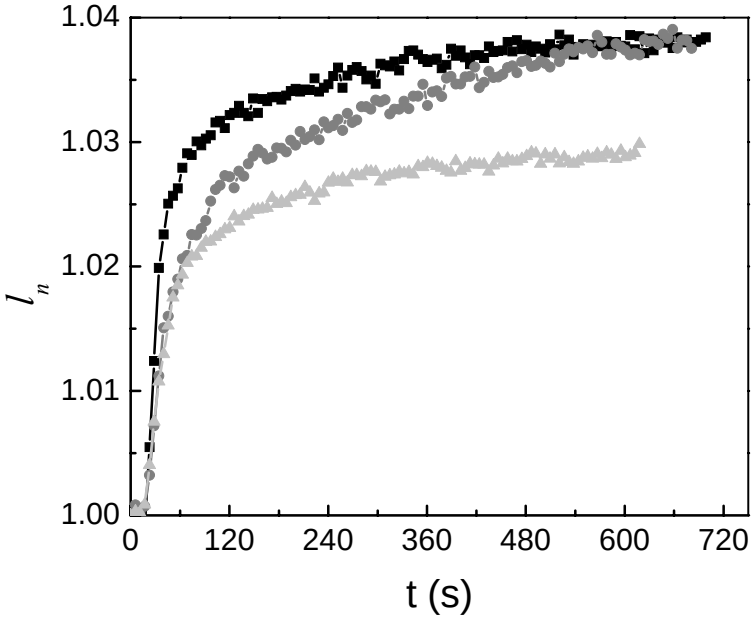

Figure **5-3**. The degree of swelling, l_n, normalized by the equilibrated thickness at 25 % RH of the thinnest sulfonated poly(styrene)-poly(methyl methacrylate) films l_0 = 21.7 nm on HMDS (■), l_0 =28.8 nm on APTMS (●), l_0 = 23.5 nm on bare silicon (▲) as humidity is increased from 25 % RH to 50 % RH.

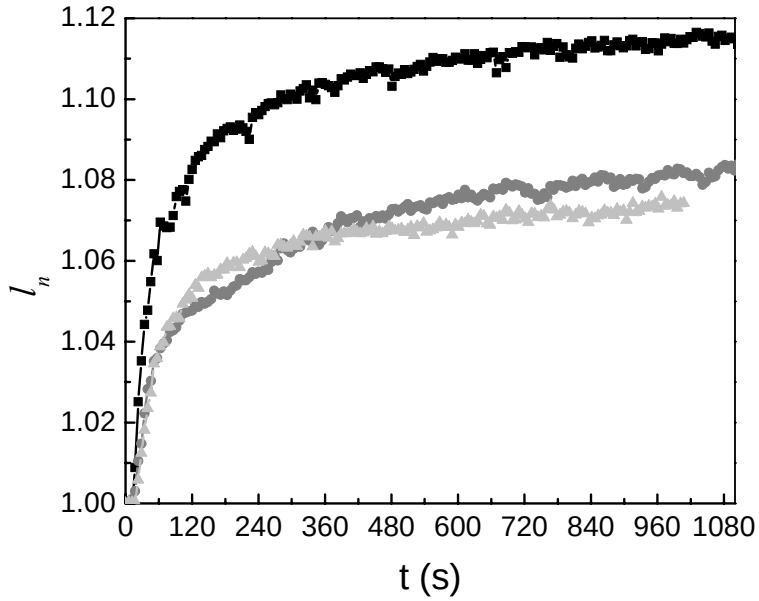

Figure **5-4**. The degree of swelling, l_n, normalized by the equilibrated thickness at 50 % RH of the thinnest sulfonated poly(styrene)-poly(methyl methacrylate) films l_0 = 22.4 nm on HMDS (■), l_0 = 29.7 nm on APTMS (●), l_0 = 24.5 nm on bare silicon (▲) as humidity is increased from 50 % RH to 75 % RH.

Figure **5-3** and **5-4** also show that the films on HMDS and APTMS reached equilibrium before the film on bare silicon. This difference in swelling rate could have been due to chain confinement from hydrogen bonding with SiO_x on the surface of the silicon. A comparison of Figure **5-3** and **5-5** shows that despite thickness, films on hydrophobic substrate treatments reached their final thickness after relative humidity increments the fastest. This behavior implies that polymer-substrate interactions have more of an effect on initial and long term swelling rate on ultra thin films. Figures **5-5** and **5-6** show that thick films swell nearly the same amount, regardless of substrate treatment, for both at the 25-50 % RH and 50-75 % RH steps.

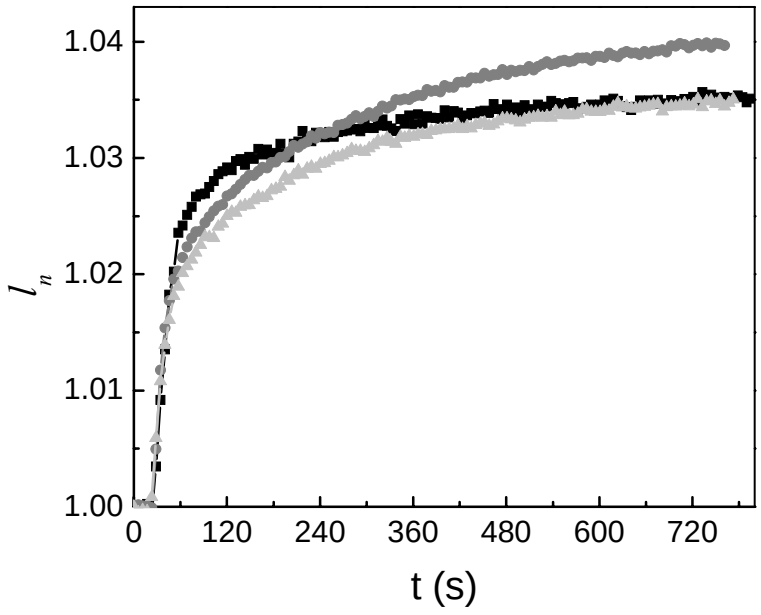

Figure **5-5**. The degree of swelling, l_n, normalized by the equilibrated thickness at 25 % RH of the thickest sulfonated poly(styrene)-*b*-poly(methyl methacrylate) films l_0 = 326.9 on HMDS (■) l_0 = 347.6 nm on bare silicon (●), and l_0 = 383.3 nm on APTMS (▲) as humidity is increased from 25 % RH to 50 % RH.

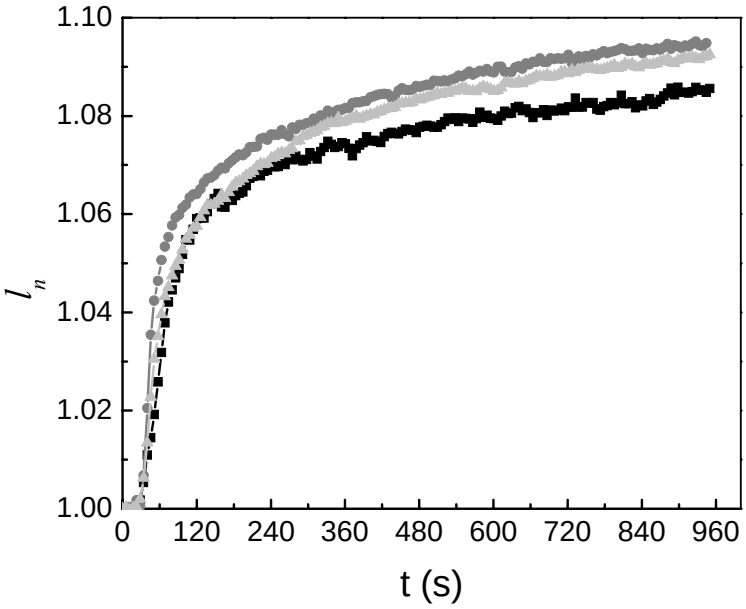

Figure **5-6**. The degree of swelling, l_n, normalized by the equilibrated thickness at 50 % RH of the thickest sulfonated poly(styrene)-*b*-poly(methyl methacrylate) films l_0 = 341.8 nm on HMDS (■), l_0 = 361.2 nm on bare silicon (●), and l_0 = 396.6 nm on APTMS (▲), as humidity is increased from 50 % RH to 75 % RH.

5.2.3. Initial Swelling Rate

Since the simple swelling model (Equation 5-1) did not fit the data well, the slope of the initial linear portion of the experimental data in Figures **5-3** through **5-6** was used to compare the initial rates of swelling for various samples. Initial slopes were compared for the 25 to 50 % RH step as well as the 50 to 75 % RH step, for the thinnest (~25 nm) and thickest films (~350 nm) of the series on three types of substrate treatments, as seen in Figures **5-7** and **5-8**. It was found that in the thinnest films, regardless of substrate treatment, the rate of water uptake is about twice as fast when humidity is increased from 25 to 50 % RH as compared to the 50 to 75 % RH step. This trend is observed when PEMs reach a point of hydration where the sulfonated groups are mostly solvated and have less of an attraction for water, therefore the swelling rate is lower as the humidity is

increased.[24] Films on hydrophobic HMDS absorbed water twice as fast as films on other substrates.

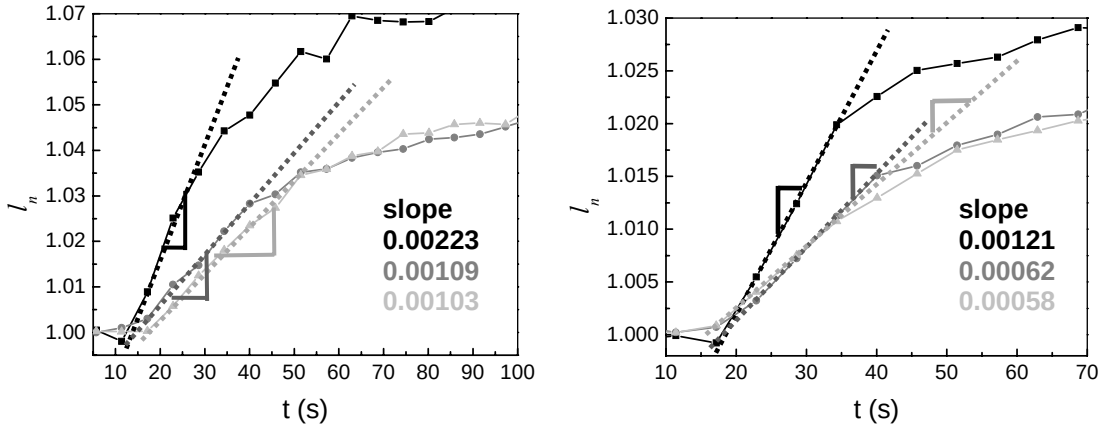

Figure **5-7**. a) The degree of swelling, l_n, normalized by the equilibrated thickness at 50 % RH of the thinnest sulfonated polystyrene-polymethyl methacrylate films l_0 =21.7 nm on HMDS (■), l_0 = 23.5 nm on bare silicon (●), l_0 = 28.8 nm on APTMS (▲), as humidity is increased from 25 % RH to 50 % RH. b) The degree of swelling, l_n, normalized by the equilibrated thickness at 50 % RH of the thinnest sulfonated poly(styrene)-poly(methyl methacrylate) films l_0 = 22.4 nm on HMDS (■), l_0 = 24.5 nm on bare silicon (●), l_0 = 29.7 nm on APTMS (▲), as humidity is increased from 50 % RH to 75 % RH. The slopes are in units of s^{-1}.

Figure **5-8** shows that for thick films, there is a 50 % increase in rate of water uptake from the 50 % RH step to the 75 %RH step for the thickest films on APTMS and the bare wafer, but the rate of water uptake for the films on HMDS did not change. Thick films did not absorb water as quickly as thin films in the 50 % RH step. These results support the theory that the confinement of chains at the substrate-polymer interface in thin films creates more free volume at the surface, allowing for faster polymer relaxation, water sorption, and thickness change.

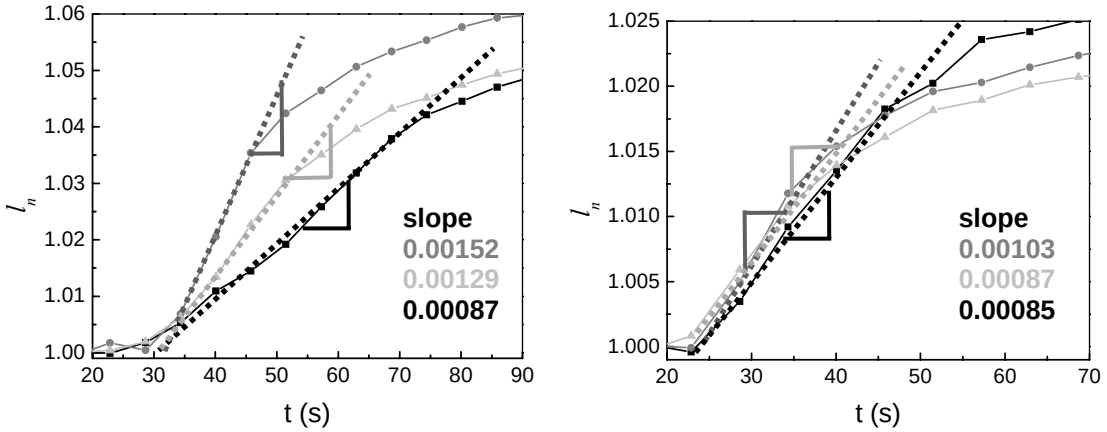

Figure **5-8**. a) The degree of swelling, l_n, normalized by the equilibrated thickness at 25 % RH of the thickest sulfonated poly(styrene)-poly(methyl methacrylate) films l_0 = 326.9 on HMDS (■), l_0 = 383.3 nm on APTMS (▲), l_0 = 347.6 nm on bare silicon (●) as humidity is increased from 25 % RH to 50 % RH. b) The degree of swelling, l_n, normalized by the equilibrated thickness at 50 % RH of the thickest sulfonated poly(styrene)-poly(methyl methacrylate) films l_0 = 341.8 nm on HMDS (■), l_0 = 396.6 nm on APTMS (●), l_0 = 361.2 nm on bare silicon (▲) as humidity is increased from 50 % RH to 75 % RH.

5.2.4. Total Thickness Change at Equilibrium as a Function of Relative Humidity

The overall degree of thickness change at equilibrium, based on substrate treatment and film thickness, was examined. Swelling, S (%), was calculated as the thickness of the equilibrated film at a given humidity, $l_{t\infty}$, divided by the dry film thickness, l_0, as shown in Equation 5-5.

$$S = \frac{l_{t_\infty}}{l_0} \tag{5-5}$$

It was observed that the thickest films (~350 nm) swelled to approximately 25 % of their original thickness regardless of substrate treatment. On the other hand, the swelling of films with initial thicknesses on the order of 25 nm, , were very sensitive to surface treatment, and the thinnest film on a hydrophobic HMDS surface swelled the most. The connection between morphology and swelling can be rationalized by the morphological data in Figure **4-7**, where the hydrophobic HMDS substrate treatment

caused the hydrophobic PMMA block to wet the substrate. This surface wetting induced by the substrate treatment increased the concentration of sulfonated polystyrene at the free surface, so film swelling was less inhibited by the glassy PMMA block.

For swelling as a function of film thickness on a particular substrate, the thinnest film on HMDS substrate swelled the most, while the thinnest film on APTMS swelled the least, with films on bare silicon between the two. Figure **5-9** shows that the thinnest film swelled the most on HMDS, while Figure **5-10** shows that the thicker the film on APTMS, the more it swelled. These opposite trends in thin films verify the influence that surface coating and film morphology has on swelling in ionic block copolymer films.

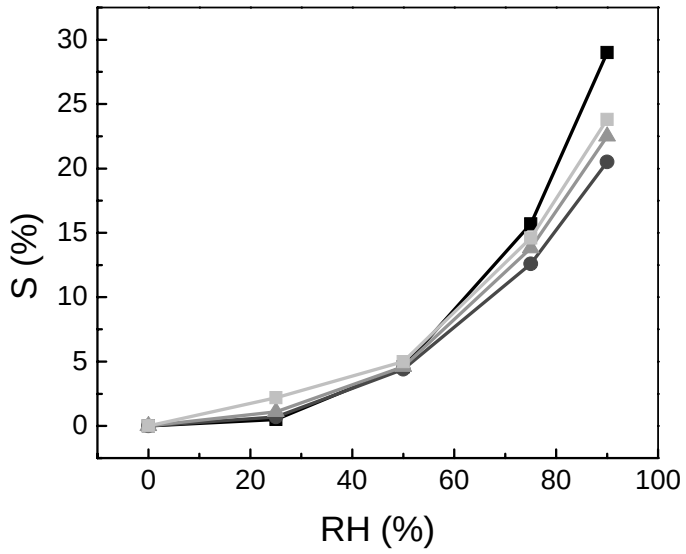

Figure **5-9**. Degree of swelling (%) at equilibrium of sulfonated poly(styrene)-*b*-poly(methyl methacrylate) films of four thicknesses, 22.8 nm (■), 43.0 nm (●), 184.5 nm (▲), 323.0 nm (■), on a hydrophobic HMDS-coated silicon wafer for relative humidities from 0 to 90 % RH.

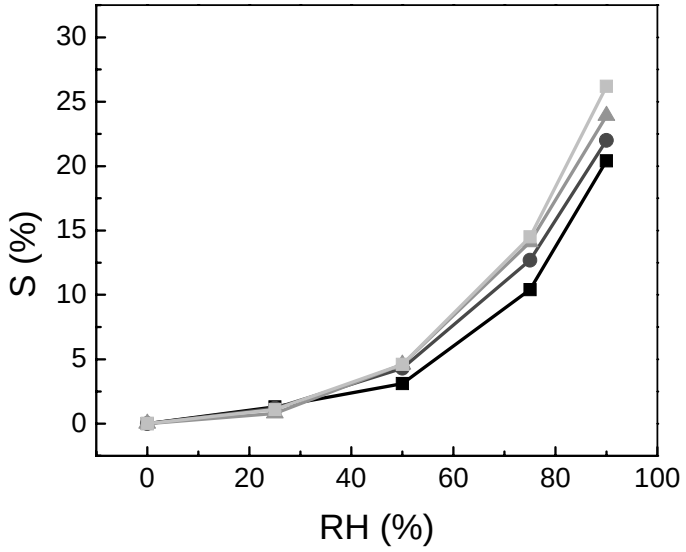

Figure **5-10**. Degree of swelling (%) at equilibrium as a function of relative humidity for sulfonated poly(styrene)-poly(methyl methacrylate) films of four thicknesses on an APTMS-coated silicon wafer. Thicknesses were 28.9 nm (■), 49.0 nm (●), 184.0 nm, (▲), 380.0 nm (■). There was a clear trend between film thickness on APTMS and the degree of swelling: the thickest film swelled the most while the thinnest film on APTMS swelled the least.

Figures **5-11** and **5-12** exemplify the significance of substrate treatment in swelling for a range of film thicknesses. For films approximately 25 nm thick (Figure **5-11**), substrate treatment greatly affected how much the film swelled from 0 to 90% RH, while films 350 nm thick showed similar overall swelling regardless of substrate (Figure **5-12**). This data confirms that polymer-substrate interactions dictate film properties for thin films with a high ratio of surface area to volume. Figure **5-12** depicts that the interfacial properties have little effect on swelling behavior in thick films.

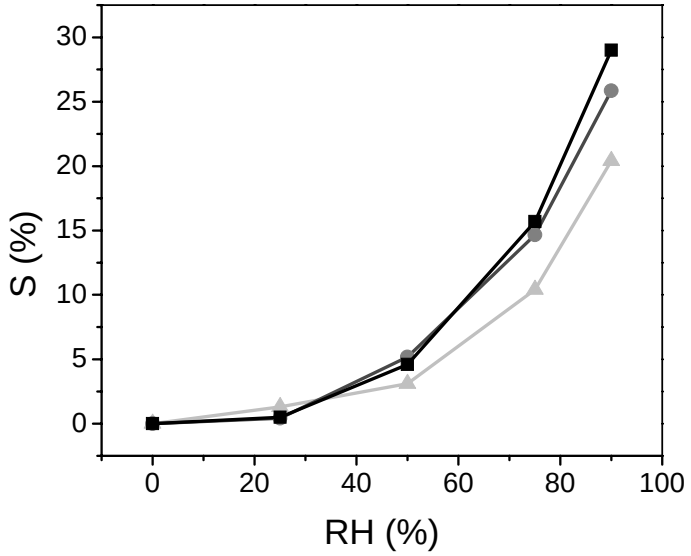

Figure **5-11**. Degree of swelling (%) at equilibrium of ultra thin films sulfonated poly(styrene)-poly(methyl methacrylate) on three different substrate treatments on silicon wafers. Films are 22.8 nm thick on HMDS (■), 23.2 nm thick on bare silicon (●) and 28.9 nm thick on APTMS (▲). The thin film on HMDS had the largest degree of swelling as humidity was increased from 0 to 90 % RH. At 90 % RH, the film on HMDS, bare silicon, and APMTS swelled 29 %, 26 %, 20 % of their original thickness, respectively.

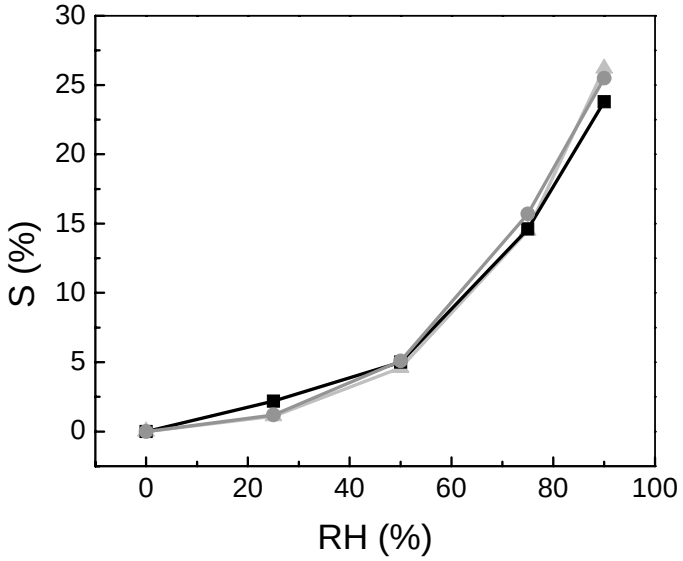

Figure **5-12**. Degree of swelling (%) at equilibrium of thick sulfonated poly(styrene)-poly(methyl methacrylate) films on three different substrate treatments on silicon wafers. Films are 323.0 nm thick on HMDS (■), 343.0 nm thick on bare silicon (●) and 380.0 nm thick on APTMS (▲). Thick films all showed similar degrees of swelling as humidity was increased from 0 to 90 % RH. At 90 % RH, the film on HMDS, bare silicon, and APMTS swelled 24 %, 26 %, 26 % of their original thickness, respectively.

5.3. Conclusions

Spectroscopic ellipsometry was used for characterizing the dynamic change in thickness while sulfonated poly(styrene)-*b*-poly(methyl methacrylate) films swelled in a humidity-controlled cell. Thickness change and swelling characteristics were compared for films over a series of thicknesses and substrate treatments. For ultra thin films 23-29 nm thick when dry, substrate treatment greatly affected how much the film swelled from 0 to 90 % RH, while films 350 nm in thickness showed similar overall swelling regardless of substrate treatment.

Substrate treatment affected both the initial swelling rate as well as the overall time it took for the film the reach an equilibrium thickness at a given relative humidity. The thinnest films on HMDS swelled the fastest and to the greatest extent, supporting the model that less confinement of chains at the substrate-polymer interface in thin films allows for faster polymer relaxation and water uptake. In ultra thin films, the rate of water uptake is twice as fast at when humidity is incremented from 25 % RH to 50 % RH, compared to the change from 50 to 75 % RH, because the sulfonate groups are more solvated and have less of a driving force for hydration at higher humidities.

It was surprising that thin films on hydrophobic substrates swelled to the greatest extent because, while hydrophobic substrates allow ionic block copolymer thin films to swell more, in other reports, they cause homopolymer thin films to swell less.[2] Attempts to fit dynamic swelling data to a basic water sorption model were unsuccessful, proving that absorption is not due to diffusion alone. Since swelling in thin films cannot be described as a first order process, this implies that film expansion is due to both diffusion of water and simultaneous polymer relaxation, the description of which is an area of

future work. The large difference in the swelling extent for thin films with different surface treatments indicates a strong correlation between thin film morphology and swelling. These results confirm that polymer-substrate interactions dictate ion-containing block copolymer film properties for thin films with a high ratio of surface area to volume. In the future, swelling of ionic block copolymer films with organized or patterned geometric structures would be an essential addition to this work.

References

1. Rubatat, L.; Li, C. X.; Dietsch, H.; Nykanen, A.; Ruokolainen, J.; Mezzenga, R., Structure-Properties Relationship in Proton Conductive Sulfonated Polystyrene-Polymethyl Methacrylate Block Copolymers (sPS-PMMA). *Macromolecules* **2008,** 41, (21), 8130-8137.
2. Vogt, B. D.; Soles, C. L.; Lee, H.-J.; Lin, E. K.; Wu, W.-l., Moisture absorption into ultrathin hydrophilic polymer films on different substrate surfaces. *Polymer* **2005,** 46, (5), 1635-1642.
3. Tan, N. C. B.; Wu, W. L.; Wallace, W. E.; Davis, G. T., Interface effects on moisture absorption in ultrathin polyimide films. *Journal of Polymer Science Part B-Polymer Physics* **1998,** 36, (1), 155-162.
4. Li, Y.; Park, E. J.; Lim, K. T. L.; Johnston, K. P.; Green, P. F., Role of interfacial interactions on the anomalous swelling of polymer thin films in supercritical carbon dioxide. *Journal of Polymer Science Part B-Polymer Physics* **2007,** 45, (11), 1313-1324.
5. Mencer, H. J.; Gomzi, Z., SWELLING KINETICS OF POLYMER-SOLVENT SYSTEMS. *European Polymer Journal* **1994,** 30, (1), 33-36.
6. Williams, G.; Watts, D. C., Non-Symmetrical Dielectric Relaxation Behaviour Arising from a Simple Empirical Decay Function. *Transactions of the Faraday Society* **1970,** 66, (565P), 80-&.
7. Vogt, B. D.; Soles, C. L.; Lee, H. J.; Lin, E. K.; Wu, W. L., Moisture absorption and absorption kinetics in polyelectrolyte films: Influence of film thickness. *Langmuir* **2004,** 20, (4), 1453-1458.
8. Hall, D. B. Experimental studies of relaxation phenomena and diffusion in thin and ultrathin polymer films. Ph.D. Thesis. . Ph.D. Dissertation, Northwestern University 1999.
9. Agra, D. M. G.; Schwab, A. D.; Kim, J. H.; Kumar, S.; Dhinojwala, A., Relaxation dynamics of rubbed polystyrene thin films. *Europhysics Letters* **2000,** 51, (6), 655-660.
10. Fujita, H.; Kishimoto, A., DIFFUSION-CONTROLLED STRESS RELAXATION IN POLYMERS .2. STRESS RELAXATION IN SWOLLEN POLYMERS. *Journal of Polymer Science* **1958,** 28, (118), 547-567.
11. Hall, D. B.; Miller, R. D.; Torkelson, J. M., Molecular probe techniques for studying diffusion and relaxation in thin and ultrathin polymer films. *Journal of Polymer Science Part B: Polymer Physics* **1997,** 35, (17), 2795-2802.
12. Kishimoto, A.; Fujita, H., Diffusion-Controlled Stress-Relaxation in Polymers, I. *Kolloid Zeitschrift* **1956,** 1, (150), 11.
13. Kishimoto, A.; Hiroshi, F., Diffusion-controlled stress relaxation in polymers. III. Stress relaxation in a swelling polymer. *Journal of Polymer Science* **1958,** 28, (118), 569-585.
14. Mundra, M. K.; Ellison, C. J.; Rittigstein, P.; Torkelson, J. M., Fluorescence studies of confinement in polymer films and nanocomposites: Glass transition temperature, plasticizer

effects, and sensitivity to stress relaxation and local polarity. *European Physical Journal-Special Topics* **2007,** 141, 143-151.
15. Burnett, D. J.; Garcia, A. R.; Thielmann, F., Measuring moisture sorption and diffusion kinetics on proton exchange membranes using a gravimetric vapor sorption apparatus. *Journal of Power Sources* **2006,** 160, (1), 426-430.
16. Edwards, D. A., Non-Fickian diffusion in thin polymer films. *Journal of Polymer Science Part B-Polymer Physics* **1996,** 34, (5), 981-997.
17. Frank, B.; Gast, A. P.; Russell, T. P.; Brown, H. R.; Hawker, C. J., Polymer mobility in thin films. *Macromolecules* **1996,** 29, (20), 6531-6534.
18. Hall, D. B.; Torkelson, J. M., Small molecule probe diffusion in thin and ultrathin supported polymer films. *Macromolecules* **1998,** 31, (25), 8817-8825.
19. Vrentas, J. S.; Duda, J. L., Molecular-Diffusion in Polymer-Solutions. *Aiche Journal* **1979,** 25, (1), 1-24.
20. Vrentas, J. S.; Jarzebski, C. M.; Duda, J. L., Deborah Number for Diffusion in Polymer-Solvent Systems. *Aiche Journal* **1975,** 21, (5), 894-901.
21. Papanu, J. S.; Hess, D. W.; Bell, A. T.; Soane, D. S., In-Situ Ellipsometry to Monitor Swelling and Dissolution of Thin Polymer Films. *Journal of the Electrochemical Society* **1989,** 136, (4), 1195-1200.
22. Singh, A.; Mukherjee, M., Swelling dynamics of ultrathin polymer films. *Macromolecules* **2003,** 36, (23), 8728-8731.
23. Sirard, S. M.; Green, P. F.; Johnston, K. P., Spectroscopic ellipsometry investigation of the swelling of poly(dimethylsiloxane) thin films with high pressure carbon dioxide. *Journal of Physical Chemistry B* **2001,** 105, (4), 766-772.
24. Mangiagli, P. M.; Ewing, C. S.; Xu, K.; Wang, Q.; Hickner, M. A., Dynamic Water Uptake of Flexible Ion-Containing Polymer Networks. *Fuel Cells* **2009,** 9, (4), 432-438.

Chapter 6

Conductivity of Ion-Containing Block Copolymer Films

6.1. Introduction

Proton conductivity is the single most important feature of a proton exchange membrane (PEM). Although bulk PEMs have been widely studied, little attention has been given to thin film ionic block copolymer swelling and conductivity. Thin ionic polymer films play a significant role in fuel cell operation: the catalyst layer is coated with ionomer to lower the resistance during proton transfer between the catalyst layer and the proton exchange membrane. Proper coating with a thin layer of ionomer (estimated to be 5-50 nm thick)[1] is essential to accessing reaction sites at all of the platinum surface area within the catalyst layer. Overall fuel cell efficiency can be improved when thin film proton conductivity in the catalyst layer is increased.[2]

Typically, it has been assumed that thin ionomer films possess the same properties, e.g. water uptake and conductivity, as bulk membranes. However, in thin ionomer films, the substrate and air interfaces affect film morphology and water uptake, as demonstrated in previous chapters. The high ratio of surface area to volume in films less than 100 nm in thickness results in a large percentage of interfacial polymer that may have different properties than what is observed for bulk films. It has been established that there is an inherent connection between the morphology of an ion-containing polymer, how much it swells with water, and its proton conductivity.[3] In this chapter, conductivity is investigated as function of thickness and film processing. Thin films were created by

drop casting and spin casting onto silicon, as well as by casting into molds to form bulk films. One limitation of the present work is that, due to experimental constraints, the conductivity of a thin film on a substrate treated with HMDS or APTMS, as described above for morphology and water uptake, cannot be measured. Since electrodes are attached to the substrate, substrate coatings would cover the electrodes and the resistance of the substrate treatment may affect the conductivity results obtained. Due to this limitation, thin film conductivity was only measured on a bare Si substrate with an insulating oxide layer of 90 nm so that the conductivity of silicon did not skew the measurement.

Yasuda, et al.[4, 5] provided the initial report on thin film ion conductivity via impedance spectroscopy. They found that the film conductivity of spin cast Nafion samples decreased as the thickness of the film on silicon decreased. As conductivity is an intrinsic material property, it is not anticipated to change for films with varying thickness. Equation 6-1 shows how the resistance of a sample is used to compute the conductivity

$$\sigma = \frac{\ell}{R \cdot A} \tag{6-1}$$

where σ is the proton conductivity, *l* is the path length between electrodes, A is the cross sectional area of the film available for proton transport, and R is the measured resistance. Yasuda, et al.[4] reported that conductivity decreased as a logarithmic factor of thickness, over a scale of bulk (500 μm) to ultra thin (5 nm) films. Thinner films were found to have higher activation energies for ionic conductivity, indicating that some inherent structural changes with thickness influence their conductive nature. It was suggested that thin films absorb less water, thus lowering conductivity. In addition to water uptake changes with film thickness, morphological effects, could have an influence on the

measured conductivity. However, neither water uptake nor morphology was investigated in Yasuda's work.

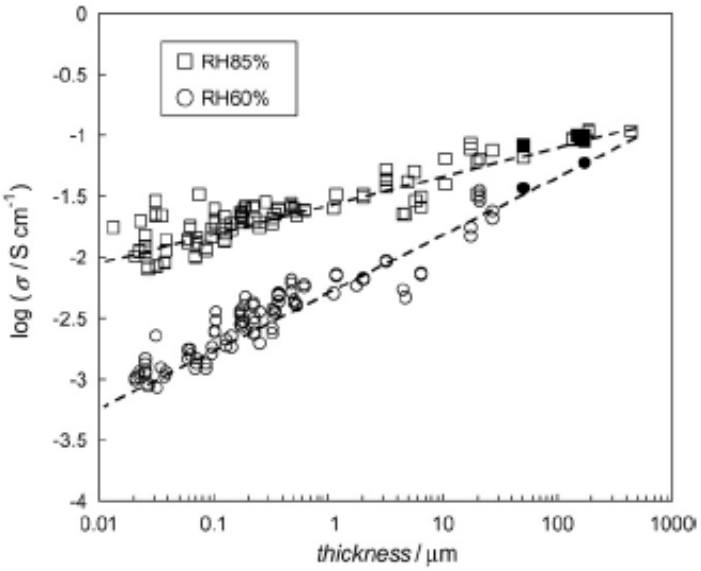

Figure **6-1**. Dependence of the conductivity of recast Nafion® thin film on film thickness. Samples were measured at 85 ºC and a relative humidity of 85 % (□) or 60 % (○). Solid data points (■) represent bulk membranes (Nafion® 112, 115, and 117).[4]

In this study, proton conductivity was measured for sPS-*b*-PMMA films 80 nm to 60 μm thick. Since morphology is greatly influenced by film processing, conductivity showed a dependence on how films were cast. Drop cast films had higher conductivities due to the longer casting times which afforded better organization of the ionic domains.

6.2. Conductivity of Spin Cast Thin Films

Since processing conditions have a strong influence on resulting polymer morphology, it is important to investigate how various film processing techniques affect conductivity. Thin film morphologies are influenced by solution concentration, spin

speed, and thickness, so creating films via spin casting can create a range of morphologies, and thus different conductivity for the same material. Films 86 nm to 2.5 μm thick were fabricated by spin casting sulfonated poly(styrene)-*b*-poly(methyl methacrylate) from 1 and 5 % w/w solutions in dimethylformamide (DMF) at spin speeds of 500 to 4000 rpm. Figure **6-2** shows that the measured proton conductivity initially decreases as the thickness of the film increases, but the thickest film has a greater conductivity than the other samples. The higher degree of interfacial area per volume could contribute to this range of conductivity as a function of thickness.

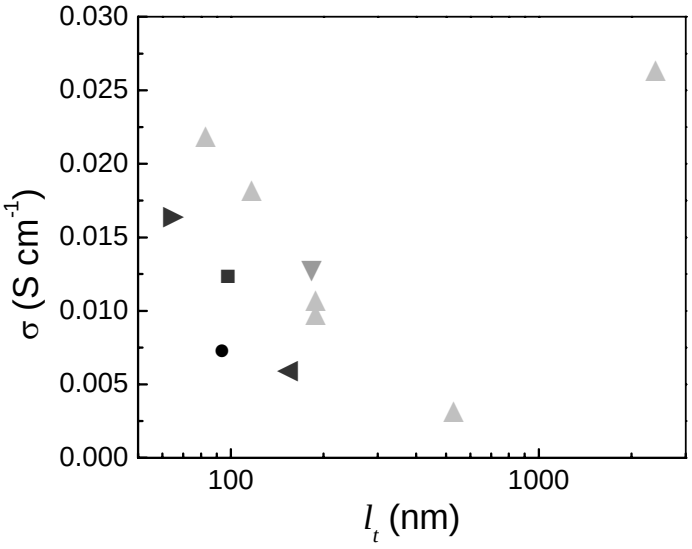

Figure **6-2**. Conductivity, σ, as a function of film thickness, l_t, for spin cast sulfonated poly(styrene)-*b*-poly(methyl methacrylate) films from 86 nm to 2.5 μm thick measured at 90% RH and 25°C. Samples include molecular weights in kg mol^{-1} and degrees of sulfonation of 403-263, DS 74 % (●), 203-165, DS 100 % (▼), 186-106, DS 93 % (■), 170-128, DS 100 % (◄), 120-90, DS 100 % (►), 80-52, DS 100 % (▲).

While the films less than 500 nm in thickness dried within a minute of spin casting, at least 5 min were required for the 2.5 μm thick film to dry, which could have allowed more time for ionic domain organization. The thicker film subsequently showed higher conductivity, displaying characteristics more like a drop cast film.

Decreasing conductivity with increasing thickness in this study was unexpected given Yasuda's initial data. However, there are reports of the conductivity of electrolyte-filled track-etched membranes increasing with decreasing pore radius.[6] Physical mechanisms for the conductivity increase with decreasing pore radius have not been provided, but there could be advantageous proton transport on the surface or at the interface of thin electrolyte layers. If protons are transported more easily at interfaces, films of various thicknesses would have similar resistances but different conductivities based on thickness (see Equation 3-1). The previous results on different pore size membranes and the results for the spin cast films with thicknesses less than 500 nm in Fig. **6-2** would tend to support one another, but further study of the mechanism of proton transport in the presence of large interfacial areas is required.

6.3. Conductivity of Drop Cast Thin Films

Drop cast films showed dependence of conductivity on film thickness. Since drop cast films are slowly dried over a period of at least 24 hours, the polymer domains have more time to kinetically arrange into a phase separated morphology. By allowing the polymer more time to phase separate, the morphology of the film, and therefore the conductivity, is less susceptible to processing effects. Figure **6-3** shows the trend between decreasing conductivity with decreasing film thickness, l_t, for samples created

by drop casting 1 and 5% w/w solutions of sulfonated poly(styrene)-*b*-poly(methyl methacrylate) in DMF.

Bulk film conductivity was measured for a series of sulfonate poly(styrene)-*b*-poly(methyl methacrylate) cast into Teflon ® molds. Films cast from 5 w/w % solution (DMF) were slowly dried for more than 10 days. Conductivities were measured as a function of relative humidity, as shown in Figure **6-3**. The outlier of the series with the lowest conductivity at 90 % RH also has the lowest degree of sulfonation. While it has the most sulfonate groups because it is the highest molecular weight, those groups are less concentrated because the polymer has a degree of sulfonation of only 74 %. Figure **6-3** shows that molecular weight has little effect on conductivity, with films over a large range of sPS-*b*-PMMA molecular weights showing similar conductivities up to 90% RH.

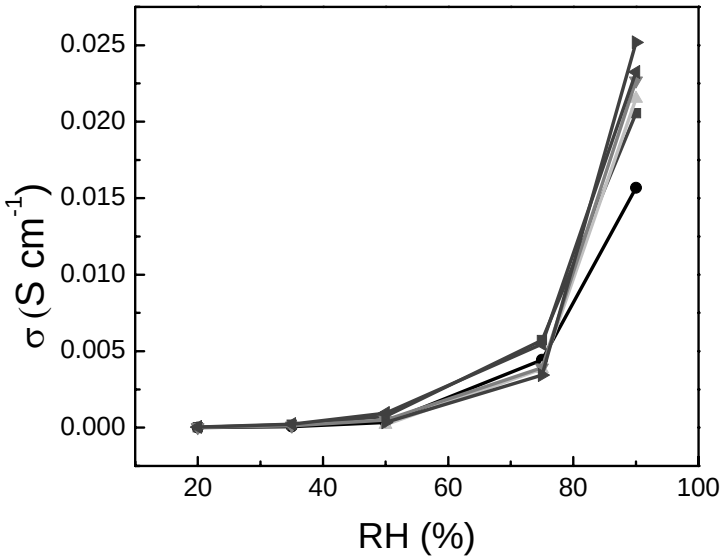

Figure **6-3**. Conductivity, σ, as a function of relative humidity for bulk films (~50 μm in thickness) for a variety of sulfonated poly(styrene)-*b*-poly(methyl methacrylate) molecular weights. Samples include molecular weights in kg mol^{-1} and degrees of sulfonation of 403-263, DS 74 % (●), 203-165, DS 100 % (▼), 186-106, DS 93 % (■), 170-128, DS 100 % (◄), 120-90, DS 100 % (►), 80-52, DS 100 % (▲).

The conductivities of sPS-*b*-PMMA films created by drop casting and bulk film casting are shown in Figure **6-4**. Drop cast films are indicated by the dotted circle while bulk films are indicated by the solid circle. Films drop cast onto silicon wafers dried over a period of at least 8 hours while bulk films dried over at least 10 days. Details of film fabrication can be found in Chapter 3. Bulk and drop cast films show that conductivity decreases logarithmically with thickness, similar to Yasuda's findings.[4] Since thicker films are made by slowly drying sPS-*b*-PMMA from solution, these films allowed for the films to reach a more favorable kinetic arrangement. Conductivity subsequently shows a clearer trend with thickness for slowly dried films than for spin cast films.

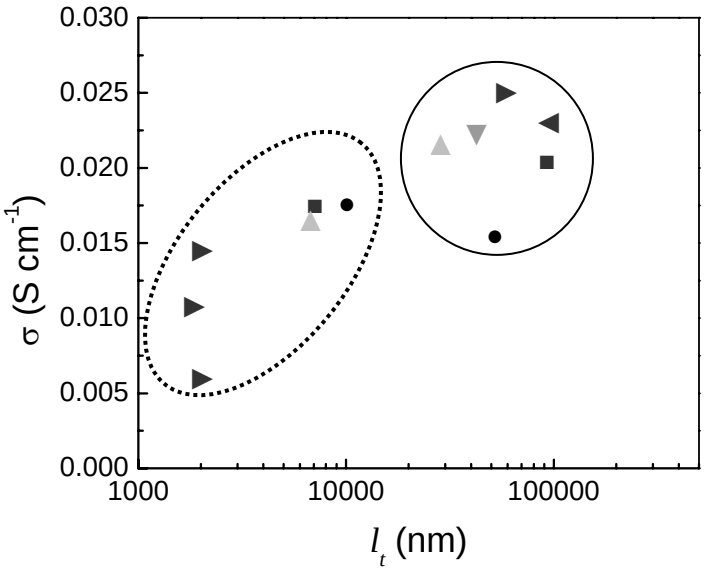

Figure **6-4**. Conductivity, σ, as a function of thickness, l_t, for drop cast and bulk films. Conductivities were measured at 90 % RH and 25 °C. The solid circle surrounds bulk films created in molds. The dotted circle indicates films that were drop cast. Samples include molecular weights in kg mol^{-1} and degrees of sulfonation of 403-263, DS 74 % (●), 203-165, DS 100 % (▼), 186-106, DS 93 % (■), 170-128, DS 100 % (◀), 120-90, DS 100 % (▶), 80-52, DS 100 % (▲).

6.4. Conclusions and Future Work

Film processing methods had an effect on the measured conductivity of ionic block copolymer samples. Films that were slowly dried from drop cast solutions showed a trend between conductivity and film thickness, while films that were spin cast did not. Creating a reliable method for repeatable conductivity measurements of thin films is an important future step. Although similar research has measured conductivity by sputtering gold electrodes onto glass slides,[3] we found this method to be far less consistent from sample to sample. The method of electrode creation using photolithography is the best option, although, more development is required to make this a robust, repeatable, and routine measurement. In the future, a larger array of samples must be characterized to ensure that these trends are accurate.

References

1. Eikerling, M., Water management in cathode catalyst layers of PEM fuel cells - A structure-based model. *Journal of the Electrochemical Society* **2006,** 153, (3), E58-E70.
2. Liu, Y. X.; Murphy, M. W.; Baker, D. R.; Gu, W. B.; Ji, C. C.; Jorne, J.; Gasteiger, H. A., Proton Conduction and Oxygen Reduction Kinetics in PEM Fuel Cell Cathodes: Effects of Ionomer-to-Carbon Ratio and Relative Humidity. *Journal of the Electrochemical Society* **2009,** 156, (8), B970-B980.
3. Rubatat, L.; Li, C. X.; Dietsch, H.; Nykanen, A.; Ruokolainen, J.; Mezzenga, R., Structure-Properties Relationship in Proton Conductive Sulfonated Polystyrene-Polymethyl Methacrylate Block Copolymers (sPS-PMMA). *Macromolecules* **2008,** 41, (21), 8130-8137.
4. Siroma, Z.; Kakitsubo, R.; Fujiwara, N.; Ioroi, T.; Yamazaki, S. I.; Yasuda, K., Depression of proton conductivity in recast Nafion (R) film measured on flat substrate. *Journal of Power Sources* **2009,** 189, (2), 994-998.
5. Siroma, Z.; Ioroi, T.; Fujiwara, N.; Yasuda, K., Proton conductivity along interface in thin cast film of Nafion (R). *Electrochemistry Communications* **2002,** 4, (2), 143-145.
6. Chen, H.; Palmese, G. R.; Elabd, Y. A., Membranes with oriented polyelectrolyte nanodomains. *Chemistry of Materials* **2006,** 18, (20), 4875-4881.

Chapter 7

Conclusions and Future Work

7.1. Summary and Conclusions

Morphology, swelling, and conductivity of thin ion-containing block copolymer films were investigated and to determine the fundamental water sorption phenomena and morphological features that may influence the conductivity of thin films. Film morphology was studied as a function of processing conditions, thickness, and substrate treatment. Spectroscopic ellipsometry was used to characterize the dynamic change in thickness and optical properties while sPS-*b*-PMMA films swelled in a humidity-controlled cell. It was established that substrate treatment has the largest effect on film morphology, which greatly influences swelling behavior in thin films. Substrate treatment affected both the initial swelling rate as well as the overall time it took for the film the reach an equilibrium thickness at a given relative humidity. The large difference in the swelling extent for thin films (~ 25 nm) with different surface treatments indicates a strong correlation between thin film morphology and swelling. These results confirm that polymer-substrate interactions dictate ion-containing block copolymer film properties for thin films with a high ratio of surface area to volume.

Film processing methods had an effect on the conductivity of ionic block copolymer samples. Films that were slowly dried from drop cast solutions showed a trend between conductivity and film thickness, while films that were spin cast did not.

Dynamic swelling data was fit to a stretched exponential model, proving that absorption is due to both diffusion of water and simultaneous polymer relaxation.

7.2. Future Directions

While this research has answered important questions for a controlled set of materials, it has elicited even more. In terms of future data modeling, since water sorption in thin sPS-*b*-PMMA films has been shown to be the result of more than simple diffusion, an equation to appropriately describe polymer relaxation during swelling must be established. In terms of future sample preparations, swelling of ionic block copolymer films with organized or patterned geometric structures would also be an essential addition to this work.

Since spectroscopic ellipsometry (SE) was the most successful aspect of characterizing dynamic changes in data, a central part of this study, future characterization will include more specialized uses of SE. Mueller matrix ellipsometry can be used to evaluate anisotropic optical changes by deriving optical properties in a particular direction. When combined with infrared light, SE would give information about the optical changes during swelling as well as molecular vibrational modes. Tracking changes in the characteristic bonding of water would give valuable information about how water interacts with itself and with the polymer as equilibrium water content varies. The behavior of water within a hydrated ion conductive polymer film is still not completely understood.

Since spectroscopic ellipsometry only gives information about the volumetric water uptake, assumptions must be made about how the mass of the film changes when

water is absorbed. If the mass and volume change could be measured simultaneously, the time lag between water sorption and polymer expansion could be determined and the real density of the film could be calculated instead of assumed. In the future, a quartz crystal microbalance (QCM) will be installed on the spectroscopic ellipsometer to simultaneously measure gravimetric and volumetric water uptake. The polymer film would have to be coated on a quartz crystal substrate that is compatible with the QCM and the relative humidity chamber would have to be built around the QCM holder. Ideally, a quartz crystal microbalance with dissipation (QCM-D) would give even more information by determining film thickness, mass, density, and viscoelastic properties by measuring both the dissipation and resonance frequency of the crystal after oscillations are stopped. QCM-Ds allow for monitoring of both structural and mass changes of a thin film, which would be a powerful tool when combined with spectroscopic ellipsometry.

A more reproducible and reliable method for conductivity measurements of thin films needs to be developed. A larger array of samples must be characterized to ensure that conductivity trends are accurate. Direct current conductivity of proton transfer in humidified membranes should be measured and compared to AC impedance results in order to better understand mechanisms of proton conduction in ion conductive thin films. Conductivity will be measured on materials with more rubbery blocks than PMMA to establish how the structural block affects overall swelling and conductivity in ionic block copolymer thin films. For such an interesting and unexplored set of materials, there is much more work to do to understand how water activity contributes to the dynamic behavior of thin ion-containing polymer films.